CONSTRAINTS ON THE EARTH'S ANELASTIC AND ASPHERICAL STRUCTURE FROM ANTIPODAL SURFACE WAVES

Thesis by

Eric Paul Chael

In Partial Fulfillment of the Requirements

For the Degree of

Doctor of Philosophy

California Institute of Technology

Pasadena, California

1983

(Submitted May 24, 1983)

To My Parents

ACKNOWLEDGMENTS

During the last six years it has been my privilege and pleasure to work among the outstanding faculty, students and staff of the Seismo Lab. I am especially indebted to Don Anderson, my research advisor. Don has been a constant source of insight, ideas and - most importantly - enthusiasm throughout this study. I thank José Rial for introducing me to the antipode project and for providing the seismograms. Hiroo Kanamori, Jeff Given and Ichiro Nakanishi answered many questions about surface waves and normal modes. They also reviewed rough drafts and offered computer programs and unpublished results of their own work. Don Helmberger served as my academic advisor and patiently taught me how to run a pass pattern.

The figures in this thesis were expertly drafted by Laszlo Lenches with the assistance of Joe Galvan. Marianne Walck proofread the text.

The Lab's coterie of footballers, softballers and skiers have done much to make life outside the office enjoyable. I will miss them.

I thank my close friends - Steve, Dan, Jim, Bruce, Paul - and especially Marianne for their encouragement and companionship.

The National Science Foundation supported this research through the Graduate Fellowship Program and through grants EAR77-14675 and EAR811-5236.

Any traveler who misses the journey
misses about all he's going to get.

- William Least Heat Moon

Think Snow!

- Anon

ABSTRACT

Seismograms recorded at antipodal distances ($\Delta \sim 180^{o}$) are used to measure the attenuation and dispersion of surface waves. The antipode is a focus for surface wave energy radiated at all directions from the source. Antipodal records thus give direct estimates of global average properties. Laterally heterogeneous Earth structure degrades the focusing and complicates the data analysis.

Group velocity and Q of 120-300 s Rayleigh waves are obtained from a record (station PTO) of the May 23, 1968 New Zealand earthquake. The effects of aspherical structure on this record are simulated by generating synthetic seismograms for an ellipsoidal Earth. The results show that the bias in antipodal Q measurements varies with time. This property is used to constrain the bias in the PTO measurements.

A seismogram of the August 19, 1977 Indonesian earthquake from station TRN is used to study 250-500 s Rayleigh waves. This record is synthesized by combining first order perturbation theory with a realistic representation of the Earth's heterogeneities. Analysis of the synthetic shows that Q measured from the TRN record is biased as much as 20% and that group velocities are virtually unbiased. The PTO and TRN data yield global average values of Rayleigh wave Q which are comparable to or slightly below those for the model PREM [Dziewonski and Anderson, 1981].

Antipodal Love wave and spheroidal overtone data are also presented. Synthetic seismograms match the observed arrivals well, demonstrating that these wave modes can be profitably studied at the antipode.

TABLE OF CONTENTS

INTRODUCTION

Accurate modeling of seismic velocities in the Earth requires an accurate knowledge of seismic attenuation. This is because attenuative materials must necessarily be dispersive: they must have phase velocities which vary with frequency. As a result, an elastic velocity profile which satisfies body wave travel time data (1-10 s periods) will be incompatible with observed periods of free oscillations (periods > 200 s). Also, elastic parameters of candidate mantle materials are measured in the laboratory at ultrasonic frequencies, so the results may not be directly comparable to seismic data. Jeffreys [1965] was among the first to suggest that attenuative dispersion is of first order in frequency. Liu et al. [1976] and Kanamori and Anderson [1977] subsequently demonstrated that the phase velocity could vary by more than 1% over the seismic frequency band for reasonable estimates of attenuation. The measurement errors of normal mode eigenperiods, surface wave phase velocities, and body wave travel times are typically less than 0.1%, so the dispersion accompanying absorption is above the level of detection by an order of magnitude. Hart et al. [1977] and Anderson et al. [1977] showed that correcting for dispersion reduced the discrepancies between body wave and normal mode data. Better estimates of the attenuation, or Q, of normal modes and body and surface waves are needed in order to construct an accurate velocity model compatible with all these data

sets.

Better attenuation estimates will also yield more accurate measurements of the seismic moment and energy release in earthquakes. Moment determinations are based on amplitudes of arrivals at stations distant from the source [e.g., Kanamori, 1970a], requiring a knowledge of decay rates along the propagation path. For large events ($M_s > 7$) the first few surface wave arrivals (R1, R2, etc.) are often off-scale at most stations, forcing the use of later arrivals. An error in the assumed attenuation of surface waves would have a proportionally larger effect on moment estimates made from later arrivals.

Rotation and aspherical structure can produce coupling between nearly degenerate normal modes of a spherically symmetric Earth model [Dahlen, 1968, 1969]. This effect may be significant at low frequencies, and should be considered in inversions for both radial Earth structure and earthquake source parameters [Masters et al., 1983]. Woodhouse [1980] demonstrated that attenuation strongly affects the specific nature of the coupling between two modes. Improved attenuation estimates will enable accurate corrections for mode coupling and hence lead to further refinements in seismic velocity models and earthquake moment tensor determinations.

Ultimately, the anelastic behavior should provide some information about materials and conditions in the Earth's interior. Q is observed to be relatively constant over seismic frequencies,

implying that a distribution of relaxation mechanisms is responsible for absorption [Liu et al., 1976; Anderson et al., 1977]. The geophysically relevant relaxation mechanisms [Jackson and Anderson, 1970; Minster, 1980] appear to be thermally activated processes, the absorption varying exponentially with temperature. Activation energies depend upon the chemical composition and the particular relaxation mechanisms. Because of the temperature dependence, the variation of Q with depth should constrain the geotherm. Steady-state creep mechanisms in the mantle may be caused by the same mechanisms responsible for attenuation of seismic waves, such as dislocation glide or climb. If so, it may eventually be possible to infer mantle viscosities from the Q profile [Anderson and Minster, 1981]. Temperature and viscosity have implications for the nature of mantle convection.

The primary objective of this thesis is to determine well constrained global average values of Q for fundamental mode Rayleigh surface waves in the 100-500 s period band. This has been the goal as well of many other investigations [Anderson et al., 1965; Kanamori, 1970b; Mills and Hales, 1977, 1978; Nakanishi, 1979; Sailor and Dziewonski, 1978; Masters and Gilbert, 1982]. These studies have employed a wide variety of techniques, but they all have one thing in common. Q values calculated from a particular record represent the attenuation only around the great circle connecting the epicenter and station. To obtain global averages of attenuation, the results for

many distinct great circles must be combined. In principle this method should work, but in practice there appear to be some problems with it. Figure 0.1a shows results of Nakanishi [1979] for two stations lying along the same great circle. Q estimates from these records differ by as much as a factor of two at some periods. Comparable uncertainties probably exist in most measurements for a particular great circle, and these errors are transmitted to subsequent global averages. In Figure 0.1b the global average estimates of five different studies are compared; discrepancies between the results average about 50% at all periods. There are many possible explanations of this scatter, including poor signal-to-noise, contamination by other wave modes, biased selection of seismograms, and effects of lateral scattering.

In this thesis, a more direct measure of average global attenuation is obtained through the analysis of recordings from the antipodal regions of earthquakes. Because the antipode is a caustic for Rayleigh wave propagation, it offers two immediate advantages. First, energy arriving from all azimuths, i.e., energy that has sampled the entire globe, contributes to the antipodal record. Such a record thus reflects average global properties, not just the structure along a particular great circle. Global averages can therefore be obtained from a single event at a single station. The Earth does the averaging; combining different events and stations, with the attendant accumulation of errors, is not necessary. Second, if the

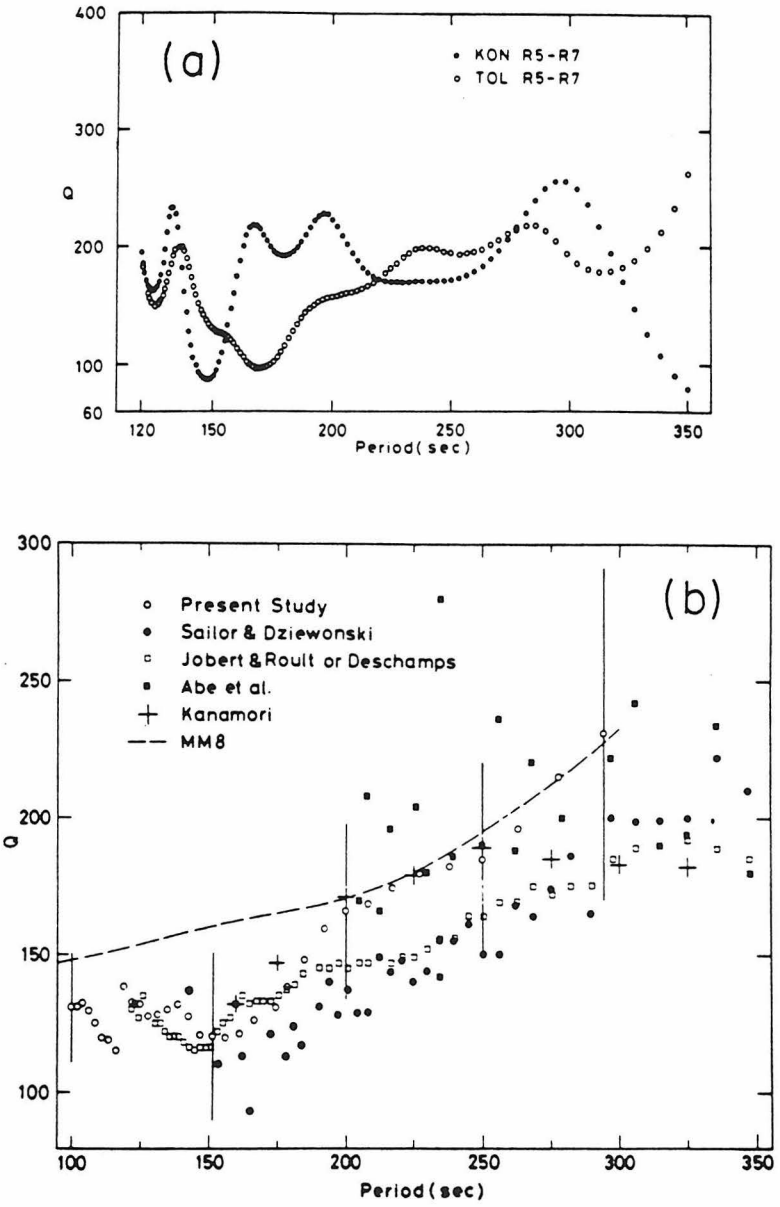

Figure 0.1 (a) Precision of conventional great circle Rayleigh wave Q measurements: results from two seismograms recorded along the same great circle path. (b) Average Rayleigh wave Q determined by 5 different studies which used conventional great circle data. Scatter is considerable at all periods. (a) and (b) are both from Nakanishi [1977].

arriving energy is consistent in phase, constructive interference produces strong amplification of the signal, reducing the effect of noise contamination. The resulting measurements are stable and reproducible, showing much less scatter than is seen in conventional studies. Both advantages are clearly dependent on the radiation pattern of the event. An isotropic explosion radiates equal energy with uniform phase at all azimuths, yielding at the antipode of a spherically symmetric globe complete constructive interference for vertical motion, and complete cancellation of horizontal motion. Of the shear-dislocation sources, a shallow, 45° dip-slip event is most favorable. The Rayleigh wave radiation pattern of such an event has two wide phase-symmetric lobes, offering the greatest degree of constructive interference at the antipode.

In a sense, the Earth behaves as a giant lens, bringing all of the Rayleigh wave energy from an earthquake to a focus at the antipode. Dispersion of the wave train, analogous to a chromatic aberration of the lens, smears out the temporal focusing. The spatial focusing is degraded by lateral heterogeneities in the Earth's velocity structure, which represent imperfections in the figure of the lens. A significant fraction of this thesis is devoted to removing from the antipodal attenuation estimates any bias caused by lateral velocity heterogeneities. Two distinct approaches are employed towards this end. For periods from 150 to 250 s, the bias is constrained by the attenuation measurements themselves, without any

a priori assumptions about the heterogeneous structure. This is accomplished by studying effects on antipodal Q values which would be common to any distribution of heterogeneities. A result of this approach is an independent constraint on the nature of such heterogeneities in the mantle; specifically, it may indicate the extent to which continental and oceanic structures differ. At longer periods (250-500 s) reliable observations of great circle phase velocities, as a function of path orientation on the Earth, are combined with perturbation methods to model the effects of a realistic distribution of heterogeneities.

Besides attenuation estimates, the antipodal seismograms yield global average phase and group velocities for Rayleigh waves. Conventional studies produce accurate velocity measurements, and most such studies agree within their limits of resolution. In this case the antipodal method cannot really improve on the uncertainties in the global averages. The results here generally corroborate existing phase and group velocity data.

While most of this thesis is concerned with Rayleigh waves and the corresponding fundamental spheroidal modes, some measurements of the dispersion and attenuation of Love waves and spheroidal overtones are also presented. Results for these wave modes complement the Rayleigh wave results and tighten the constraints on inversions for the radial Earth structure. Unfortunately, the antipodal Love and overtone data collected so far are rather limited. Still, few global

averages for these modes are to be found in the literature, so the measurements here should prove useful despite their relatively large uncertainties and limited frequency range.

Chapter 1

THE PTO RECORD OF THE INANGAHUA, NEW ZEALAND EARTHQUAKE

The first antipodal Rayleigh arrivals analyzed are from a seismogram of the Inangahua, New Zealand, earthquake of May 23, 1968 (M_s=7.1, latitude=41.72°S, longitude=172.03°E, h=21 km, time=1724:17 (ISC)), recorded at WWSSN station PTO (Porto, Portugal; latitude=41.14°N, longitude=8.60°W). Body waves on this record have been previously studied by Rial [1978a, b]. Focal mechanism studies reveal this event to have been of predominantly thrust type [Robinson et al., 1975] (see Figure 1.1), satisfying the need for constructive interference of the Rayleigh lobes at the antipode. The station lies at a distance of 179.25° from the epicenter, or about 80 km from the true antipode, assuming a spherical Earth of radius 6371 km. The wavelengths of the long period (120-300 s) waves on this record vary from about 500 to 1600 km, so PTO is for these periods only a fraction of a wavelength from the antipode. As a result, the seismogram should exhibit the features of a true antipodal recording.

Before asserting that measurements from the PTO record represent global averages, one must consider how the radiation pattern of the Inangahua event affected the sampling of the mantle. Rial [1978b], studying the body waves, modeled the earthquake as a triple event. The three sources shared a common epicenter and focal

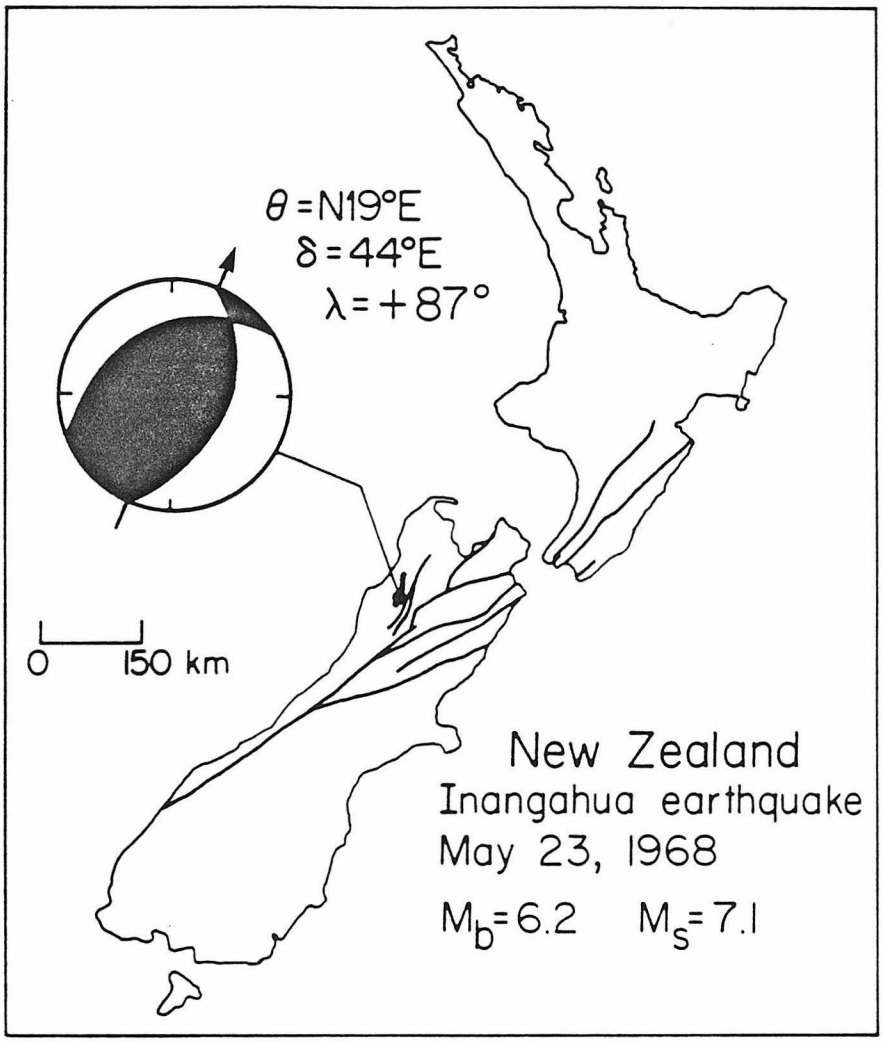

Figure 1.1 Location of the Inangahua, New Zealand earthquake of May 23, 1968. The focal mechanism (lower hemisphere projection) was determined by Robinson et al. [1975]. The earthquake occurred on the Glasgow Fault, a branch of the Alpine-Wairau system.

mechanism (strike=19°, dip=44°, rake=+87°) but differed in depth, seismic moment, and origin time. For long period Rayleigh waves, these differences are inconsequential, and Rial's triple source can be portrayed as a single event. The Rayleigh wave radiation pattern for this event displays the double-lobed nature typical of a thrust event. Assuming the Earth was well sampled between the half amplitude azimuths of the lobes, the Inangahua event's radiation pattern yields a coverage range of about 200°, greater than half of the globe. Figure 1.2 shows the radiation pattern superimposed on the epicenter, with great circles drawn through the half-amplitude points. Because the preferentially sampled zone includes a representative distribution of oceanic, continental, and tectonic regions, results from the PTO record should reflect an accurate measure of average global properties.

Group Velocity Measurements

The long period vertical record from PTO was digitized and interpolated to a sampling interval of 2 s. The first three Rayleigh wave arrivals were then extracted using conservative group velocity windows covering roughly 2.7 to 4.4 km/s. Beyond the third arrival the Rayleigh waves were too dispersed and attenuated to be above the noise. Because at the antipode the conventionally labeled arrivals R1 and R2 overlap, the first Rayleigh arrival will be referred to as

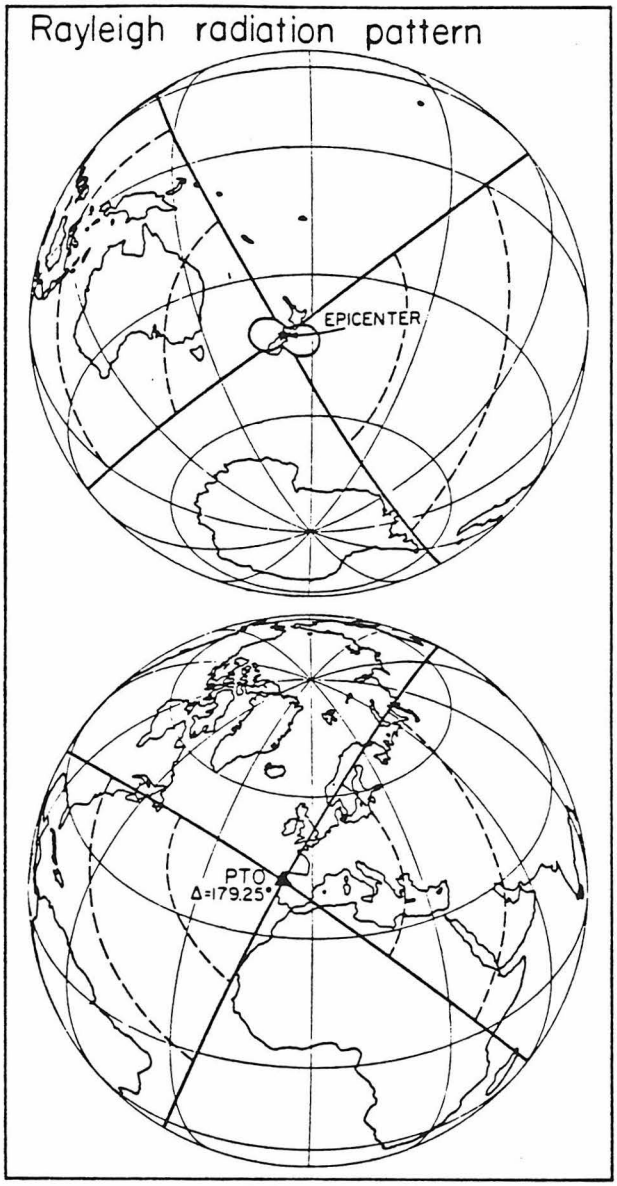

Figure 1.2 Global projection of the Rayleigh wave radiation pattern of the Inangahua earthquake. The upper diagram shows the long period radiation pattern at the epicenter, and the lower diagram illustrates the focusing at the antipodal station PTO. The dashed lines indicate the regions most strongly sampled.

R1R2; similarly, the second is called R3R4 and the third, R5R6. These arrivals correspond to propagation distances of 180^{o}, $360^{o}+180^{o}$, and $2\times360^{o}+180^{o}$, respectively. Unfiltered spectra of the three Rayleigh arrivals extracted from the PTO record are shown in Figure 1.3. Also shown is a representative noise spectrum, obtained by digitizing about one hour of the record ahead of the P wave arrival. The third Rayleigh arrival (R5R6) falls into the noise at periods below 150 s, and the second (R3R4) does so below about 100 s. At periods longer than 300 s the decay is too slow to be reliably measured using the available length of record. As a result the usable frequency range of this record is limited to periods between 100 and 300 s.

Each window was next convolved with a succession of narrow-band filters of the form

$$H(t) = \frac{\delta}{2\sqrt{\pi}} \cos(\omega_o t)\exp(-\delta^2 t^2\ 4) \qquad 1.1$$

where

δ = filter half-width, equal to $(\omega_1 - \omega_2)/2$;

ω_o = central frequency, equal to $(\omega_1 + \omega_2)/2$;

ω_1 = high-frequency cutoff;

ω_2 = low-frequency cutoff.

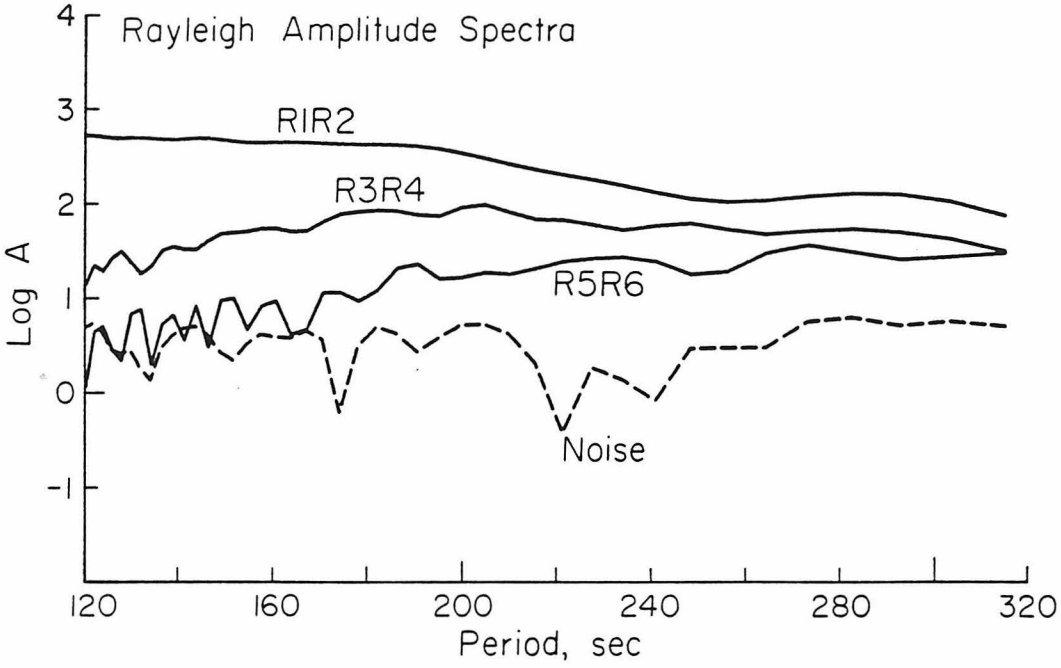

Figure 1.3 Amplitude spectra of the vertical component of the first three Rayleigh arrivals at PTO (unfiltered). The noise spectrum (dashed) was determined from a portion of the PTO record before the event.

This filter has a Gaussian shaped frequency response. Best results were obtained for a filter half-width δ of 10 mHz; 10 different filters were used, spanning the 120 to 300 s period range. In most cases, the filtered traces exhibited well-defined, dispersed wave groups. As a representative example, Figure 1.4 shows waveforms of the three Rayleigh arrivals convolved with a 170-250 s filter. Group velocities were calculated from the peak amplitude time of each filtered wave group using the formula

$$U(\omega) = \left(t_p(\omega) - t_o\right)/\Delta \qquad 1.2$$

where

$t_p(\omega)$ = peak amplitude time of group
with central frequency ω;

t_o = origin time of event;

Δ = propagation distance.

Here, the propagation distance Δ was based on a mean Earth circumference of 40,030 km, and the assumption that the station lies at the true antipode. No corrections were made for source or instrumental group delay times. Following Kanamori and Abe [1968], these combined corrections were estimated to be no greater than 0.7% of the travel time of the first (R1R2) arrival.

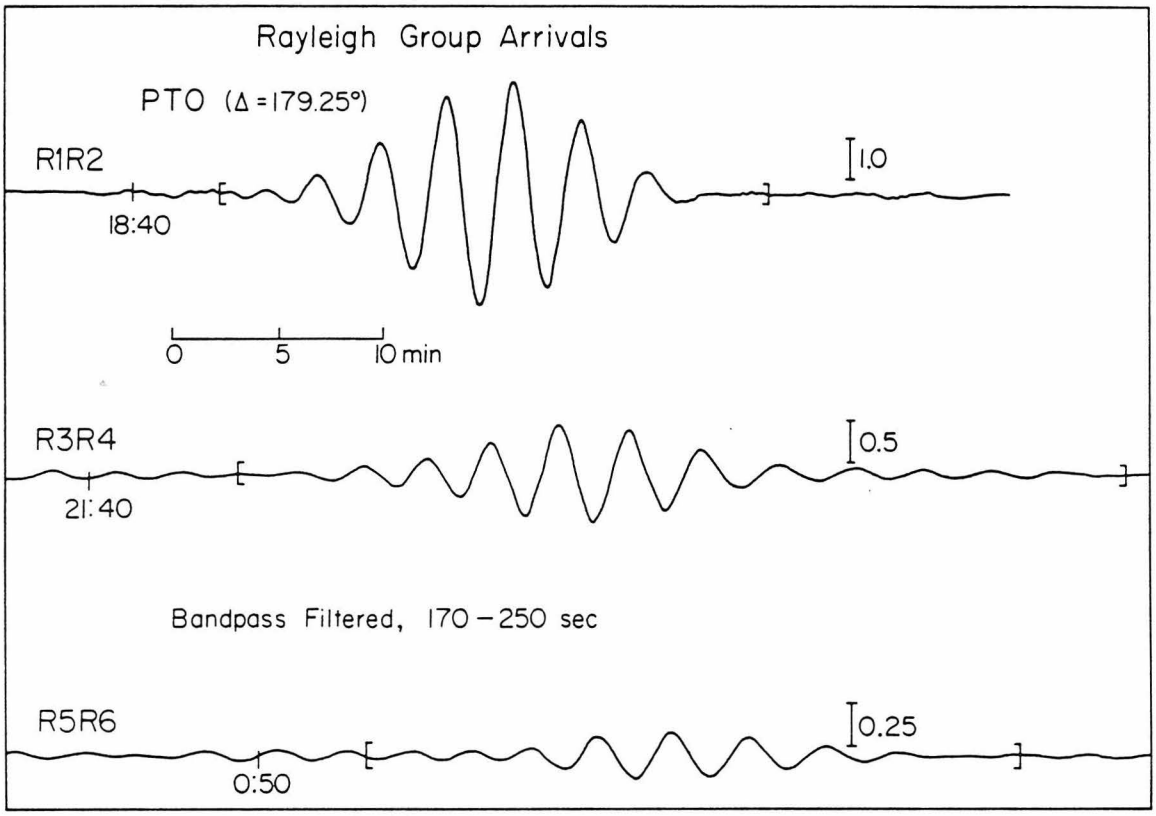

Figure 1.4 Bandpass filtered (170-250 s) vertical component records of the first three Rayleigh arrivals at PTO. Note changes in amplitude scales. Arrivals were windowed between the brackets and then Fourier transformed in order to measure spectral amplitude ratios. This process was repeated for several filter bands in the 120-300 s period range.

Rayleigh wave group velocities measured from the PTO record are listed in Table 1.1. Figure 1.5 compares the antipodal group velocity values with the global averages given by Mills and Hales [1977]. These authors used a least squares parabola-fitting technique to determine group velocities for many great circle paths. Their results were very well constrained and showed little deviation between paths. A recent study by Nakanishi and Anderson [1982] gives global averages which agree closely with Mills and Hales' values. The excellent agreement (generally within 0.01 km/s or 0.3%) of the antipodal measurements with results of both these studies demonstrates that PTO was located near enough to the geometric antipode and that the focusing there was sufficiently sharp to enable measuring of global average properties using this single record.

Attenuation Measurements

To measure the attenuation, the prominent Rayleigh wave groups were extracted from the broad-windowed, bandpass-filtered traces. This was essentially equivalent to restricting the time windows to a group velocity range appropriate for the pass band of each filter. In this way it was possible to remove from the signals energy outside of the wave groups but perhaps within the originally wide arrival windows. Each wave group was padded with zeroes to a length of 4096 samples and transformed to the frequency domain by using a standard

Table 1.1 - Rayleigh Wave Group Velocity

T, s	U^a, km/s	$U_{NA}{}^b$	$U_{PREM}{}^c$
120	3.75	3.750	3.716
130	3.72	3.728	3.698
140	3.69	3.704	3.681
150	3.67	3.675	3.665
160	3.64	3.664	3.649
170	3.62	3.645	3.633
180	3.61	3.626	3.617
190	3.60	3.611	3.603
200	3.59	3.596	3.589
210	3.58	3.585	3.579
220	3.58	3.577	3.571
230	3.58	3.573	3.568
240	3.58	3.577	3.570
250	3.59	3.583	3.578
260	3.60	3.601	3.593
270	3.61	3.622	3.615
280	3.63	3.654	3.645

[a]PTO record, this study.
[b]Nakanishi and Anderson [1982].
[c]Dziewonski and Anderson [1981].

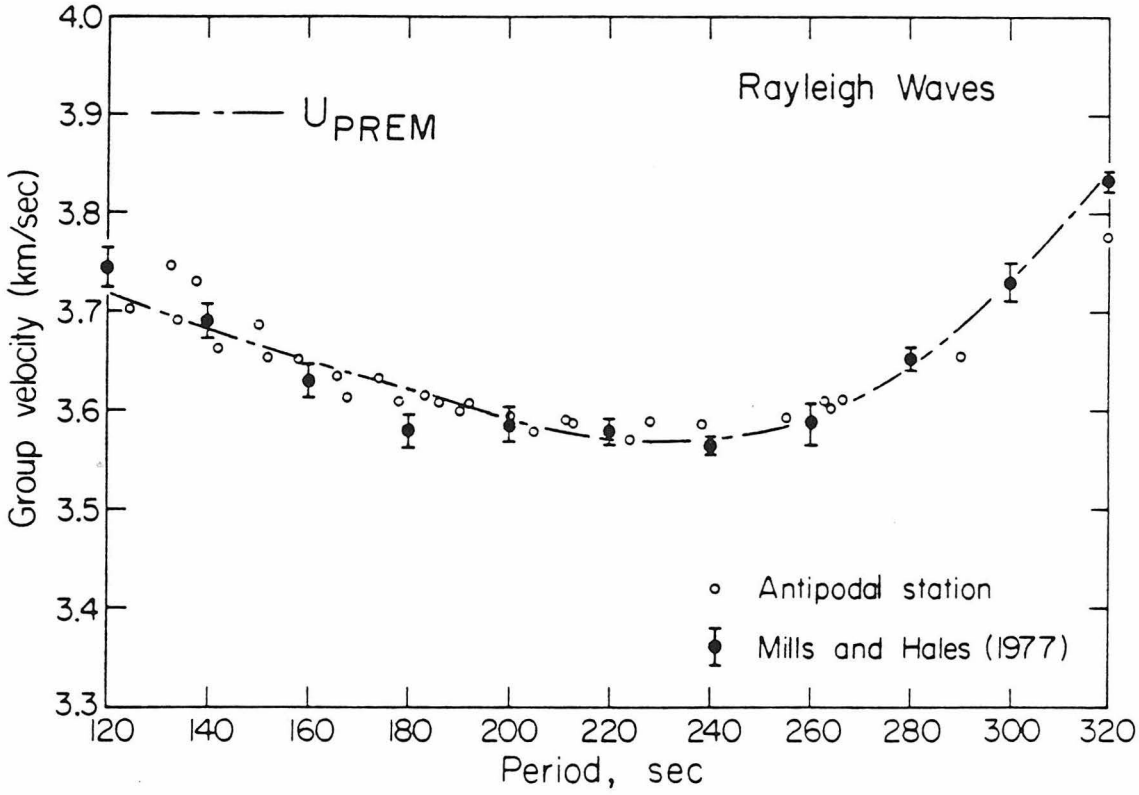

Figure 1.5 Rayleigh wave group velocity measurements from the PTO record. Also shown are Mills and Hales' [1977] average values for many great circle paths, and the dispersion curve for model PREM of Dziewonski and Anderson [1981].

FFT routine. No smoothing of the resulting amplitude spectra was considered necessary. The attenuation coefficient $\gamma(T)$ was calculated from [Satô, 1958; Ben-Menahem, 1965]

$$\gamma(T) = \frac{\ln[A_i(T)/A_j(T)]}{\Delta_j - \Delta_i} \qquad 1.3$$

where $A_i(T)$ is the spectral amplitude at period T of the ith arrival and Δ_i is the propagation distance of the ith arrival. This single station spectral ratio technique [Aki and Richards, 1980] removes effects common to all the Rayleigh arrivals, such as the source spectrum and instrument response. The ratio A_i/A_j is a measure only of the attenuation, or spectral energy decay, between arrivals. The attenuation coefficient γ is related to the quality factor Q through the relation [Brune, 1962]

$$Q(T) = \frac{\pi}{T\gamma(T)U(T)} \qquad 1.4$$

Values of γ were determined at several frequency points across the band of each of the filters; the considerable overlap in the frequency response of successive filters resulted in redundant measurements at each frequency, the spread of which indicates the effects of noise and the windowing methods. By measuring the decay between both the first and second (R1R2/R3R4) and first and third (R1R2/R5R6) arrivals, two essentially independent determinations of

$\gamma(T)$ were made. In Figure 1.6, the $\gamma(T)$ values from the PTO record are plotted using different symbols for the R1R2/R3R4 and R1R2/R5R6 measurements. Also shown are the global average results of Mills and Hales [1977]. The error bars ($\pm 1\sigma$) on their results typify the scatter seen in great circle studies not only between different great circles but also for repeated measurements along a single path. At periods less than 200 s the antipodal results fall outside the $\pm 1\sigma$ error bars of Mills and Hales [1977] but within the total scatter of their data. This scatter may result from lateral refractions of the propagating Rayleigh wave, contamination of the signal by overtone energy, or poor signal-to-noise ratios. In contrast, the PTO values display a very smooth, stable trend, indicating that amplification at the antipode has significantly improved the signal level. The PTO results also exhibit excellent consistency between the R1R2/R3R4 and R1R2/R5R6 measurements. This consistency immediately confirms that the windowed Rayleigh arrivals are sufficiently isolated from significant overtone energy. In the following chapter this consistency will be used as a constraint on the possible bias induced by a laterally heterogeneous velocity structure.

Another antipodal recording with clean Rayleigh arrivals in the same period range was produced by an intermediate depth South American earthquake on February 21, 1971, centered near the junction of Chile, Argentina, and Bolivia (M_S=6.8, latitude=23.81^{o}S, longitude=67.20^{o}W, h=166 km, time=1035:20 (ISC)). The WWSSN station HKC in Hong Kong

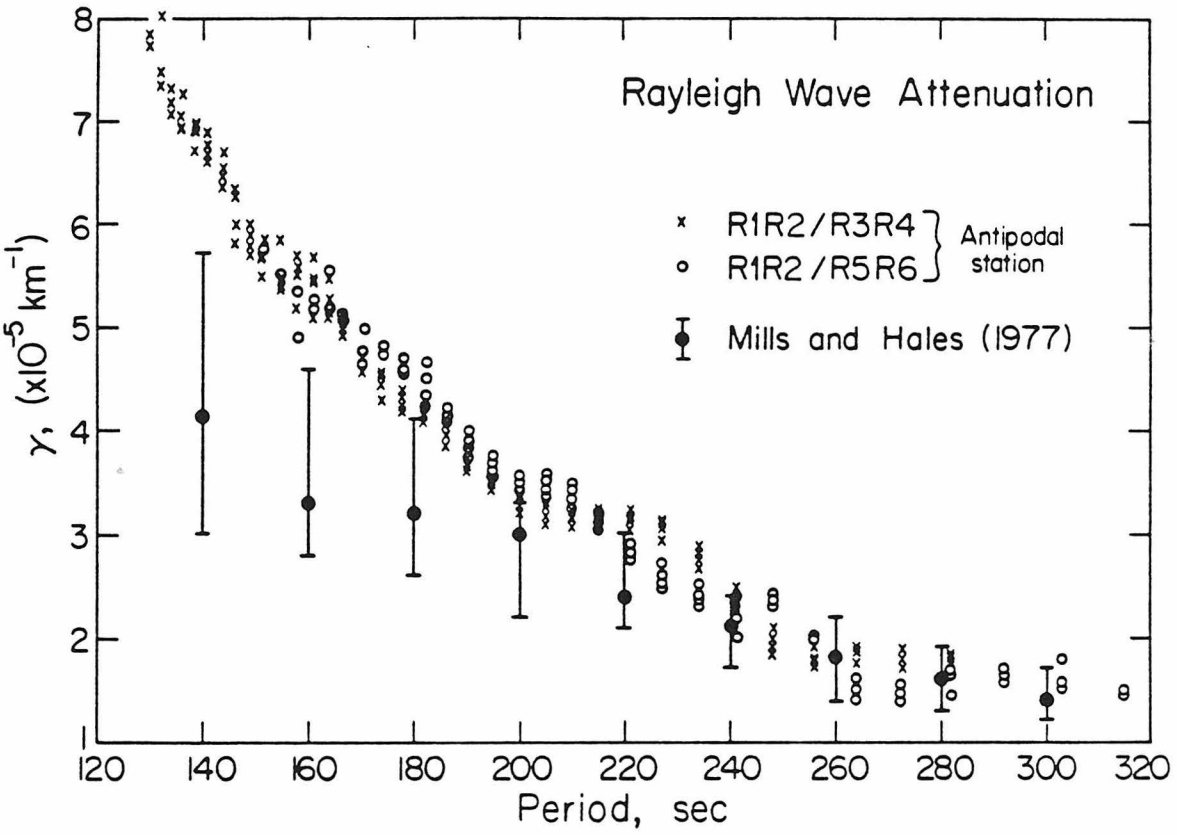

Figure 1.6 Values of the Rayleigh wave attenuation coefficient γ as a function of period, obtained from the PTO record. Note both the small amount of scatter and the consistency of the R1R2/R3R4 and R1R2/R5R6 trends. The average-Earth values of Mills and Hales [1977] are plotted for comparison.

(latitude=22.30°N, longitude=114.17°E) falls at an epicentral distance of 178.05°, putting it within half a wavelength of the antipode for 120 s and longer Rayleigh waves. The long period vertical record was processed in the manner described above. The Rayleigh waves were weaker on this record than on the PTO record due to the depth and size of the event, so only the first two arrivals (R1R2 and R3R4) proved useful.

The attenuation coefficients determined from these arrivals are shown in Figure 1.7. The values are in good agreement with those obtained from the PTO record, especially at periods shorter than 220 s. The source-station orientation on the globe for this second event was totally different from that for the first, resulting in a much different sampling of the Earth by this event's radiation pattern. Yet the attenuation values measured in both cases were virtually identical. The agreement is in fact better than that commonly seen in conventional studies between two different stations along the same great circle (see Fig. 0.1a). This agreement of the antipodal records strongly implies that in each case the sampling of the Earth was sufficient to reveal global average properties. Also, any biasing due to lateral heterogeneities must be similar for the two events.

Horizontal Components

The first Love and Rayleigh arrivals (G1G2 and R1R2,

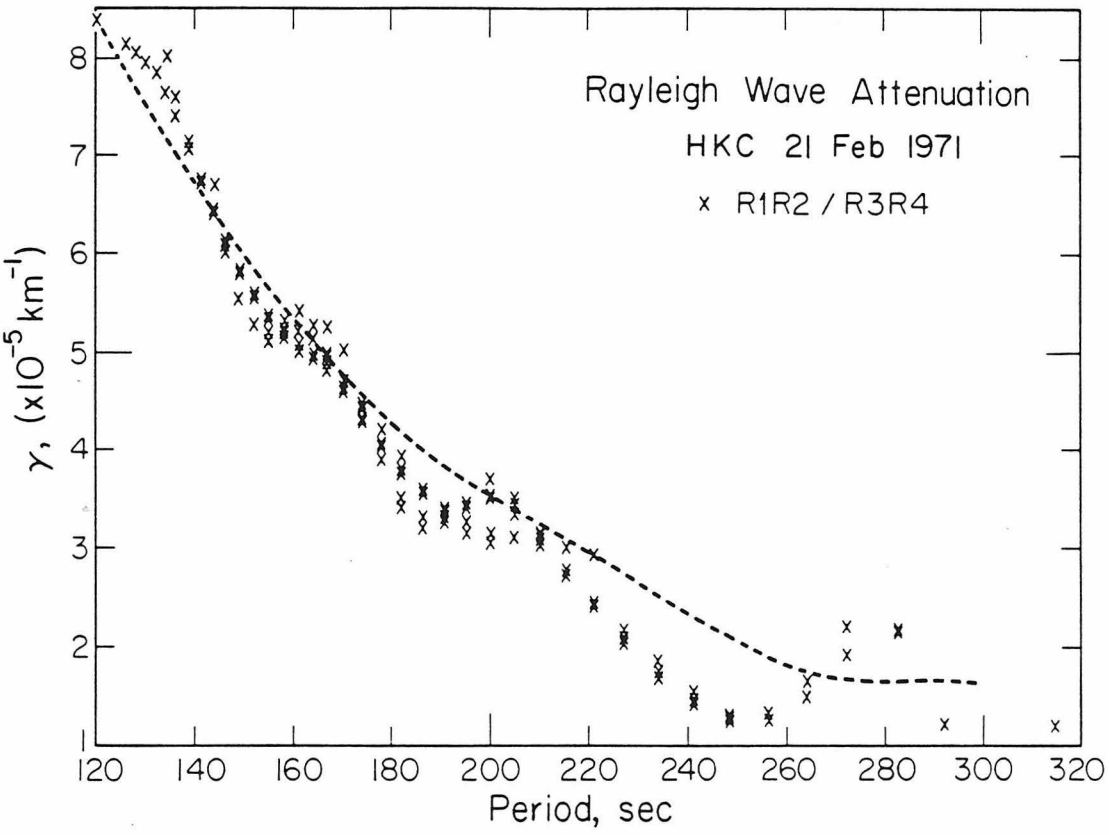

Figure 1.7 Values of the attenuation coefficient γ obtained from the HKC record of a South American event (Δ=178.05°). The dashed line gives the smoothed average trend of the measurements from the PTO record (Fig. 1.6).

respectively) produced very clean signals on the horizontal long period instruments at PTO. Figure 1.8a shows the seismograms for all three components of the first arrivals. A 100-300 s bandpass filter was applied to the traces. The traces were normalized to the same peak-to-peak amplitude in Figure 1.8a; the true amplitude (cm) is given at the right end of each trace. The Love wave (G1G2) is very prominent on the east-west (E) component and just barely above the noise on the north-south (N). It is totally absent on the vertical (Z), as it should be. The N and E components of the Rayleigh wave (R1R2) are similar in amplitude and are about one-half the amplitude of the vertical.

The three traces in Figure 1.8a were combined in pairs to produce the three seismoscope-style plots of Figure 1.9a. Each of these plots shows a two-dimensional projection of the filtered ground motion during the Love and Rayleigh arrivals. The two axes of each plot are scaled the same, but the scaling differs between plots. Both arrivals are very strongly polarized. The Love wave is seen clearly on the horizontal projection, polarized along the direction N85^{o}E. On each vertical projection the Love wave is properly confined to the horizontal axis. The horizontal Rayleigh wave motion is polarized along N35^{o}E; the two vertical projections show the amplification of the Z component relative to the horizontals. The polarization plots show two rather surprising things. First, the horizontal motions are substantial. The exact antipode of a shallow earthquake source should

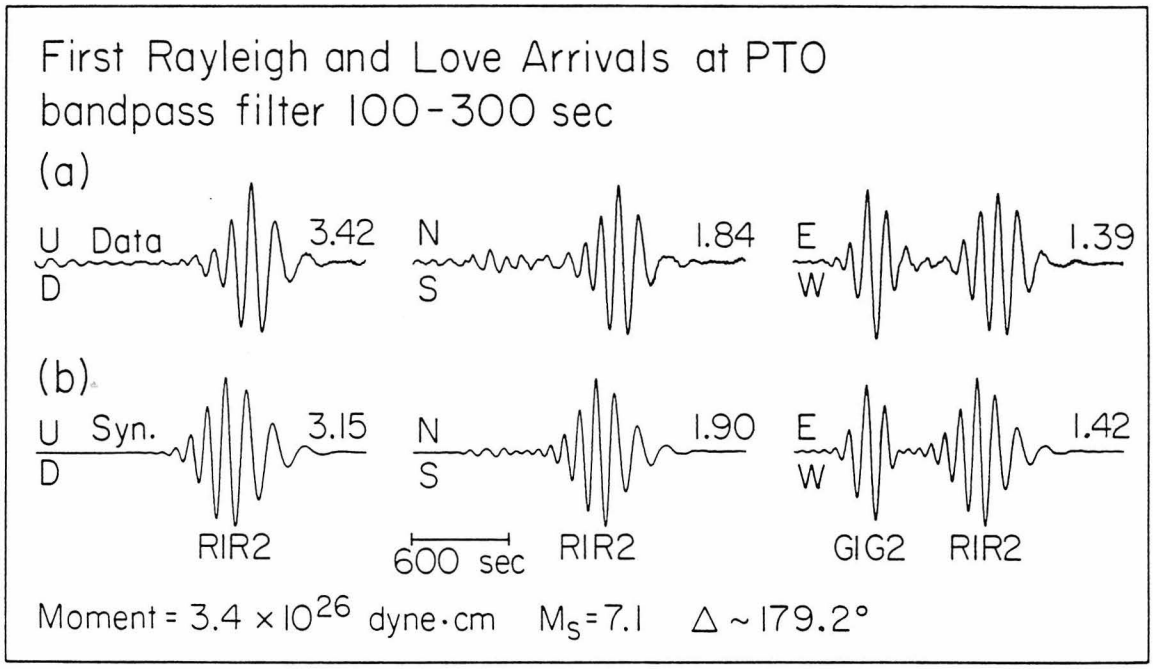

Figure 1.8 (a) Observed three-component Rayleigh (R1R2) and Love (G1G2) first arrivals at PTO. (b) Best-fit spherical-Earth synthetics of the traces in (a). All traces were convolved with a 100-300 s bandpass filter. Peak-to-peak amplitude (cm) is given at the right end of each trace. Amplitudes of synthetic traces are based on a moment of 3.4×10^{26} dyne-cm.

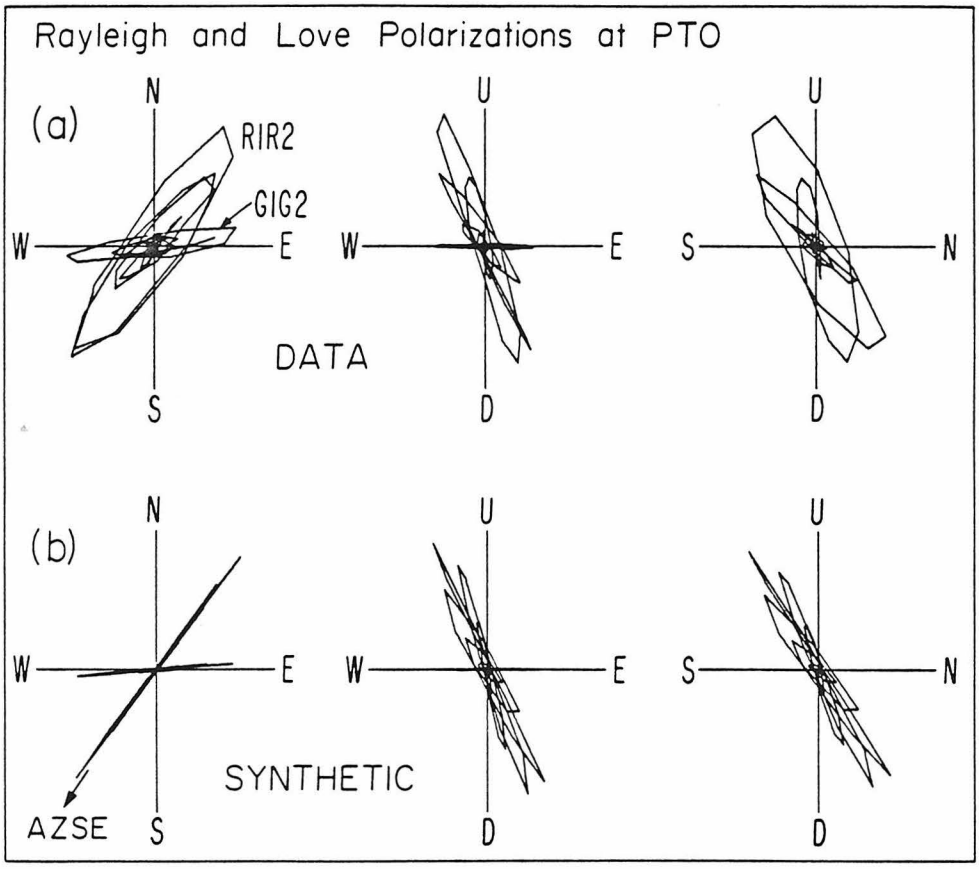

Figure 1.9 (a) Two-dimensional projections of the observed ground motion at PTO made by combining the traces of Figure 1.8(a). The two axes of each plot are scaled the same, but the scaling differs between plots. (b) Corresponding projections for the synthetic traces of Figure 1.8(b). The arrow labeled AZSE gives the back-azimuth to the epicenter used in generating the synthetics.

be a node for Love waves and the horizontal component of Rayleigh waves. Actually, the station PTO lies 0.75° from the true antipode of the Inangahua earthquake, which is far enough to permit observable horizontal motions. Second, the Love and horizontal Rayleigh signals are not polarized perpendicularly to each other. This unusual phenomenon is expected in the antipodal region, where the transverse spheroidal and longitudinal toroidal components can become significant if the source has a non-isotropic radiation pattern.

Synthetic seismograms were generated in order to determine if the details of the observed Rayleigh and Love polarizations could be matched. The synthetics were produced by summing the fundamental spheroidal and toroidal modes of the spherical Earth model 1066A [Gilbert and Dziewonski, 1975], using the Q values of model SL2 [Anderson and Hart, 1978]. A point source at 11 km depth with a step time function was assumed. The focal mechanism of the Inangahua earthquake used by Rial [1978b] and the ISC epicenter of the event were used as starting parameters. The location and fault plane strike were then varied to obtain the best agreement with the observed polarizations (Fig. 1.9a).

The angle between the Rayleigh and Love arrivals on the horizontal projection was very sensitive to the strike of the fault plane. The observed angle of 50° was best matched using a strike of 36°; this is only 17° from the strike used by Rial [1978b]. The amended mechanism still satisfies the P-wave first motions plotted by

Robinson et al. [1975]. After adjusting the mechanism to fit the relative orientations of the Rayleigh and Love polarization directions, the absolute directions were satisfied by moving the epicenter. The epicenter preferred for the synthetics is at latitude 41.94°S, longitude 171.79°E. This is about 30 km southwest of the ISC location, near the opposite end of the aftershock zone observed by Robinson et al. [1975].

The three components of the best-fit synthetic seismograms are shown in Figure 1.8b. The synthetic waveforms compare very well with those observed. The most notable discrepancy is in the arrival time of the R1R2 group. Model 1066A gives Rayleigh group velocities at periods below 200 s which are known to be higher than appropriate global averages [H. Kanamori, personal communication]. The number near the right end of each synthetic trace gives the peak-to-peak amplitude (cm) predicted for a seismic moment of 3.4×10^{26} dyne-cm. The values are in good agreement with those observed for all three components. According to Kanamori and Anderson [1975], this moment value is consistent with the event's surface wave magnitude (M_S=7.1). Figure 1.9b shows the polarization plots obtained from the synthetic traces. The vertical projections show that the synthetic Rayleigh wave has the proper ratio between the horizontal and vertical amplitudes. This ratio is sensitive to the distance of the station from the exact antipode and, to a lesser extent, to the source depth. On the horizontal projection, the synthetic arrivals are polarized

along the same directions as the data. The relative amplitudes of the Rayleigh and Love waves also match the data well. The observed horizontal polarizations are not as linear as the synthetics predict. This could be the result of source finiteness, random noise and imperfect focusing due to lateral velocity variations. The overall agreement of the synthetic and observed polarizations dramatically demonstrates the high quality of the Earth lens.

Love Wave Group Velocity

Relatively few investigators have presented estimates of average Earth Love wave group velocities. Kanamori [1970b] averaged the Love group velocities observed for 12 great circle paths and Dziewonski et al. [1972] measured the average dispersion by first summing 13 autocorrelograms of horizontal seismograms. Nakanishi and Anderson [1983b] performed a spherical harmonic inversion of Love group velocities observed for many great circles. Because there are few such studies and most average only a small number of great circles, antipodal records may offer improved constraints on Love wave group velocities.

The first Love wave arrival at PTO (G1G2) produced a clean signal on the east-west instrument (Fig. 1.8a). Group velocities were measured from this arrival for the period range 50 to 250 s using a bandpass filtering technique similar to that used for the Rayleigh

waves. In this case the group arrival time was corrected for both source and instrument group delays. The instrument delay as a function of period was determined following Kanamori and Abe [1968]. Furumoto and Nakanishi [1983] determined the empirical relation $M_o=2.5\times10^{22}\tau^3$ between the seismic moment M_o (dyne-cm) and the source time τ (s). Using $M_o=3.4\times10^{26}$ dyne-cm for the Inangahua earthquake yields τ=24 s. The source group delay is one-half the source time. The group velocity measurements from the PTO record are compiled in Table 1.2. Figure 1.10 compares the PTO results to the Love group velocity curve for Earth model PREM [Dziewonski and Anderson, 1981]. The average Earth values of Nakanishi and Anderson [1983b] are in close agreement with the PREM curve.

The antipodal Love wave yields group velocities somewhat higher than PREM at most periods (Fig. 1.10). The difference is generally less than 1%, which may not be significant considering the possible errors in the antipodal measurements. The G1G2 arrival traveled a relatively short distance, so errors in source and instrument delay times and in the assumed path length (20,015 km) could introduce some bias. The arrival's energy is concentrated at periods below 170 s so the results at longer periods are suspect. At the shorter periods, below about 100 s, lateral heterogeneities and the offset of PTO from the true antipode should affect the results. In light of the possible errors, the Love wave group velocities from the G1G2 arrival at PTO are consistent with existing Earth models. This is perhaps best

Table 1.2 - Love Wave Group Velocity

T, s	U^a, km/s	$U_{NA}{}^b$	$U_{PREM}{}^c$
50	4.33		
75	4.42		
100	4.42	4.387	4.385
125	4.38	4.385	4.385
150	4.40	4.385	4.385
175	4.42	4.385	4.383
200	4.43	4.387	4.382
225	4.40	4.388	4.382
250	4.37	4.391	4.386

[a]PTO record, this study.
[b]Nakanishi and Anderson [1983b].
[c]Dziewonski and Anderson [1981].

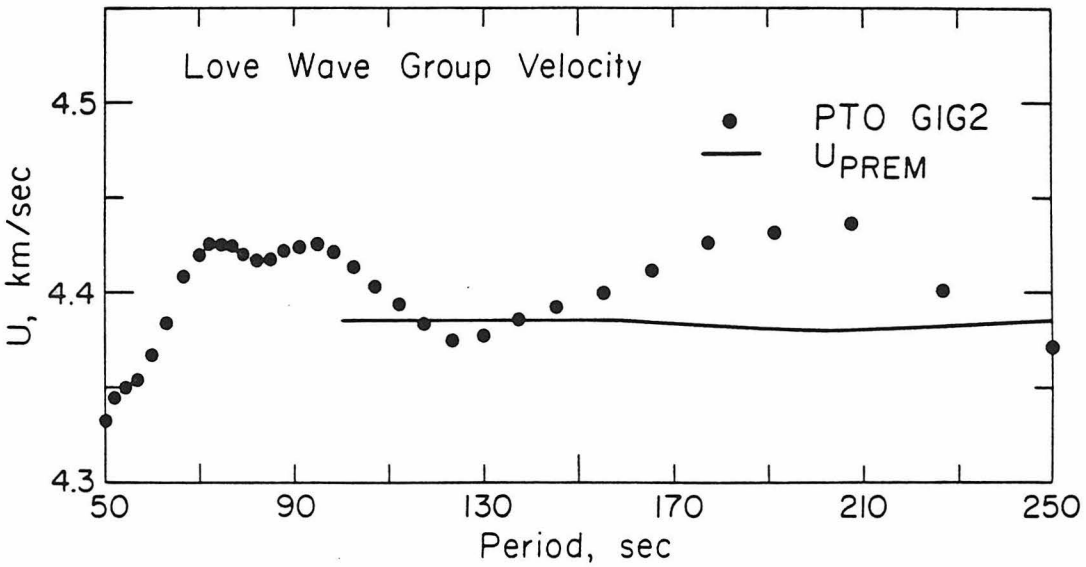

Figure 1.10 Love wave group velocity measurements obtained from the G1G2 arrival at PTO. Also shown is the group velocity curve of the model PREM [Dziewonski and Anderson, 1981].

reflected not by the group velocity values themselves (Fig. 1.10) but by the timing and overall fit of the synthetic Love waveform to the data (Fig. 1.8).

Unfortunately, the second Love wave arrival at PTO (G3G4) was too weak to be identified above the noise on the record. As a result, attenuation estimates for Love waves could not be determined.

Spheroidal Overtones

Because the depth dependence of the spheroidal overtones (${}_nS_\ell$, with $n \geq 1$) differs from that of the fundamental modes, measurements of the dispersion and attenuation of overtones should improve the resolution of the Earth's radial structure. Shallow earthquakes excite the fundamental modes more efficiently than the overtones, making analysis of the overtones difficult. The overtones are typically studied by measuring their eigenperiods and Q in the frequency domain. This requires seismograms of long duration, which are produced only by large earthquakes. Eigenperiods of various overtone modes have been presented by Derr [1969], Dziewonski and Gilbert [1972, 1973] and Mendiguren [1973]; measurements of Q were made by Sailor and Dziewonski [1978] and Masters and Gilbert [1982]. Most of the overtone modes observed in these studies have periods greater than 300 s. At periods below this the overtone modes are usually overpowered on the spectra by the fundamental modes.

Overtones with periods less than 300 s can however be observed on many seismograms as isolated wave groups which are separated in time from the fundamental surface wave arrivals. The overtone groups are not readily analyzed by standard traveling wave techniques for two reasons. First, they are very dispersive, so the groups are not identifiable after the first few arrivals. More troublesome is the fact that several overtone branches have group velocity curves which intersect (Fig. 1.11) An individual overtone branch (fixed n) cannot be isolated in the time domain: an observed arrival represents the complex interference of many branches. As a result, the group velocity and attenuation as functions of period cannot be independently determined for each branch by a traveling wave analysis. In this section, forward modeling of antipodal time domain overtone arrivals is used to corroborate models of the velocity and attenuation profiles in the upper mantle.

Okal [1978] divided the spheroidal modes among 5 families. The 0102 and 0304 arrivals represent the 'R' (Rayleigh) family of modes, in which the horizontal and vertical motions are coupled. Within each family, the modes ${}_nS_\ell$ are rearranged in 'pseudo-overtone' branches, e.g., ${}_pR_\ell$. In the new classification the angular order ℓ is unchanged; a new radial order p is assigned in place of the old value n. Physical properties such as phase velocity, attenuation and excitation vary smoothly along each branch of constant p. The 0102 and 0304 arrivals were synthesized by summing all modes of model 1066A

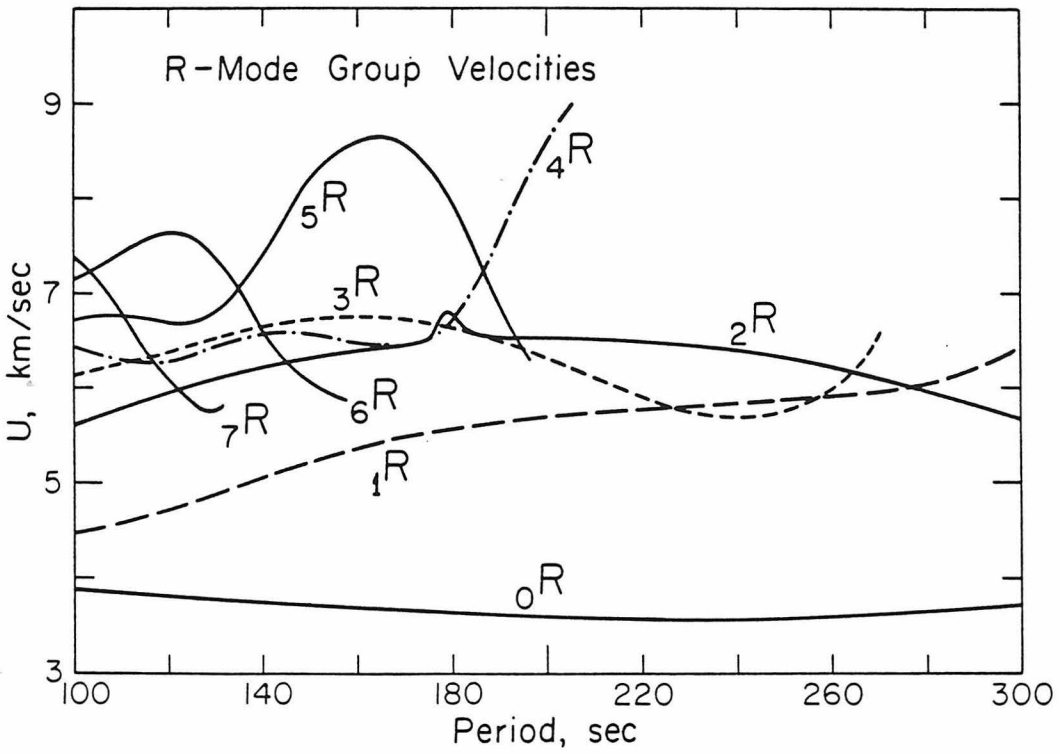

Figure 1.11 Group velocity curves of model 1066A [Gilbert and Dziewonski, 1975], for the spheroidal `R' mode branches defined by Okal [1978]. The branch $_0R$ corresponds to the fundamental Rayleigh wave.

in the branches ${}_1R_\ell$ to ${}_7R_\ell$ with periods down to 45 s. Tests demonstrated that the higher R branches and the other mode families contributed no significant energy in the time windows of the 0102 and 0304 arrivals. The same source location and mechanism used in modeling the Rayleigh and Love arrivals were employed here. The synthetics were generated by a program based on the method outlined by Kanamori [1970a]. Each synthetic was convolved with an instrument operator and a 100 to 300 s bandpass filter.

The Inangahua earthquake of 1968 produced clean overtone arrivals at the antipodal WWSSN station PTO. The first two such arrivals (0102 and 0304) on the long period records were extracted with group velocity windows covering 5 to 9 km/s. These arrivals were well separated from the fundamental Rayleigh and Love arrivals. The vertical 0102 and 0304 traces, bandpass filtered for 100 to 300 s energy, are shown in Figure 1.12. The peak-to-peak amplitude (cm) is given near the right end of each trace.

Synthetics of the two arrivals were produced using three different Q models: MM8 [Anderson et al., 1965], SL2 [Anderson and Hart, 1978] and PREM [Dziewonski and Anderson, 1981]. The waveforms for all three Q models were virtually identical. The only noticeable difference between the synthetics for the three Q models was in the ratio r of the maximum amplitudes of the 0102 and 0304 arrivals. Model MM8 gave r=3.0, SL2 gave r=3.5 and PREM gave r=3.7. The observed ratio was r=3.7. This indicates that, of these three models,

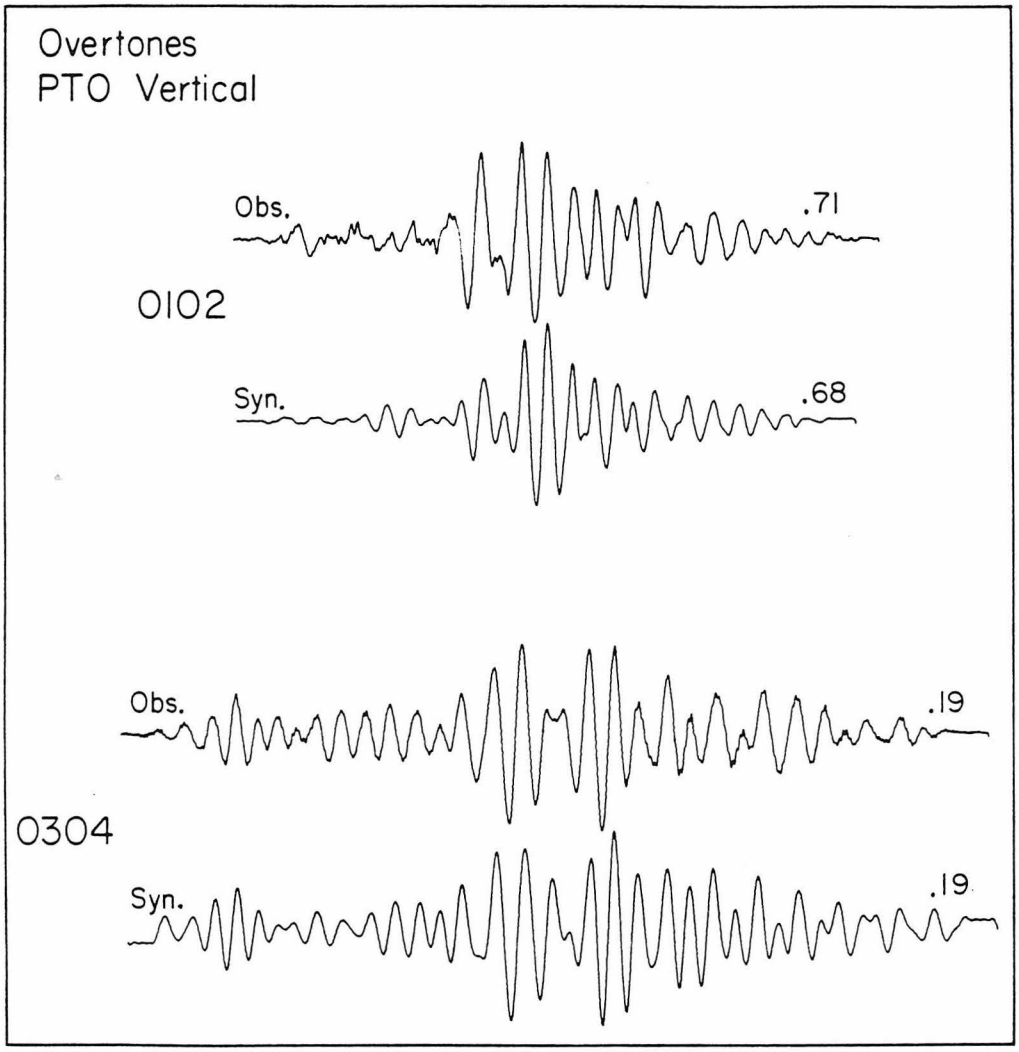

Figure 1.12 Vertical components of the observed and synthetic spheroidal overtone arrivals 0102 and 0304. Each trace was convolved with a 100-300 s bandpass filter. Peak-to-peak amplitude (cm) is given at the right end of each trace. Amplitudes of synthetic traces are based on a moment of 3.4×10^{26} dyne-cm.

PREM best matches the observed attenuation.

Figure 1.12 shows the synthetic vertical traces for the PREM Q model, beneath the observed traces. The agreement of the observed and synthetic 0304 traces is very impressive. Amplitude and phase match very well across most of the window. The visual fit of the 0102 traces is less satisfying, primarily due to an underestimate by the synthetic of the first large pulse on the data. The dominant contributions to this pulse come from the p=3,4,5 branches. The phase of this pulse, and the phase and amplitude of the remainder of the 0102 waveform are accurately reproduced by the synthetic. The peak-to-peak amplitudes of the synthetics for a seismic moment of 3.4×10^{26} dyne-cm are listed near the traces; the values are very close to those of the observed traces. This is the moment value determined from the first Rayleigh and Love arrivals, so the overtones have the predicted amplitudes relative to the fundamentals.

The horizontal components of the 0102 and 0304 arrivals were also synthesized. Figure 1.13 compares the observed and synthetic north-south signals, and Figure 1.14 compares the east-west. The synthetic fits for the horizontals are not quite as good as for the vertical seismogram. The timing and overall envelope amplitudes for the horizontal synthetics match the data reasonably well. The data may include significant contributions from toroidal overtone modes, which have not been included in the synthetics. Portions of some toroidal branches of 1066A have the proper group velocities. Adding

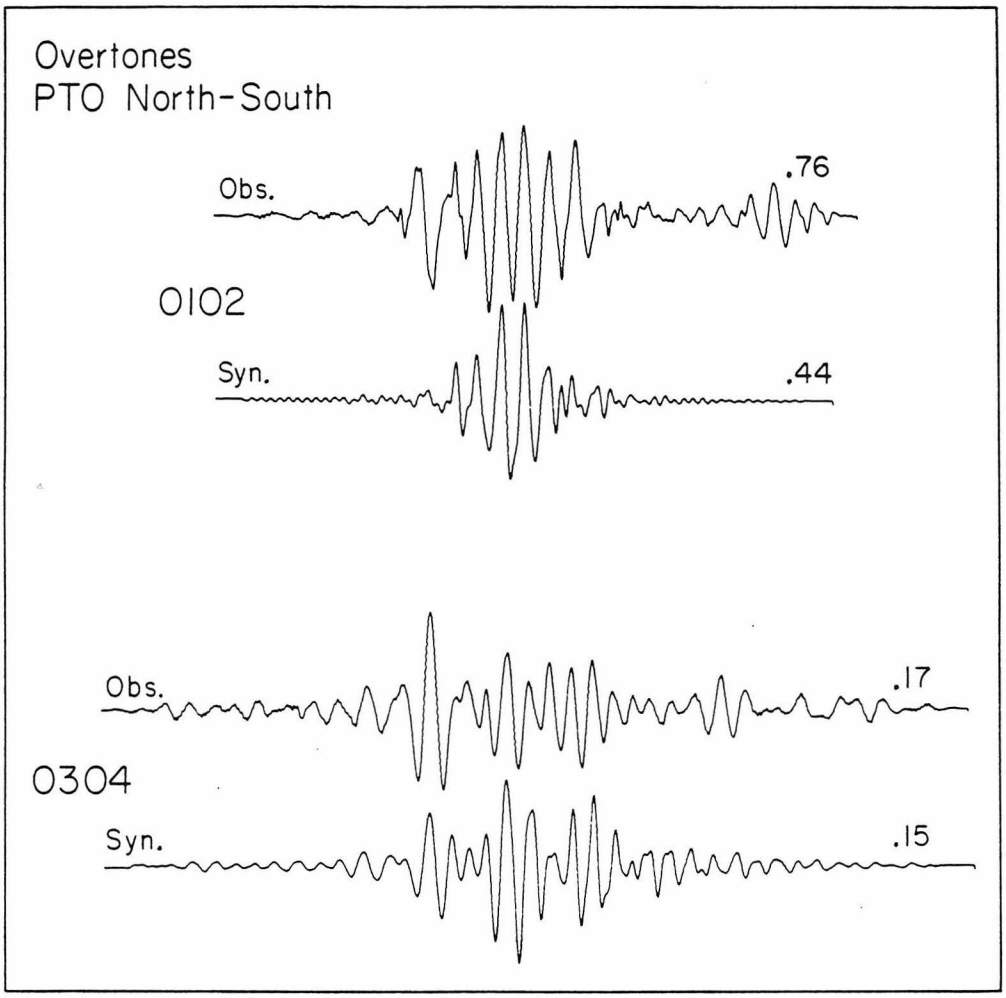

Figure 1.13 Same as Figure 1.12, for the north-south components.

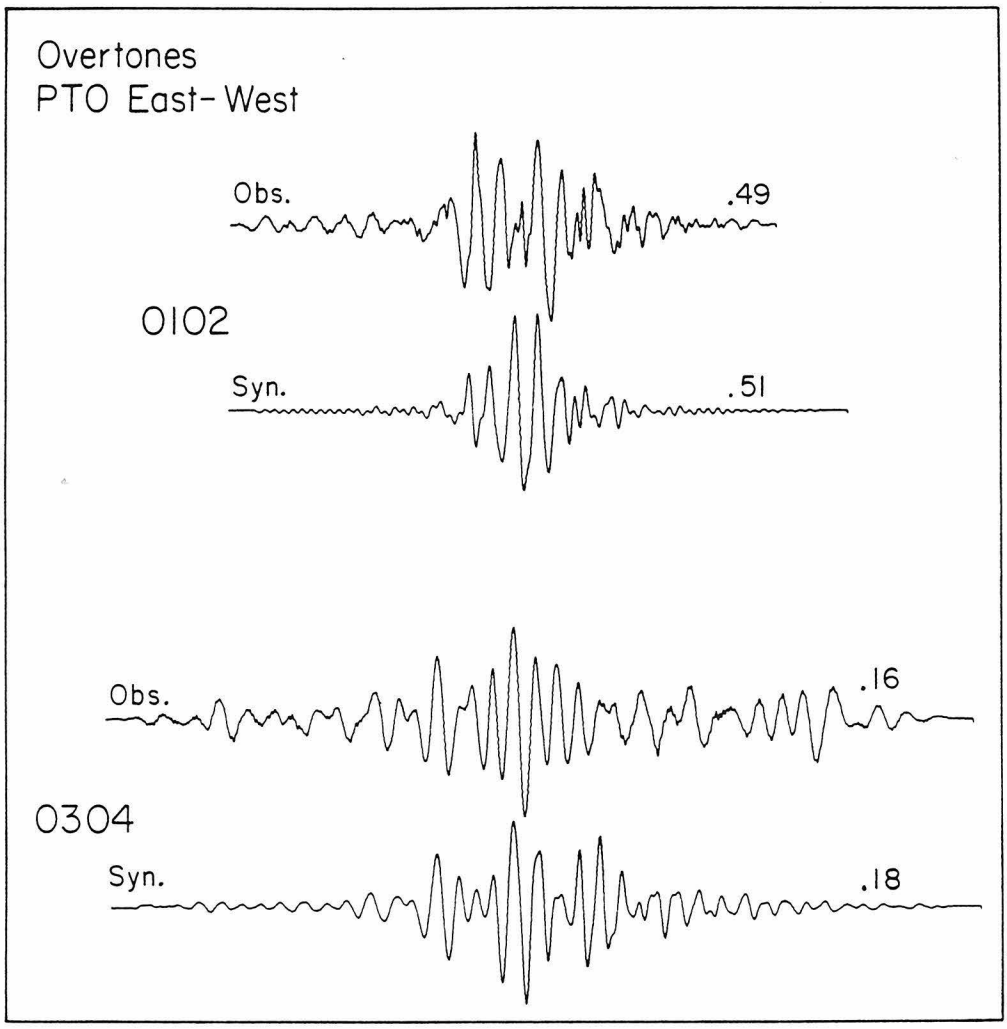

Figure 1.14 Same as Figure 1.12, for the east-west components.

the toroidal modes might therefore improve the fits of the horizontal synthetics.

Modeling the overtone arrivals at the antipode suggests that the PREM attenuation profile yields appropriate average Earth Q for the ${}_1R_\ell$ to ${}_7R_\ell$ spheroidal-mode branches defined by Okal [1978]. This is the first attempt to constrain the attenuation of these modes. Because the observed arrivals are formed by the interference of as many as 7 mode branches, it is not possible to independently measure the Q of any single branch. This study shows the PREM model to be consistent with the antipodal overtone records at periods between 100 and 300 s. It is conceivable that attenuation profiles for the upper mantle somewhat different from PREM could also satisfy the data.

It may be possible to use overtone arrivals in a waveform inversion scheme to further refine estimates of the attenuation profile. Dziewonski and Steim [1982] have presented a waveform inversion technique (WIT) in which an Earth model is perturbed to improve the fit of synthetic seismograms to observed data. This method could lead to velocity and attenuation profiles which give optimal agreement to several mode branches simultaneously. Overtone recordings from conventional as well as antipodal distances remain to be exploited.

Chapter 2

EFFECTS OF ASPHERICAL STRUCTURE: ELLIPSOIDAL EARTH MODEL

Various investigators [e.g., Dahlen, 1979a, b; Sleep et al., 1981] have suggested that the Earth's lateral heterogeneities may systematically bias measurements of attenuation. A general aspherical perturbation in the structure of the Earth removes the $2\ell+1$-fold degeneracy in eigenfrequency of the singlets ${}_nS_\ell^m$ comprising the normal mode peak ${}_nS_\ell$. If this splitting of the singlets is of the same order as the attenuative broadening, it will be unresolvable; it will act to broaden further the overall peak shape. If naively assumed to be unsplit, the peak would yield an erroneously low Q estimate. Dahlen [1979a, b] argues that the bias should be insignificant for conventional single-station analyses, while attenuation measurements based on stacked or antipodal records may be strongly biased toward lower Q.

Stacked records are produced by summing the signals from all available stations, and antipodal records similarly add up the arrivals from a continuum of paths. If different great circle paths have different average velocities, the constructively interfering signals in both cases then differ somewhat in phase. As a result, the antipodal and stacked arrivals are reduced in amplitude. The discrepancy in phase increases with each successive orbit, so the

amplitude of each composite arrival successively decreases. Antipodal and stacked signals decay faster than signals along individual great circles and give low apparent Q estimates. Stacking seismograms has been used several times to increase signal-to-noise in studies of mantle Q [Jordan and Sipkin, 1977; Sailor and Dziewonski, 1978]. The records which go into the stack are either selected on the basis of high signal-to-noise or else represent an indiscriminate sampling of available records. It is therefore difficult to estimate the net bias of the resulting Q measurements or even to determine its sign since the unavailable or discarded data are not included in the analysis.

The antipodal attenuation measurements presented in the preceding chapter may be significantly biased and do in fact yield lower Q at periods below 240 s than most great circle studies. Averages from these conventional great circle determinations may be biased as well, not by lateral heterogeneity effects but by sampling problems. For example, a representative number of low Q paths may not be included in the averages because of the low amplitudes of the later arrivals. In contrast to this the antipodal experiment involves a uniform sampling, weighted by the radiation pattern. The low Q paths are automatically included in the 'stack'. A unique aspect of the antipodal method is that the sign of the bias is known. The initial antipodal results therefore set an upper bound on global attenuation (or a lower bound on Q). Antipodal estimates are a useful complement to conventional surface wave and free oscillation measurements of Q

even if the bias cannot be estimated precisely. The intrinsic advantages of the natural Earth 'stack' warrant an effort to estimate the bias. This is not possible in conventional experiments because of the missing data.

To quantify the bias in the antipodal Q measurements rigorously, one requires both an accurate representation of the Earth's three-dimensionally heterogeneous structure and a theory which correctly models surface wave propagation on this body. The latter problem has been approached using perturbation theory [Dahlen, 1980; Woodhouse and Dahlen, 1978; Woodhouse and Girnius, 1982] and variational methods [Usami, 1971; Geller and Stein, 1978]. Different techniques impose somewhat different restrictions, concerning among other things the magnitudes of lateral velocity contrasts and length scales of the heterogeneities. Whether or not a certain set of restrictions is satisfied for the real Earth is not always clear. Determining the heterogeneous structure of the upper mantle is the topic of much current research and some controversy. The most common practice has been to perform a 'pure path' analysis [Toksöz and Anderson, 1966; Okal, 1977; Nakanishi, 1979; Silver and Jordan, 1981]. Typically, the Earth's surface is divided into continental, oceanic, and tectonic regions. Great circle average phase velocity data are then inverted to yield an optimum dispersion curve for each regional type. Crucial to this method is the assumption that the structure throughout the upper mantle reflects the surface

heterogeneity, and the validity of this assumption is open to question. Regionalized Earth models from different studies show significant differences; the results of such a study are strongly dependent on both the regionalization scheme and the data set used in the inversion [Kawakatsu, 1983]. At present then, the three-dimensional structure of the upper mantle is poorly resolved. In consequence the attenuation biasing caused by lateral heterogeneity cannot be unambiguously determined using forward modeling. The only alternative is to estimate the bias by studying effects which would be common to any distribution of heterogeneities. This is the method employed in this chapter.

Method

To put limits on the possible bias in antipodal attenuation measurements, lateral heterogeneity is represented as an ellipsoidal perturbation in shape. For 120 to 300 s periods, the Earth's actual ellipticity (f~1/298) has a negligible effect on the PTO record (Fig. 2.1). The effects of an exaggerated ellipticity are examined: the regular azimuthal variation in great circle path length on the ellipsoid replaces the real situation of an irregular azimuthal distribution of great circle average phase velocity. Velocity perturbations can be modeled as path length perturbations since both cause travel times to the antipode to be path dependent, so that the

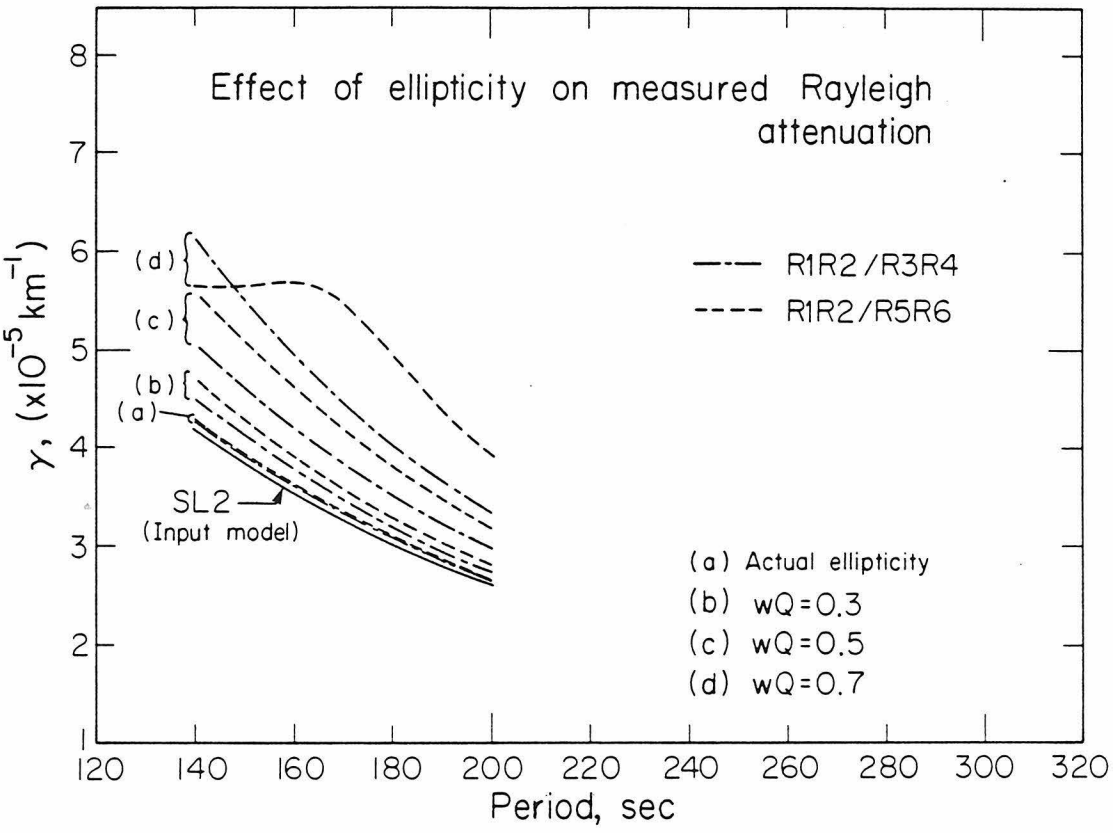

Figure 2.1 Effect of ellipticity on measurements of the attenuation coefficient γ, for observations near the antipode. Synthetic Rayleigh arrivals were generated for an ellipsoidal Earth using attenuation model SL2 of Anderson and Hart [1978]. Values of γ measured from the synthetic arrivals show greater bias from the SL2 curve as the asphericity (wQ) increases. As the bias increases, so does the separation of the 'measured' R1R2/R3R4 and R1R2/R5R6 curves. Note that the Earth's actual ellipticity has a negligible effect (for the proper source-station geometry).

constructive interference there of energy arriving from different azimuths is degraded. Because the splitting caused by the real Earth is unresolvable, one need not know the specific frequencies and amplitudes of the singlets under a particular peak. Rather, one is concerned only with the character of the resultant peak itself and with any side effects that the splitting may have on the time domain signals. Thus, one can order the singlets using an elliptical heterogeneity and attempt to 'statistically' imitate the behavior of mode peaks produced by the Earth's velocity heterogeneities. An observable side effect is then sought which can be used to constrain the amount of splitting (and hence the bias in antipodal attenuation measurements) caused by the real Earth.

There are both theoretical and observational reasons for believing that the effects of the true Earth structure on antipodal seismograms may be modeled reasonably well by a simple ellipsoidal perturbation. Like conventional great circle experiments, the antipodal experiment is sensitive only to the cumulative effects of propagation over a complete orbit around the Earth. Because of this, the odd order spherical harmonic components of the lateral heterogeneity do not affect the singlet locations [Madariaga, 1972] and so induce no bias in attenuation estimates. In addition, the 'complete orbit' nature of the experiment preferentially emphasizes the order-two harmonic of the heterogeneity [Backus, 1964; Kawakatsu, 1983; Nakanishi and Anderson, 1983a]. The real Earth may therefore

behave much like an ellipsoid, which is an order-two perturbation to a sphere. Observations which support this argument have been presented by Masters et al. [1982]. Their plots of mode eigenfrequency (or, equivalently, great circle average phase velocity) as a function of great circle pole position show a dominant order-two pattern. Kawakatsu [1983] and Souriau and Souriau [1983] have shown that regionalized Earth models from several studies would also appear to be order-two dominant to a 'complete orbit' experiment. Understanding the effects of an ellipsoidal heterogeneity is therefore relevant for studying antipodal seismograms.

Theory

Following the treatment given by Dahlen [1979b], let $u(\underline{r},\omega)$ represent the spectrum of the radial component of the fundamental mode Rayleigh wave at $\underline{r}$ on an ellipsoidal, nonrotating Earth due to a source at $\underline{r}_s$. To first order in the eigenfrequencies and zeroth order in the eigenfunctions, this spectrum can be expressed as

$$u(\underline{r},\omega) = \sum_{\ell=0}^{\infty} \sum_{m=0}^{\ell} A_\ell^m(\underline{r}) c_\ell^m(\omega) \qquad 2.1$$

The amplitude term A_ℓ^m is a rather complicated combination of the source moment tensor elements, the displacement scalars U and V, and factors determined by the source and station locations. Spectra of

the two horizontal components are given by formulas identical to Equation 2.1, with somewhat different expressions for the amplitude terms. Complete expressions for the amplitude terms for all three components are given in the Appendix. The term $c_\ell^m(\omega)$ defines the spectral shape of a singlet peak

$$c_\ell^m(\omega) = -\frac{1}{2}\left[\alpha_\ell + i\left(\omega-\omega_\ell^m\right)\right]^{-1} - \frac{1}{2}\left[\alpha_\ell + i\left(\omega+\omega_\ell^m\right)\right]^{-1} \qquad 2.2$$

where α_ℓ is the attenuation coefficient. The eigenfrequencies ω_ℓ^m of an ellipsoidal Earth are given by

$$\omega_\ell^m = \omega_\ell^d\left[1+a_\ell\left(1-\frac{3m^2}{\ell(\ell+1)}\right)\right] \qquad 2.3$$

where ω_ℓ^d is the degenerate eigenfrequency for a spherically symmetric Earth. The splitting of the eigenfrequencies is determined by the single parameter a_ℓ, which is proportional to the ellipticity. Defining w_ℓ as the (dimensionless) total splitting width $w_\ell=(\omega_\ell^0-\omega_\ell^\ell)/\omega_\ell^d$, one finds from Equation 2.3 that $w_\ell \simeq 3a_\ell$ (for $\ell>>1$). The eigenfrequencies given by Equation 2.3 are doubly degenerate, i.e., $\omega_\ell^{-m}=\omega_\ell^m$; this fact is included in Equation 2.1. The ellipsoidal perturbation alters the spherically symmetric spectra only through the frequency shifts of the singlet peaks. The singlet amplitudes A_ℓ^m are unaffected by the ellipticity. Transforming Equation 2.1 into the time domain yields

$$u(\underline{r},t) = -\sum_{\ell=0}^{\infty} \sum_{m=0}^{\ell} A_\ell^m(\underline{r})\exp(-\alpha_\ell t)\cos(\omega_\ell^m t) \qquad 2.4$$

The above treatment assumes the attenuation to be laterally homogeneous. More realistically, each singlet should have a distinct value, α_ℓ^m, as its decay rate. If the excitation of the singlets is sufficiently uniform, as it should be for antipodal stations, then the width of the composite peak, neglecting splitting, would be the average of the singlet widths. In this case it is reasonable in the modeling procedure to replace the distinct values α_ℓ^m by the average value α_ℓ. The corresponding average Q can be obtained from $Q_\ell=\omega_\ell^d/2\alpha_\ell$. This is just another way of saying that the antipode acts as a natural averager of global attenuation, assuming there is sufficiently complete sampling of the globe by the event's radiation pattern. The fact that the results from two different events agree so closely (Figures 1.6 and 1.7) argues in favor of sufficient sampling.

Again, it is not the Earth's actual ellipticity of figure which is of interest; an elliptical Earth model is used as an arbitrary deviation from spherical symmetry to simulate the effects of lateral heterogeneities in the Earth's elastic parameters. Because of this, the event can be located anywhere on the ellipsoid. Furthermore, the strike of the fault plane can be oriented as desired. The receiver is then located at the proper distance from the event along the azimuth appropriately oriented relative to the event strike.

Synthetic time domain Rayleigh waves were generated by a program based on Equations 2.3 and 2.4, using Earth model 1066A of Gilbert and Dziewonski [1975] and Q model SL2 of Anderson and Hart [1978]. The synthetic Rayleigh arrivals were convolved first with an instrument operator, and then with a 143-200 s narrow-band filter as used in the analysis of the real data. As suggested by Dahlen [1979b], the splitting parameter a_ℓ was chosen to vary with ℓ such that the product $w_\ell Q_\ell$ remained constant. The 120 to 300 s period range involves orders ℓ of roughly 80 to 25. Since Q decreases with increasing ℓ in this range, the condition $w_\ell Q_\ell$=const means that w_ℓ increases for shorter periods. This, in turn, means that for shorter periods the ellipticity becomes greater, so that the modeled Earth was, like the real earth, increasingly heterogeneous at shorter wavelengths. Other recipes for w_ℓ could be devised, such as a more general power law model. Since the splitting should not change drastically over a narrow bandwidth and all synthetics were narrow-band filtered, the splitting effects displayed by the synthetics would not be sensitive to the specific recipe employed.

Estimating the Bias

The consistency of the R1R2/R3R4 and R1R2/R5R6 measurements was used to estimate the bias in the antipodal attenuation values. From a time domain perspective, the lateral heterogeneities act to degrade

the constructive interference at the antipode, so that the signal amplification will decrease for each successive Rayleigh arrival. This reduction in amplification is a nonlinear function of the phase mismatch of the energy approaching the antipode from different azimuths. One might thus expect the R1R2/R5R6 attenuation values to be biased somewhat differently than the R1R2/R3R4 values. This argument was examined by generating synthetics of the first three Rayleigh arrivals at PTO, for various values of the splitting factor wQ, and then measuring the apparent attenuation between the three arrivals. The agreement of the R1R2/R3R4 and R1R2/R5R6 attenuation values can be used to estimate the amount of bias in those values caused by lateral heterogeneities and this estimate can be reasonably established by representing the heterogeneities as a simple ellipsoidal perturbation.

Figure 2.1 was produced with the source on the equator of the ellipsoid. Notice in Figure 2.1 that, as the bias from the input attenuation curve increases, so does the separation of the R1R2/R3R4 and R1R2/R5R6 'measured' curves. For sufficiently large wQ the usual trend of a curve toward greater bias at shorter periods would reverse. This is seen in Figure 2.1 on the R1R2/R5R6 curve for wQ=0.7, below 160 s. This occurred because the range in path lengths with azimuth for the R5R6 arrival exceeded half a wavelength. The separation of the R1R2/R3R4 and R1R2/R5R6 curves is decreased only over a very narrow period band. It was not possible to obtain both large bias and

small separation of the two curves across the full 143 to 200 s band. The behavior of the curves in Figure 2.1 was found to be independent of the source-station orientation on the ellipsoid. For wQ=0.7, the synthetic R1R2/R3R4 and R1R2/R5R6 curves are separated much more than the observed trends plotted in Figure 2.2. Thus the bias in the observed measurements must be less than the difference shown in Figure 2.1 between the SL2 curve and the curves for wQ=0.7. At a fixed period T, it is the relative separations of the SL2, R1R2/R3R4, and R1R2/R5R6 curves which are important, and these are strictly determined by the value of the splitting width w. The shifts between the curves are independent of the specific input attenuation model. The separation of the two curves which was produced using wQ=0.5 represents a reasonable upper limit to the observed separation. The amount by which the synthetic 'measured' curves are shifted above the input Q model for wQ=0.5 is thus the best estimate of the amount by which the observed attenuation values can be biased from the actual intrinsic attenuation. Subtracting this amount of bias from the observed values, the solid curve in Figure 2.2 is obtained. This corrected curve establishes the best estimate of average global attenuation consistent with the antipodal measurements. At periods below 150 s, the R5R6 signal fell into the noise, so that stable R1R2/R5R6 γ values could not be determined. As a result, there is no real constraint on the bias below 150 s. The solid curve was extrapolated down to 120 s, but the bias there may be even greater.

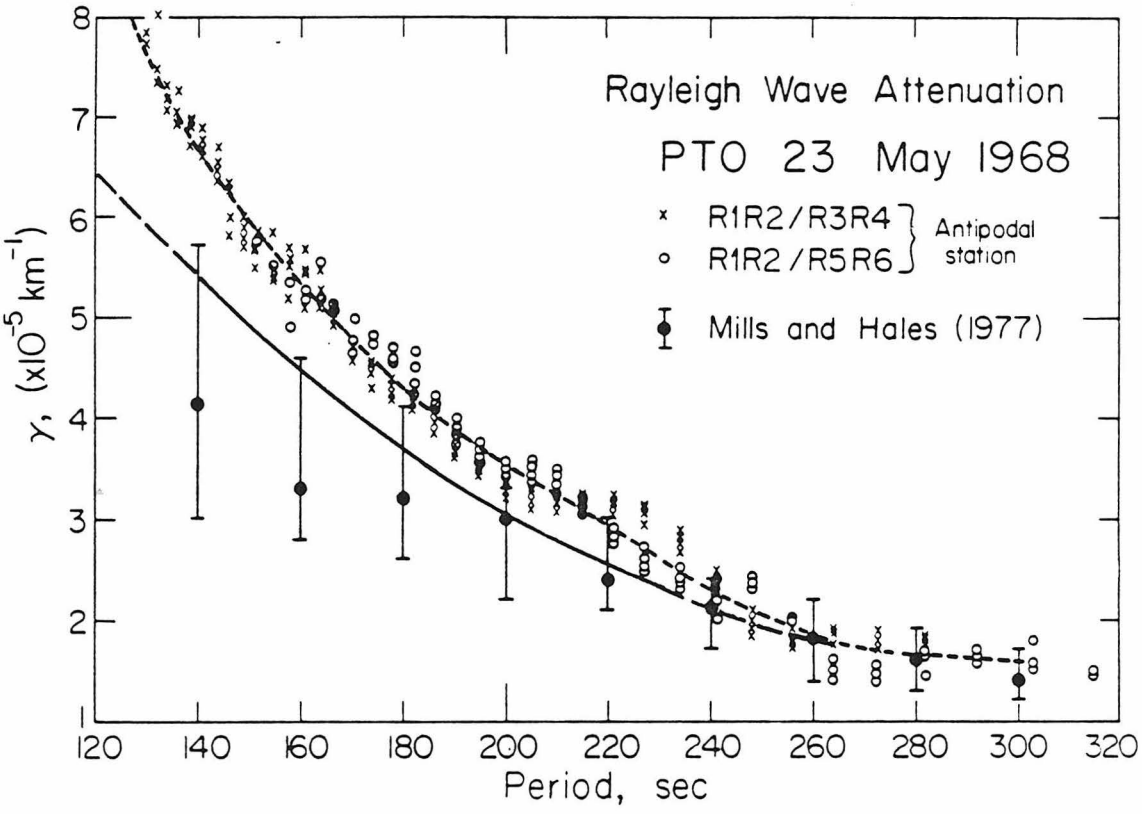

Figure 2.2 Antipodal observations of Rayleigh wave attenuation. The upper (dashed) curve follows the smoothed average trend of the measurements from the PTO record. The solid curve beneath the measured values represents the best estimate of average γ after correcting for bias.

Above 240 s, the uncorrected attenuation values are in agreement with great circle studies, so the bias there is probably negligible. At all periods the corrected curve is within 1σ of the Mills and Hales [1977] estimate, although at periods below 200 s the corrected antipodal γ is greater than their mean value. A recent study by Dziewonski and Steim [1982] supports the antipodal results down to 165 s, the minimum period of their analysis.

As mentioned earlier, the biasing effect shown in Figure 2.1 is independent of the orientation on the ellipsoidal Earth model. This means that Figure 2.1 would look the same if either the event's strike or its location on the ellipsoid were changed, with the station kept at the proper distance and azimuth. Actually, if such changes were made, different values of the parameter wQ would be necessary to reproduce Figure 2.1 exactly. This would not affect the discussion of the allowable amount of bias in the measurements, which relied on the fact that the R1R2/R3R4 and R1R2/R5R6 curves split further apart as the bias increased. It does, however, affect the interpretation of the splitting width w as a measure of the Earth's structural asymmetry. As it turns out, the value of w needed to induce a certain amount of bias is fairly insensitive to the event strike, and it varies as $(\cos^2\theta)^{-1}$ with the event latitude θ. For example, consider the results for wQ=0.5 in Figure 2.1, produced with the event on the ellipsoid's equator. If the event were moved to a latitude of 45°, one would require $wQ=0.5/\cos^2(45^\circ)=1.0$ in order to get the same

results. Remember that all great circles through the event intersect at the antipode. With the event at latitude θ, the difference in path length δL between the longest and shortest great circles is

$$\delta L = 2\pi r_o\left(\frac{f}{2}\cos^2\theta\right) \simeq 2\pi r_o\left(w\cos^2\theta\right) \qquad 2.5$$

where f is the flattening of the ellipsoid. So the change in w needed to maintain a constant bias effect is just the change needed to keep constant the azimuthal variation in path length, or travel time, to the antipode.

Figure 2.3 demonstrates how the relationship between splitting width and event latitude affects the spectrum of the peak ${}_0S_{54}$, which falls near the center of the 143 to 200 s period band. Figure 2.3a shows the singlet amplitudes ${}_0A_{54}^m$, for an event on the equator and wQ=0.5. Figure 2.3b shows the spectral amplitude and phase of the composite peak ${}_0S_{54}$. Below these, in Figures 2.3c and 2.3d, are the corresponding plots for an event at latitude 45^o with wQ=1.0. The distributions of singlet amplitudes are markedly different for the two cases, but the shapes of the composite peaks are identical, consistent with the fact that in both cases attenuation measurements are biased by the same amount. In Figure 2.3a, the singlets are all of comparable amplitude, so that the spectral power is smeared fairly uniformly over the full width w. However, in Figure 2.3c the singlets m=40 to m=54 are very weak, so although the splitting width is

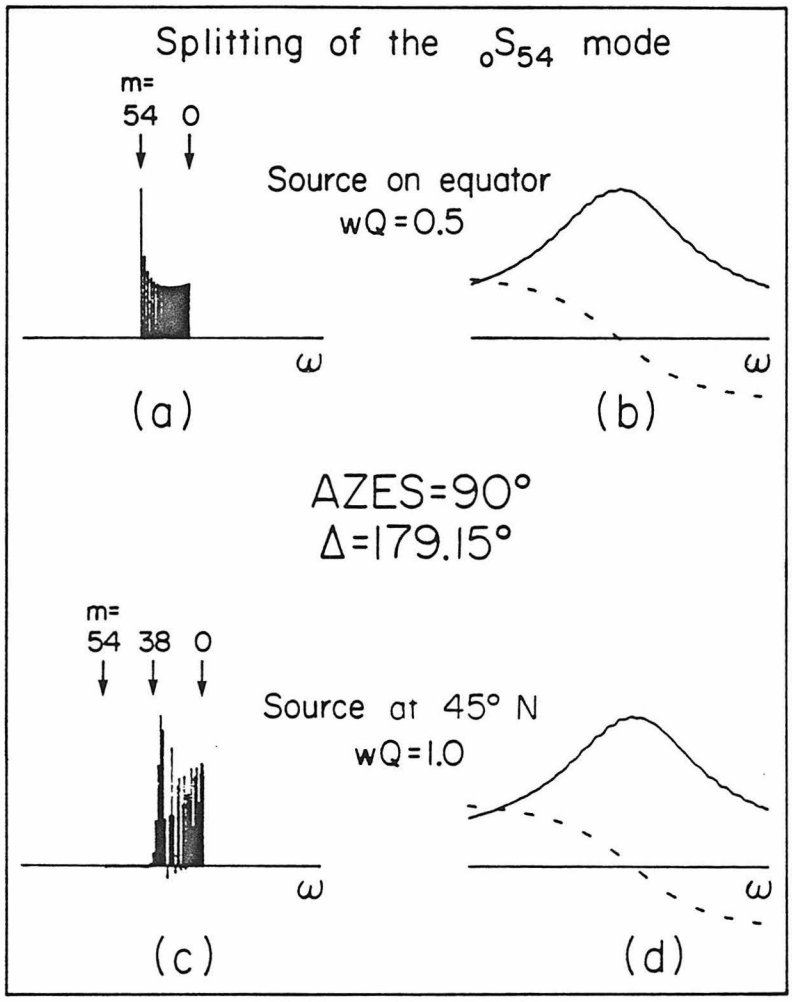

Figure 2.3 (a) The frequencies and amplitudes of the singlets of $_oS_{54}$, for a source located on the equator of an ellipsoid characterized by wQ=0.5. (b) The amplitude (solid curve) and phase (dashed curve) of the multiplet produced by the singlets in (a) with attenuative broadening. (c) and (d) Corresponding results for a source at 45°N and wQ=1.0. See text for discussion.

nominally twice that of Figure 2.3a, the 'effective splitting width' is essentially the same.

One could now imagine a third case, that for the real Earth. The singlets for the real Earth would not show such a regular variation in eigenfrequency, and the amplitude distribution among them would be fairly random. But the composite peak for the real Earth should look very much like, and result in time domain behavior very much like, the peaks of Figures 2.3b and 2.3d. This is the crucial assumption made in using results based on the ellipsoidal model to estimate the bias in real data.

To justify this assumption the effects of a random distribution of singlet eigenfrequencies beneath each mode peak were examined. First, the singlet amplitudes were calculated for the source-receiver geometry used in Figures 2.3c and 2.3d. As Figure 2.3c shows, the singlet amplitudes for this geometry scatter over a wide range of values. Each singlet was next assigned an arbitrary eigenfrequency within the range $(1\pm w/2)\omega_d$, using a random number generator. The singlet eigenfrequencies were generated independently for each mode ${}_0S_\ell$. The full spectrum in this random case was even more pathological than for the real Earth, for which one would expect the singlet pattern under ${}_0S_\ell$ to resemble that under ${}_0S_{\ell+1}$ (for $\ell >> 1$). Time domain synthetics were computed and analyzed as before. The 'measured' attenuation curves for the random case (Fig. 2.4) behaved almost exactly like the curves produced by the ellipsoidal Earth.

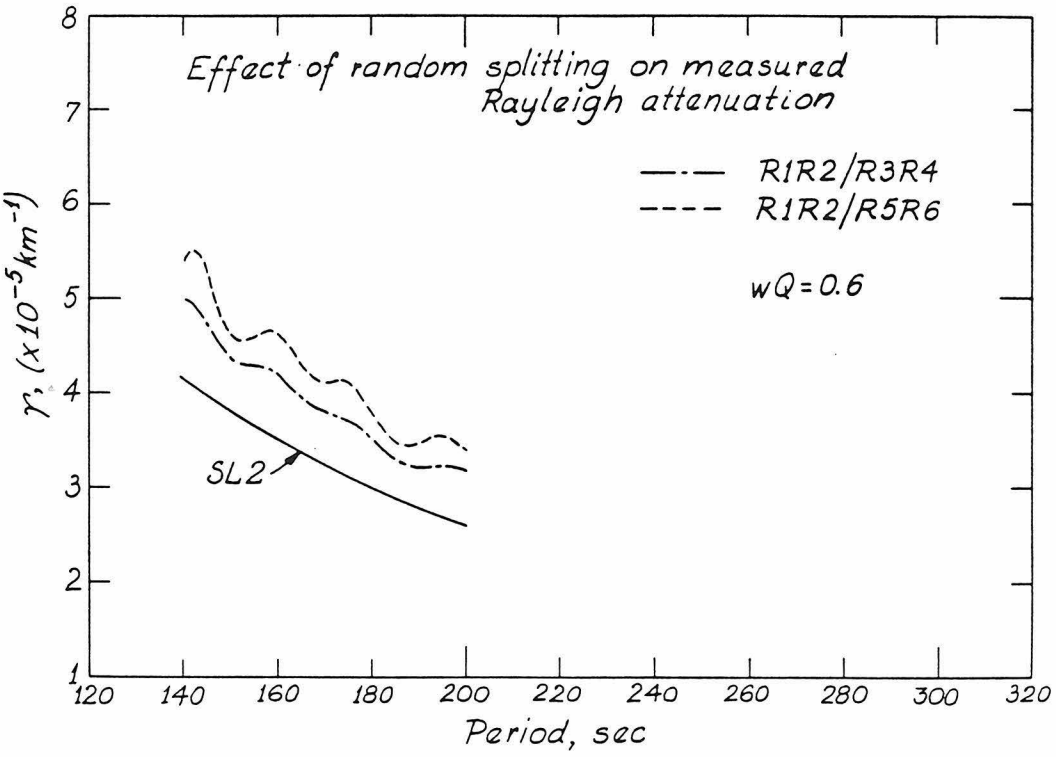

Figure 2.4 Effect of random splitting of the normal modes on antipodal attenuation measurements. The singlets of each mode were randomly distributed within a width characterized by the parameter wQ. Compare with Figure 2.1.

Individual curves oscillated slightly about the corresponding curves for the ellipsoidal model; the pattern of this oscillation changed for different sets of random eigenfrequencies. The important property of Figure 2.1 was reproduced identically: for comparable splitting widths, the R1R2/R3R4 and R1R2/R5R6 curves diverged from the input curve, and from each other, in the same fashion as in Figure 2.1. One can conclude that this figure demonstrates an inescapable side effect of unresolved split mode peaks, an effect which is independent of the singlet distributions beneath the peaks. The splitting widths and bias measures which have been determined are not dependent upon the ellipsoidal model used to estimate them.

Discussion

In Table 2.1 are compiled the results of the antipodal Rayleigh wave Q observations. The directly measured Q values, in the column labeled Q_o, are almost certainly biased due to the effects of a laterally heterogeneous velocity structure. These values establish a lower bound on global average Q values. The consistency of the R1R2/R3R4 and R1R2/R5R6 trends indicates that the bias cannot be very large, or alternatively that the focusing at the antipode is quite sharp. The observed polarizations of the Rayleigh arrivals also support this conclusion. The consistency of the measurements has been used as a constraint to estimate the amount of bias. The column of

Table 2.1 - Rayleigh Wave Q

T, s	$\delta\omega/\omega \times 100$[a]	Q_o[b]	Q_c[c]	Q_{DS}[d]	Q_{PREM}[e]	Q_{ABM}[f]
120	0.37	83	108		122	114
130	0.36	86	109		125	119
140	0.35	91	112		128	123
150	0.34	97	116		132	127
160	0.34	101	121		136	130
170	0.33	106	127	135	140	133
180	0.32	111	132	138	144	137
190	0.31	120	138	140	148	140
200	0.30	123	143	146	153	144
210	0.29	128	150	150	157	147
220	0.28	134	155	156	162	153
230	0.27	146	164	160	166	158
240	0.27	157	170	166	171	164
250	0.26	170	180	172	176	170
260		188	188	179	182	176
270		192	192	185	188	183
280		187	187	190	194	191

[a] Based on $wQ_{SL2} = 0.5$ ($w = \delta\omega/\omega$).
[b] From observed trend (dashed line) of Figure 2.2.
[c] From corrected trend (solid line) of Figure 2.2.
[d] Dziewonski and Steim [1982].
[e] Dziewonski and Anderson [1981].
[f] Anderson and Given [1982].

corrected Q values, Q_c, gives the most reasonable global average Q consistent with the data, after removing the bias.

For periods below 250 s the corrected Q are still somewhat lower than the average values given in most conventional great-circle studies. The corrected Q are, however, within the standard deviations given by Mills and Hales [1977]. The antipodal records analyzed here are of high quality, yielding stable, smoothly varying measurements of attenuation. They are also very consistent: radiation from the two events sampled the mantle in different ways, yet the results from the two events agree closely. Existing mantle attenuation models, such as SL2 of Anderson and Hart [1978] and that from the recent Preliminary Reference Earth Model (PREM) of Dziewonski and Anderson [1981], were constructed using the great circle results as constraints. In Figure 2.5 the antipodal results are compared to these two models. Model SL2 gives Q which are decidedly too high across the usable frequency band of the PTO record. The PREM model comes closer to the corrected antipodal Q but is still rather high at periods below 220 s. Above 280 s, the antipodal Q from the PTO record are possibly suspect due to very low signal amplitude and relatively short record length for these long periods. If the antipodal Q are indeed better global averages, then the upper mantle is more attenuative than has been generally recognized. Dziewonski and Steim [1982] have recently analyzed an extensive great circle data set to obtain high precision estimates of global Rayleigh wave attenuation down to periods of 165 s. From 280

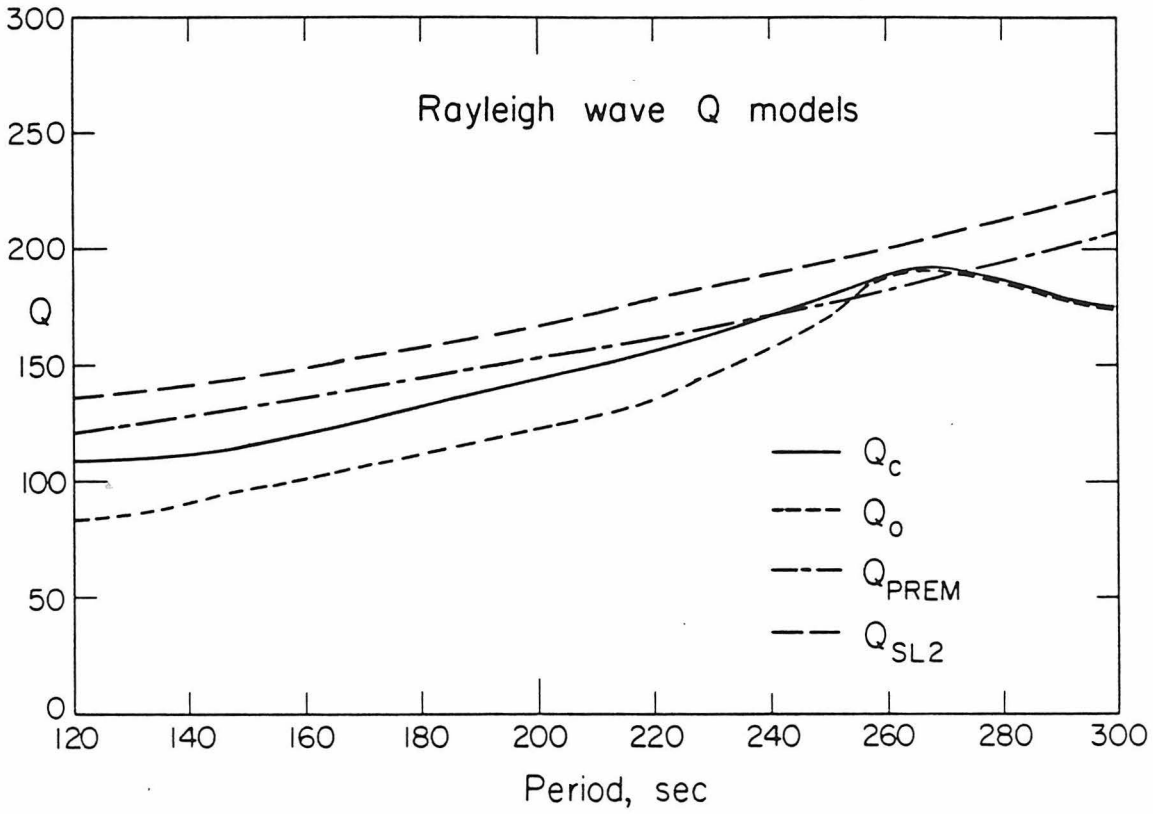

Figure 2.5 Observed (Q_o) and corrected (Q_c) trends of globally averaged Q of Rayleigh waves as a function of period, obtained from antipodal data. The attenuation models PREM and SL2 are shown for comparison.

to 165 s their results (see Table 2.1) are virtually identical to those presented here (average difference ~3%). This gives strong support to the method of correcting for bias.

Also listed in Table 2.1 are estimates of the splitting widths of the Rayleigh modes with periods between 120 and 250 s. Madariaga and Aki [1972] and Luh [1974] have calculated splitting widths of various modes for Earth models with distinct continental and oceanic velocity profiles. Luh [1974] used the Canadian shield model CANSD [Brune and Dorman, 1963] for the continental structure and model 5-5-1 [Saito and Takeuchi, 1966] for the oceans. These models differ most significantly in the upper 120 km of the Earth, with smaller differences extending to depths of 400 km. Luh [1974] calculated a splitting width for the mode ${}_0S_{40}$ (period = 212 s) of 0.32%. This compares favorably with the antipodal estimate of 0.29% for the splitting width at 210 s. The antipodal observations thus suggest that the differences between continental and oceanic structures are comparable to the differences between the CANSD and 5-5-1 models. Of course, greater variations may occur locally, but such variations are not important on a global scale.

The splitting widths determined here can also be compared directly to observed ranges in great circle average phase velocities. Nakanishi [personal communication] has plotted great circle average Rayleigh wave phase velocity at a period of 200 s as a function of take-off azimuth from the source for 28 different earthquakes. For

sources near New Zealand, the difference between the minimum and maximum phase velocities (δc) is typically 0.02 to 0.03 km/s (Fig. 2.6). The splitting width w at 200 s determined here represents a corresponding range given by

$$\delta c = (c/U)wc = 0.02 \text{ km/s}$$

The factor c/U is necessary because Nakanishi's measurements were made at fixed frequency while w was determined at fixed wavenumber [Dziewonski, 1970]. One might expect the observed range to be greater than that determined from the antipodal record because of random errors in the great circle velocity estimates. Also, as mentioned above, there could be localized anomalies which have little effect on the full antipodal 'stack' but which cause a particular great circle measurement to differ greatly from the norm. In light of these arguments the width w determined here seems to agree very well with independent observations of the Earth's heterogeneity.

Conclusions

The uncorrected antipodal results provide a lower bound for mantle Rayleigh wave Q values and, as such, provide an important constraint on absorption in the upper mantle. Because the 'stack' is complete an attempt was made to estimate the bias due to lateral

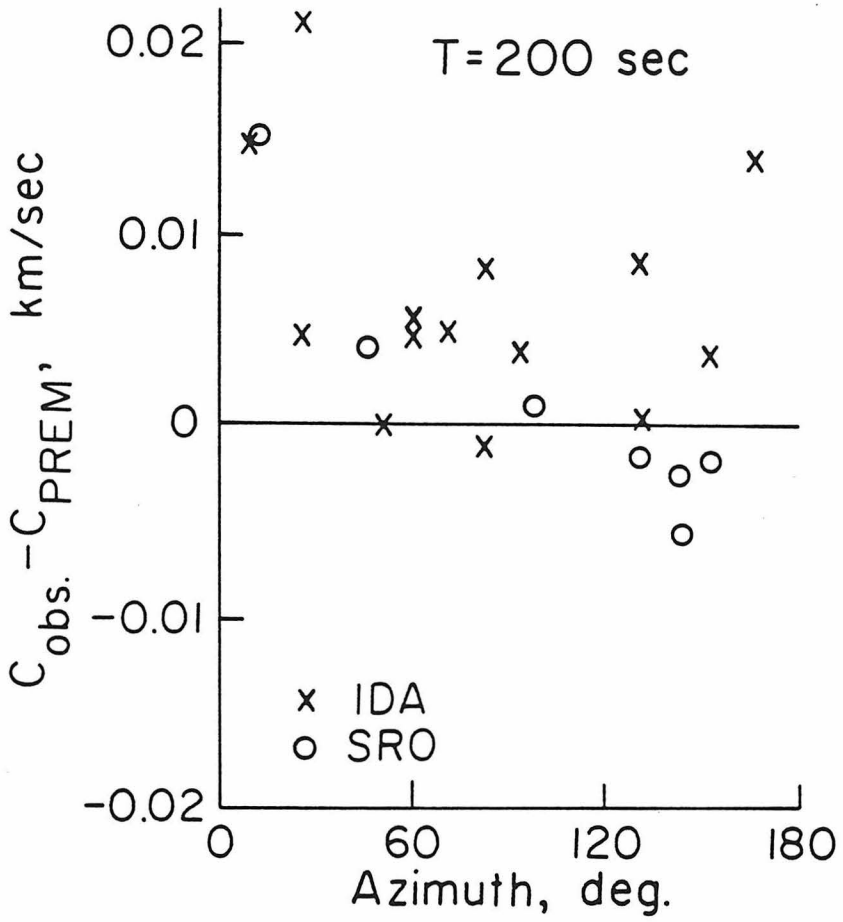

Figure 2.6 Variation of great circle Rayleigh wave phase velocity (period=200 s) with take-off azimuth from the source, for an epicenter in the vicinity of the Inangahua event. Base line corresponds to the model PREM. Circles and crosses denote measurements from SRO and IDA instruments, respectively. Measurements were made by I. Nakanishi [personal communication].

velocity heterogeneity and to correct the observed Q values for this effect. Although accounting for the effects of an unknown lateral heterogeneity may appear to be an intractable problem, one can have confidence in these results for the following reasons:

1. The antipodal records give excellent agreement with previous great circle group velocity values.

2. The observed Rayleigh polarization indicates that focusing at the antipode is quite sharp.

3. Attenuation values are smooth, stable, and reproducible.

4. There is excellent consistency between successive passages of the Rayleigh wave groups.

5. Different events give almost identical results.

6. The method used to synthesize mode splitting allowed the heterogeneity to increase toward shorter periods.

7. The property used in estimating the bias, namely, the relative biasing of the R1R2/R3R4 and R1R2/R5R6 curves, is a general feature of mode splitting.

8. The corrected attenuation values are in excellent agreement with the most complete and precise recent studies.

9. The estimates of the splitting widths due to lateral heterogeneity are consistent with previous studies.

The uncorrected measurements of the attenuation coefficient γ lie, as they should, above previous estimates of global attenuation. The deviation increases at short periods which is consistent with the

assumption that lateral heterogeneity is greatest near the surface and decreases with depth. Uncorrected estimates of γ for periods greater than 200 s are lower than the Mills and Hales [1977] 'upper bound' (+1 standard deviation). Since the uncorrected estimates set lower bounds on Q, this indicates that the minimum Q of the mantle at these periods is more tightly constrained than before. Corrected estimates of γ at shorter periods are at the upper end of the Mills and Hales [1977] estimated range, indicating that the Q of the shallow mantle is less than would be inferred from their estimate. The corrected Q values, however, are within the stated errors ($\pm 1\sigma$) of the Mills and Hales [1977] data at all periods, and they agree with the Dziewonski and Steim [1982] data to within an average error of 3%.

Chapter 3

THE TRN RECORD OF THE SUMBAWA, INDONESIA EARTHQUAKE

The Sumbawa, Indonesia earthquake of August 19, 1977 (M_S=7.9, latitude=11.08°S, longitude=118.46°E, h=33 km, time=0608:55 (PDE)) produced an antipodal seismogram at the WWSSN station TRN near Trinidad, British West Indies (latitude=10.65°N, longitude=61.40°W). Because of its size this event has been used in several studies of free oscillations and long period surface waves [Buland et al., 1979; Geller and Stein, 1979; Silver and Jordan, 1981; Masters and Gilbert, 1982]. The event itself is of tectonic significance because it was a rare large normal slip event which occurred near a subduction zone [Stewart, 1978]. The event location, mechanism and aftershock area [Stewart, 1978] are shown in Figure 3.1. Like a thrust event, a shallow normal event has a two-lobed radiation pattern. Vertical motions interfere constructively at the antipode producing an amplified signal. The source and station coordinates put TRN at a distance of 179.5° from the epicenter. In fact the true antipode of the station falls within the aftershock area of the Sumbawa event. If the aftershock area represents the extent of rupture then the source and station are really as antipodal to one another as is possible. The large magnitude of this event caused the long period vertical instrument at TRN to be driven off scale by the earlier arrivals so

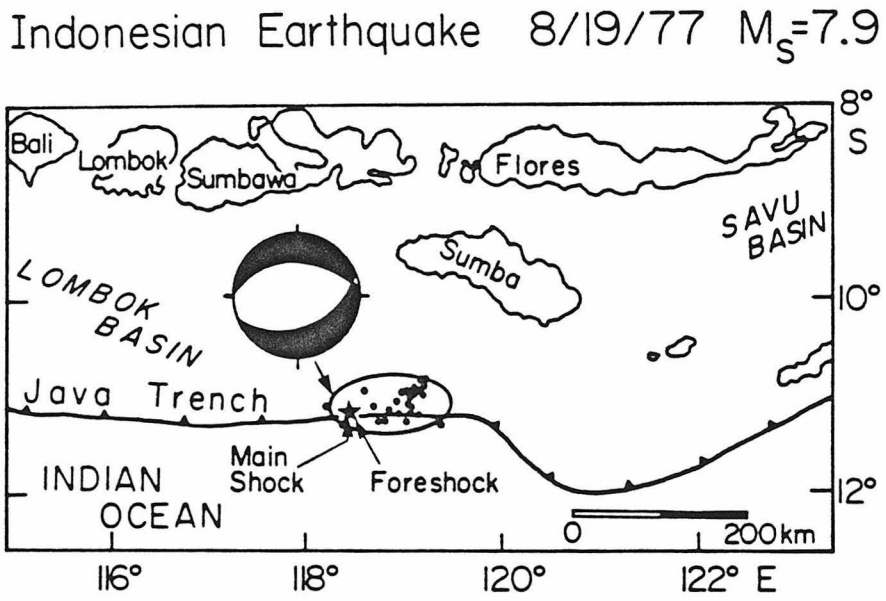

Figure 3.1 Location, focal mechanism and aftershock distribution of the Sumbawa, Indonesia earthquake of August 19, 1977 (M_S=7.9). Figure provided by G. Stewart [personal communication].

that the first 6.5 hours of the record were unusable.

The trace analyzed in this chapter began at 1245:00 and continued for 17.5 hours until falling into the noise. This record was digitized and interpolated to a sampling interval of 2 s, filtered to remove energy at periods shorter than 100 s, then decimated to a 20 s sampling interval. The first 8 hours of data are shown in Figure 3.2, and the amplitude spectrum of the 17.5 hour trace is plotted in Figure 3.3. The trace was dominated by periods between 200 and 500 s. The fundamental modes ${}_0S_9$ through ${}_0S_{35}$ appear as prominent simple peaks on the spectrum. Attenuation reduced periods shorter than 200 s before the signal came on scale and the instrument removed periods longer than 500 s. The data began during the third Rayleigh arrival (R5R6). Over the 200 to 500 s band Rayleigh group velocities range from 3.6 to 5.0 km/s. As a result the subsequent Rayleigh arrivals were very dispersed and eventually began to overlap. The arrivals could not be separated by simple group velocity windowing, so the straightforward procedure used to measure velocities and Q for the PTO record could not be employed here. A somewhat more complicated procedure was necessary.

Dispersion Analysis

Analysis of the TRN record of the Sumbawa earthquake for phase and group velocities and attenuation relied heavily on the `residual

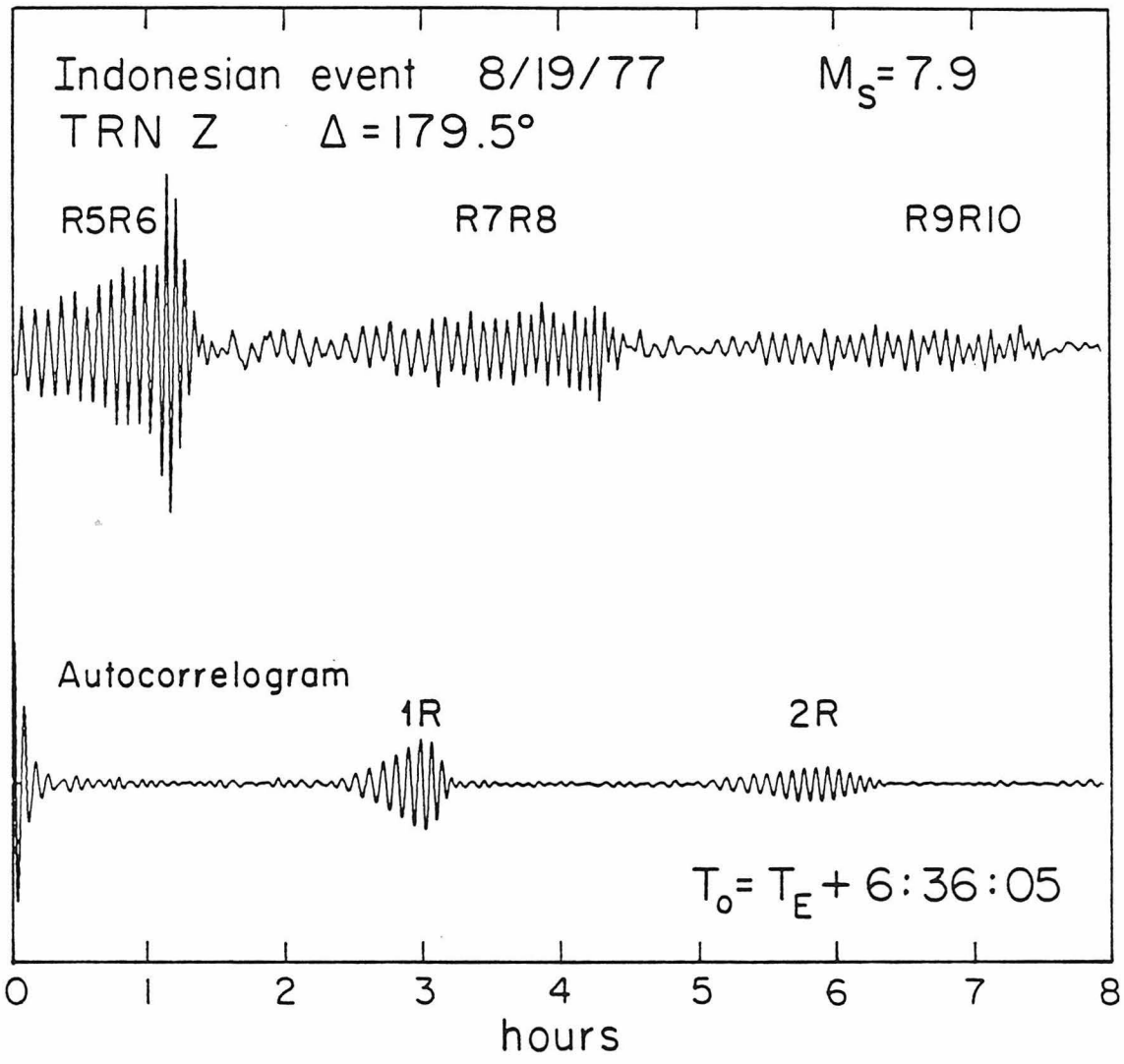

Figure 3.2 (Top) The first 8 hours of the long period vertical record of the Sumbawa event from WWSSN station TRN (Δ=179.5°). The trace begins 6 hr 36 mn 5 s after the origin time of the event. (Bottom) Autocorrelogram of 17.5 hours of the TRN record with boxcar windowing.

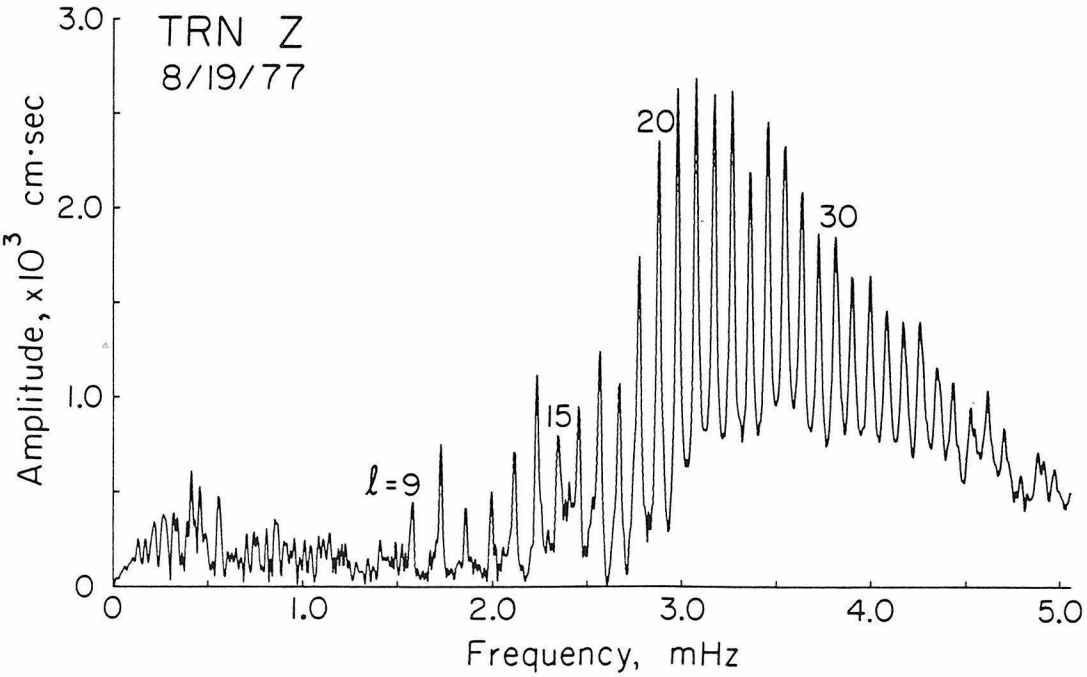

Figure 3.3 Amplitude spectrum of 17.5 hours of the TRN record with boxcar windowing. The numbers above the peaks give the angular order ℓ of the fundamental modes ${}_0S_\ell$.

dispersion' technique of Dziewonski et al. [1972]. In this method, the record to be analyzed is compared to a synthetic signal of known dispersion and the differences in phase and group velocity are measured. A major advantage is that an arrival of interest can be compressed in time and isolated from other arrivals and from energy in other modes. The residual dispersion technique also reduces systematic errors which are introduced if the group velocity changes rapidly with frequency.

The residual dispersion method was actually applied not to the original data trace but to its autocorrelogram. The autocorrelogram was generated by multiplying the spectrum of the data by its complex conjugate and inverse transforming the product. Actually, two versions of the autocorrelogram were generated. For the first version, used to measure phase and group velocity, the data trace was first multiplied by a Hanning window W(t)

$$W(t) = \frac{1}{2}\left(1-\cos(2\pi t/t_L)\right) \qquad 3.1$$

where t_L is the total record length (17.5 hr). Dahlen [1982] has shown that such windowing is necessary in order to avoid systematic errors in dispersion measurements. In the frequency domain the Hanning window has much smaller side lobes than a boxcar window of the same length [Oppenheim and Schafer, 1975] and so reduces the interference effects between adjacent normal modes on the record's

spectrum. Dahlen [1982] and Masters and Gilbert [1982] have suggested that boxcar windowing can produce systematic errors in attenuation measurements as well, but neither study demonstrated this assertion. In the following chapter a synthetic record is used to show that a boxcar window is actually preferable to the Hanning window for this purpose. The finite length of the data trace introduces effects which must be considered in the attenuation analysis. The second version of the autocorrelogram, then, was produced from the spectrum of the original trace without any tapered windowing and was used for measuring attenuation.

Figure 3.2 shows the first 8 hours of the autocorrelogram which was produced using a boxcar window. Following the large pulse at zero lag, this trace has a series of dispersed pulses occurring at 3-hour intervals. Consider the first such 'arrival', labeled 1R. This arrival gives a measure of the dispersion of Rayleigh waves over one complete orbit of the earth, or between two successive arrivals on the original data trace. Source and instrument phase and group delays, common to all arrivals on the actual seismogram, are not present in the autocorrelogram arrivals. The pulse 1R can be thought of as the sum of the crosscorrelograms of R5R6 with R7R8, R7R8 with R9R10, etc. [Dziewonski and Landisman, 1970]. Similarly, 2R gives the net dispersion over two orbits. The autocorrelogram can also be interpreted as the 'seismogram' that would be obtained at TRN for a source directly beneath the station. In this view the zero-lag pulse

is the source pulse (which is zero-phase) and 1R, 2R, etc. are successive Rayleigh arrivals which are subjected to dispersion as well as attenuation. The absence of significant energy between these arrivals on the autocorrelogram proves that the original seismogram was recorded at the antipode [Dziewonski and Landisman, 1970] and that it was dominated by fundamental mode energy.

Phase and group velocities were measured from the 1R, 2R and 3R pulses on the autocorrelogram using the residual dispersion method [Dziewonski et al., 1972]. A crosscorrelogram h(t) was computed from each observed pulse F(t) and a synthetic $F_s(t)$

$$h(t) = \frac{1}{2\pi} \int_{-\infty}^{\infty} F(\omega) F_s^*(\omega) \exp(-i\omega t) d\omega \qquad 3.2$$

The synthetic pulse has a unit amplitude spectrum given by

$$F_s(\omega) = \exp(ik_s(\omega)r + n\pi) \qquad 3.3$$

where r is the propagation distance for the pulse and $k_s(\omega)$ is a specified dispersion curve (wavenumber vs. frequency) and n is the autocorrelogram arrival number (n=1 for 1R, etc.). The term $n\pi$ in the expression for the synthetic corrects for the polar phase shifts [Brune et al., 1961]. The spectrum of the crosscorrelogram is

$$h(\omega) = |F(\omega)| \exp(i\bar{k}(\omega)r) \qquad 3.4$$

where $|F(\omega)|$ is the amplitude spectrum of the observed pulse and $\bar{k}=k-k_s$ is the difference between the dispersion curves of the data and synthetic. The dispersion curve for the model 1066A [Gilbert and Dziewonski, 1975] was used for $k_s(\omega)$ in the analysis here. The spheroidal mode wavenumbers and eigenfrequencies for this model were interpolated to produce a continuous dispersion curve. A crosscorrelogram was generated and evaluated separately for each of the pulses 1R, 2R and 3R. Figure 3.4a shows the crosscorrelograms used to measure dispersion residuals between the three arrivals and their corresponding 1066A unit-amplitude synthetics. If the 1066A dispersion curve precisely matched the dispersion in the data, then all three of the crosscorrelograms would be symmetric about zero lag. This is very nearly the case for all three signals, demonstrating both the accuracy of 1066A and the quality of the data. The slight deviations of the crosscorrelograms from zero-lag symmetry were analyzed to measure the dispersion residuals.

The crosscorrelograms were analyzed using a multiple filtering technique [Dziewonski et al., 1969] to give estimates of the phase and group velocity residuals between the data and model 1066A. The trace h(t) was convolved with a series of narrow band filters having regularly spaced center frequencies. These filters were zero-phase with Gaussian-shaped amplitude spectra. The instantaneous amplitude and phase, as functions of time, were determined by combining each

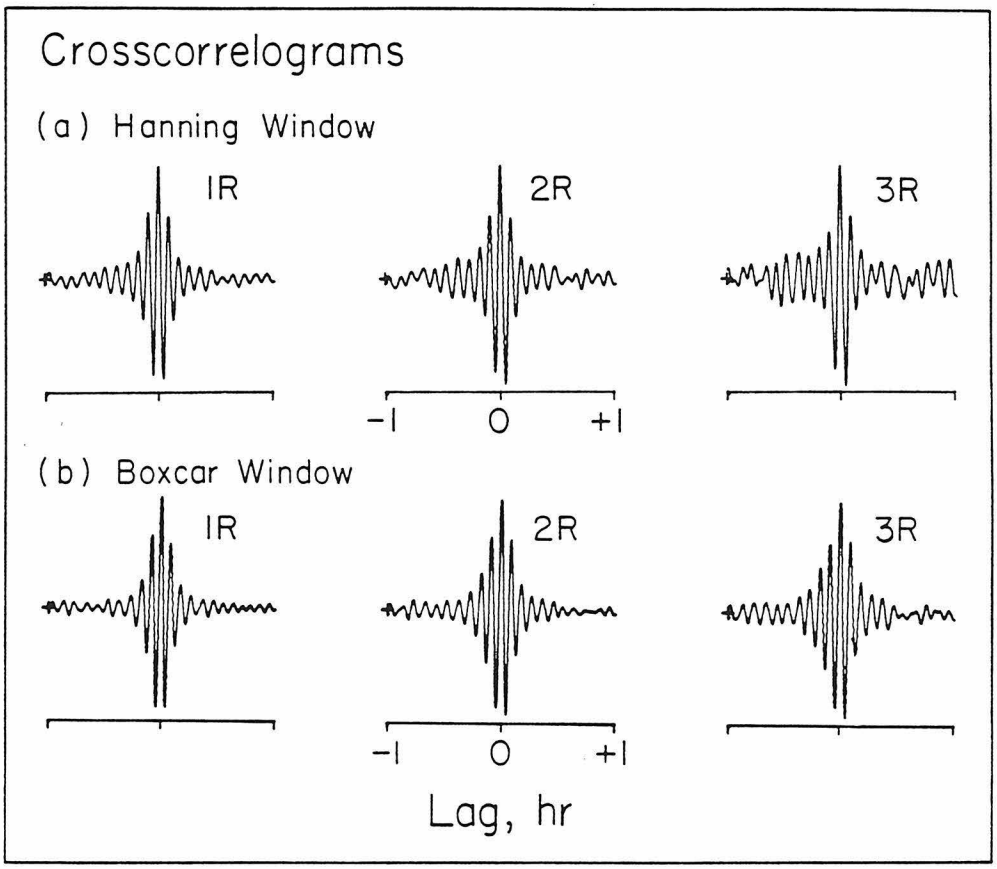

Figure 3.4 (a) Crosscorrelograms between the pulses 1R, 2R and 3R from the autocorrelogram of the Hanning-windowed TRN record and their corresponding 1066A unit-amplitude synthetics. These signals were used to measure phase and group velocity. (b) Same as (a), but produced from the boxcar-windowed TRN record. These signals were used to measure attenuation.

filtered trace with its quadrature signal [Goodman, 1960]. The instantaneous phase at zero lag gave the phase velocity residual at the center frequency of the narrow band filter. The group velocity residual was determined from the time at which the filtered crosscorrelogram attained its maximum instantaneous amplitude.

There are two principal advantages of the residual dispersion method over a direct analysis of the dispersed arrivals on the autocorrelogram. Most important is that the residual dispersion analysis greatly reduces systematic errors in standard group velocity measurements which are introduced when the signal is strongly dispersed. These errors are due to the fact that the group velocity, defined as the first derivative of frequency with respect to wavenumber, is not rigorously equal to the propagation velocity of a wave group's amplitude maximum [see Dziewonski et al., 1972]. The crosscorrelation procedure also concentrates an arrival's energy into a narrow time window, yielding the second advantage. This concentration in time improves the isolation of the desired arrivals from each other and from noise.

Results of the phase and group velocity measurements are shown in Figures 3.5 and 3.6, respectively. The data are plotted at the center frequencies of the filters used in the analysis. The multiple filtering technique causes structure in the dispersion curves to be smeared over a range of frequencies. This smoothing is a function of the filter bandwidths. Estimates from the autocorrelogram arrivals

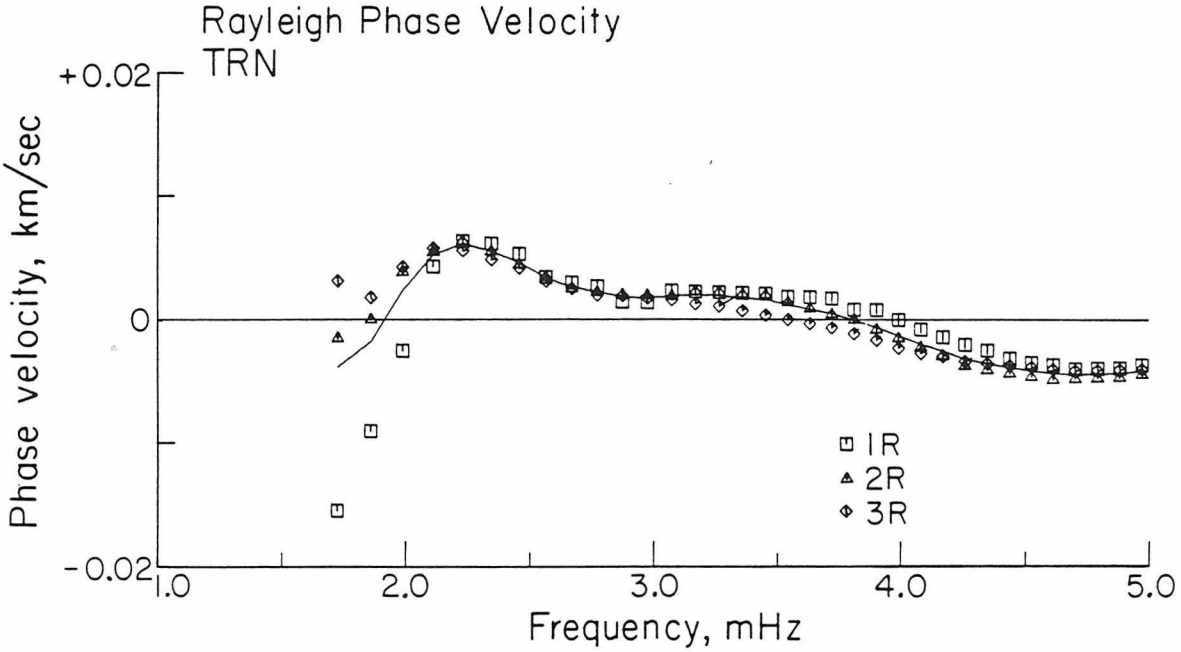

Figure 3.5 Rayleigh wave phase velocity measured from the TRN record. The data are plotted relative to the phase velocity of model 1066A [Gilbert and Dziewonski, 1975].

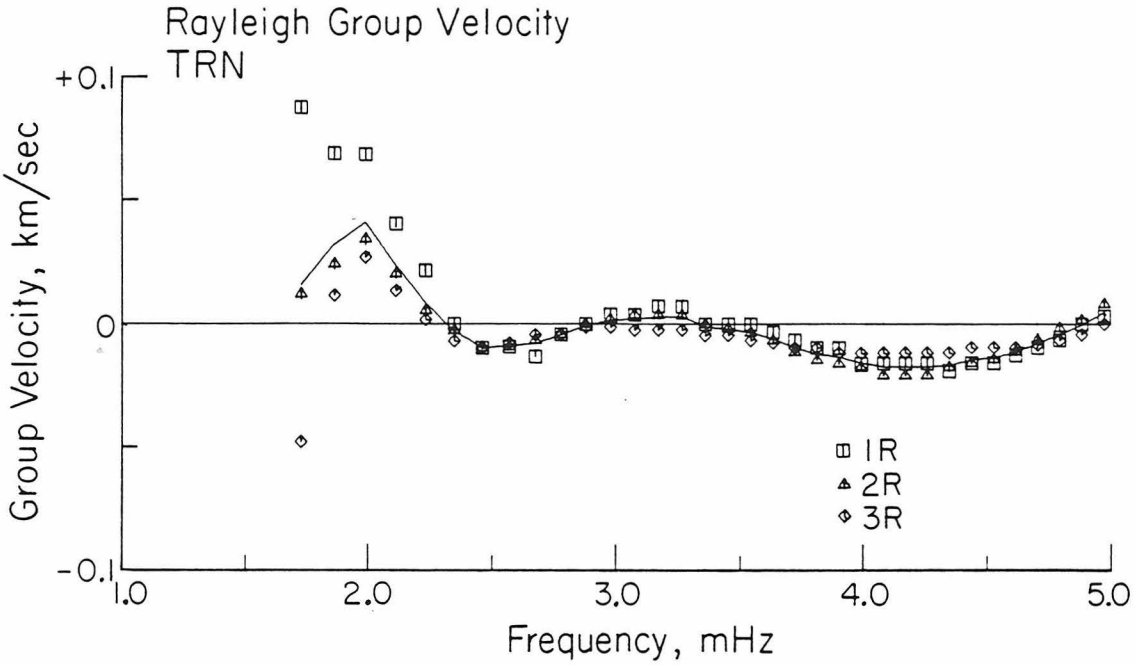

Figure 3.6 Rayleigh wave group velocity measured from the TRN record. The data are plotted relative to the group velocity of model 1066A [Gilbert and Dziewonski, 1975].

1R, 2R and 3R are plotted using different symbols. Both the phase and group curves show very stable results for frequencies between 2 and 5 mHz. The phase velocity difference between the data and 1066A is less than 0.01 km/s at all frequencies, and the group velocity residual is always less than 0.05 km/s. The results here cannot be immediately interpreted as global averages because of a sampling bias due to the focal mechanism of the Indonesian event. Based on the focal mechanism determined by Given and Kanamori [1980], the maxima of the two-lobed Rayleigh wave radiation pattern were directed nearly due north and south of the event. This resulted is a biased sampling of the geoellipsoid, with polar paths over-represented. Because such paths are the shortest great circles around the Earth and an average Earth circumference (40,030 km) was used in the analysis, one might expect the observed phase velocities to be shifted toward higher values. The effect of biased sampling on the phase and group velocity curves is examined in the next chapter using synthetic seismograms.

Attenuation Analysis

The concentration in time of the arrivals afforded by crosscorrelating with a synthetic facilitated the measurement of Q from the TRN record. Amplitude spectra of the 2 hour portions of the crosscorrelograms shown in Figure 3.4b were calculated with an FFT routine. Q was measured as a function of frequency by taking spectral

ratios between the 1R and 2R, then the 1R and 3R, crosscorrelograms. The expressions relating Q to the spectral ratios are given in Chapter 1 of this thesis. The crosscorrelograms can be used to measure Q because their amplitude spectra are the same as those of the dispersed 1R, 2R and 3R signals on the autocorrelogram (Equation 3.4). This procedure for measuring Q was first used by Sailor [1978]. The results of the Q analysis are shown as solid lines in Figure 3.7. The two curves in this Figure, 1R/2R and 1R/3R, are not directly analogous to the R1R2/R3R4 and R1R2/R5R6 curves obtained from the PTO record (Fig. 1.6). The PTO curves were obtained from the actual arrivals on the original seismogram, while for the TRN results the autocorrelogram 'arrivals' were used. The entire TRN record contributes to each of these 'arrivals'. One effect of using the autocorrelogram is a window length bias caused by the finite length of the TRN seismogram. This effect is significant only for periods longer than 400 s, and no corrections have been made for it here. This effect is included in the synthetic experiments which follow.

The Q results are stable over a more limited frequency range than the velocity measurements displayed in Figures 3.5 and 3.6. This is to be expected since the attenuation estimates employ spectral ratios between two arrivals which both include noise. Some of the noise can be attributed to contamination by other mode branches. Because spheroidal overtones are likely to be present in the data, their potential effects on the attenuation measurements should be

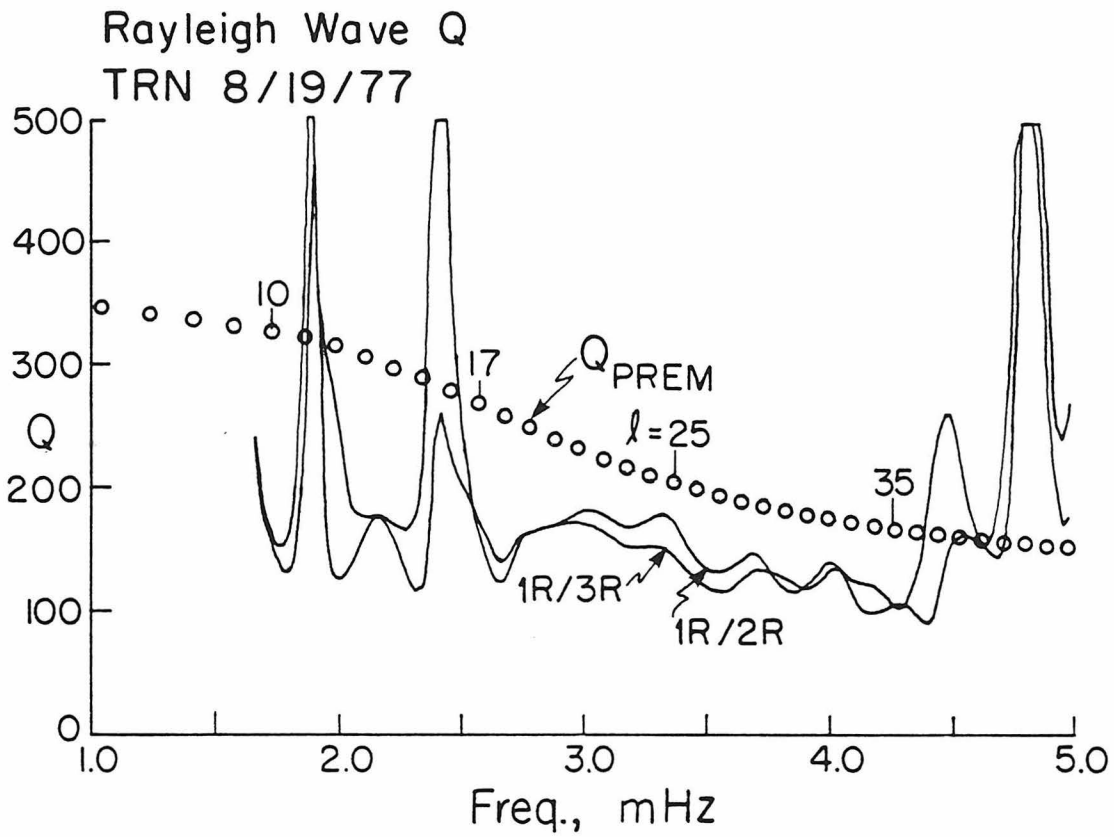

Figure 3.7 Rayleigh wave Q measured from the TRN record. The open circles give Q of the modes ${}_0S_\ell$ for the PREM attenuation model [Dziewonski and Anderson, 1981].

considered. Coupling between the fundamental spheroidal and toroidal modes may also influence the results.

Spheroidal Overtones

Synthetic versions of the TRN seismogram were generated in order to test the effects of the spheroidal overtones. The normal modes of the spherically symmetric Earth model 1066A [Gilbert and Dziewonski, 1975] were summed to produce the synthetics; the method was described by Kanamori [1970a]. The attenuation model SL2 [Anderson and Hart, 1978] gave the Q of the modes. This model was chosen because a complete catalog of all the spheroidal mode Q values existed for it. The event was modeled as a point source at 40 km depth with a focal mechanism as determined by Given and Kanamori [1980].

One synthetic was made using only the fundamental (${}_0S_\ell$) modes, and another was made using all spheroidal modes with periods longer than 150 s. The overtone excitation was much weaker than that of the fundamental branch, so the two time domain synthetics looked very similar. The overtones had a more apparent effect in the frequency domain. Figure 3.8 shows the amplitude spectrum of the synthetic with overtones. The fundamental modes ${}_0S_\ell$ clearly dominate this spectrum. There is considerable complexity between the modes ${}_0S_8$ to ${}_0S_{20}$ due to the presence of the overtone modes, primarily the ${}_2S_\ell$ branch, and

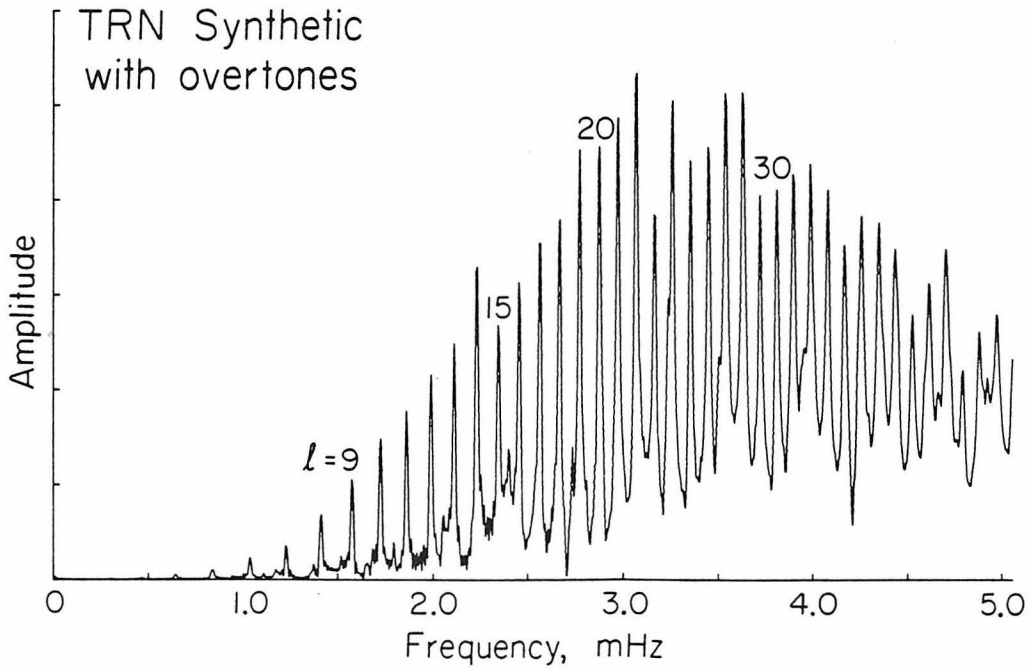

Figure 3.8 Amplitude spectrum of a spherical Earth synthetic of the TRN seismogram which included all spheroidal modes with periods longer than 150 s (fundamentals and overtones). The numbers above the peaks identify the modes ${}_0S_\ell$. Compare with Figure 3.3.

partly due to the finite record length. Beyond ${}_0S_{20}$ the small glitches on the sides of some of the fundamental modes are caused entirely by the overtones. In this region the ${}_1S_\ell$ modes are the strongest of the overtones. Besides introducing structure between the fundamental modes, overtones also affect their peak amplitudes. Without the overtones the amplitudes of the ${}_0S_\ell$ modes vary smoothly with angular order, while the pattern seen in Figure 3.8 is rather erratic. The spectrum in Figure 3.8 can be compared with that in Figure 3.3 to get a sense of the actual contribution of the overtones to the motion observed at TRN. For orders ℓ larger than 20 the observed modes (Fig. 3.3) vary more smoothly in amplitude and show less complexity than the synthetics. In this region the model apparently over-predicts the strength of the overtones relative to the fundamentals. Just the opposite holds for orders ℓ less than 20. Here the overtones seem to have a slightly larger effect on the data than predicted.

To study the influence of the overtones on measurements of fundamental mode attenuation, the synthetics were analyzed in the same manner as the data. The spectral amplitude ratios 1R/2R and 1R/3R were calculated from the autocorrelogram 'arrivals', resulting in two curves of Q versus frequency for each synthetic. The results are shown in Figure 3.9. The two dashed curves which merge near 4 mHz represent the synthetic with fundamental modes only. These curves are very smooth and agree with the input SL2 fundamental mode Q at

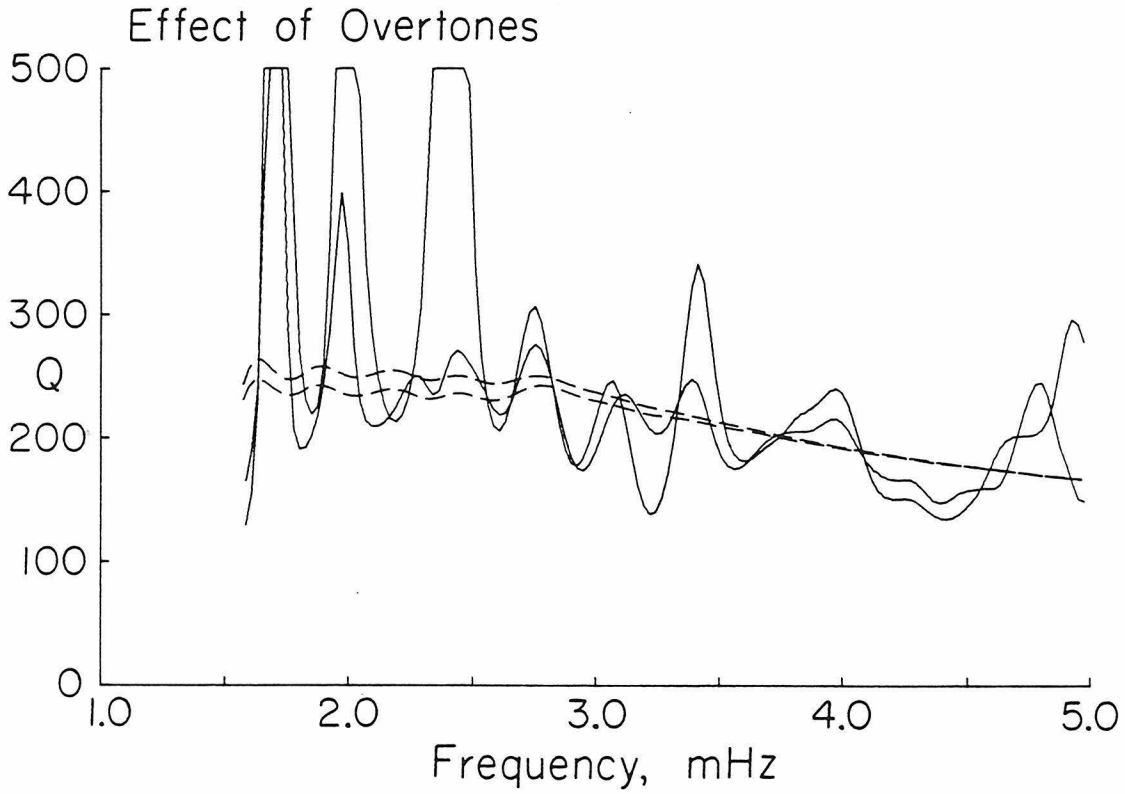

Figure 3.9 Effect of overtones on measurements of fundamental mode attenuation. The dashed curves give Q measured from a synthetic which included only fundamental modes. The solid curves result for a synthetic with spheroidal overtones added to it.

frequencies above about 2.8 mHz. At lower frequencies the dashed curves give Q below the input values because of the finite record length. The synthetic which included overtones produced the two solid curves in Figure 3.9. These curves oscillate erratically about the dashed ones and differ substantially from each other. The overtones cause the measurements to be unstable and to depend on the arrivals compared, but do not result in systematic biasing toward higher or lower Q.

The attenuation curves for the observed TRN signal (Fig. 3.7) are more stable and in better agreement than the solid curves of Figure 3.9 for frequencies between 2.8 and 4.3 mHz (modes ${}_0S_{20}$ to ${}_0S_{36}$). This indicates that the data are not seriously contaminated by overtones in this band and that the Q measurements here reflect properties of the fundamental modes only. The previous comparison of the observed and synthetic spectra also indicated this. Above 4.3 mHz the instabilities in the data are probably due as much to low signal levels as to overtones. Below 2.8 mHz, or for angular orders ℓ less than 20, the observed curves show instabilities comparable with the synthetic ones. In particular, Figures 3.7 and 3.9 both have a large spike near 2.4 mHz. This spike coincides with the prominent contamination near ${}_0S_{15}$ which is seen in both spectra (Figs. 3.3 and 3.8). Because the overtones corrupt the data below 2.8 mHz, and because resolution of Q below this frequency is limited by the window length, accurate estimates of fundamental mode Q for angular orders

less than 20 cannot be obtained from the TRN record.

Why are the overtones between ${}_0S_{20}$ and ${}_0S_{36}$ weaker in the data than in the synthetic? The discrepancy may be due in part to the velocity and attenuation models employed. Errors in the assumed source model, however, are likely to be chiefly responsible. A point source at 40 km depth has been used here. Moving the source up to 15 km would increase the fundamental mode excitation in this range, while decreasing that of the overtones. The effect on the lower frequency modes would not be as large, so the overtones would remain significant there. The Sumbawa earthquake produced a tsunami, indicating that the rupture extended to the surface. A finite rupture extent would be more realistic. Given and Kanamori [1980] argued that the faulting extended from the surface to below 60 km depth. Evidence on the contribution of overtones to the TRN seismogram is somewhat indirect, based largely on the stability of the attenuation measurements. Still, the results here suggest that antipodal records may prove useful for studying seismic sources as well as Earth structure.

Mode Coupling

Another possible cause of contamination in the TRN attenuation measurements is mode coupling. If two normal mode multiplets of a spherical Earth model have nearly equal eigenfrequencies, then small perturbations to the model will result in an interaction between the

two multiplets which can drastically alter the eigenfrequency, eigenfunction and Q of each [Dahlen, 1968, 1969; Luh, 1973, 1974]. Realistic perturbations to existing Earth models would include rotation, ellipticity, aspherical structure and anisotropy. Dahlen [1969] suggested that mode coupling between the fundamental spheroidal and toroidal branches may be significant between angular orders 10 and 25. In this band a mode ${}_0S_\ell$ is nearly degenerate with ${}_0T_{\ell+1}$. Woodhouse [1980] showed that coupling depends on the attenuation rates of the modes involved as well as their frequency spacing. Masters et al. [1983] tested the effects of rotation, ellipticity and lateral heterogeneity on the coupling between modes in the fundamental spheroidal and toroidal branches. They concluded that the Coriolis force due to the Earth's rotation dominates the coupling behavior for angular orders less than 40. This coupling is most efficient between nearest neighbor ${}_0S_\ell$ and ${}_0T_{\ell\pm1}$ modes. The coupled multiplets both display mixed spheroidal and toroidal character [Dahlen, 1969].

Masters et al. [1983] calculated the shifts in center frequency and Q of the ${}_0S_\ell$ modes of 1066A induced by rotation and ellipticity coupling. The modes ${}_0S_{10}$ to ${}_0S_{20}$ were shifted noticeably towards lower Q, with especially large shifts for ${}_0S_{11}$ and ${}_0S_{19}$. These two modes are very close in frequency to ${}_0T_{12}$ and ${}_0T_{20}$, respectively. A large shift in Q was also found for ${}_0S_{32}$, but the predicted coupling of this mode to ${}_0T_{31}$ is very sensitive to the reference model and 1066A may not be sufficiently accurate for these

modes [Masters et al., 1983]. Except for ${}_0S_{32}$, the Q of the fundamental spheroidal modes beyond angular order 20 were not significantly affected by coupling.

Besides changing the frequency and Q of a mode, coupling can alter its eigenfunction. Coriolis coupling imparts a vertical component to the toroidal mode eigenfunctions [Dahlen, 1969]. As a result toroidal modes may sometimes be observed on vertical records [Masters et al., 1983]. In most such cases they should have an effect on the vertical spectrum comparable to that of the spheroidal overtones. No attempt has been made to model the effects of coupled toroidal modes on the TRN attenuation results. Such effects could only be important between ${}_0S_{10}$ and ${}_0S_{20}$, where the coupling is strong, and would act in addition to the contamination caused by the spheroidal overtones. It is suggestive that the TRN data (Fig. 3.7) show a large spike in Q near the frequency of ${}_0S_{11}/{}_0T_{12}$, one of the most strongly coupled mode pairs.

The Q measurements from the TRN record are compared in Figure 3.7 to the Q of the corresponding fundamental spheroidal modes for the Preliminary Reference Earth Model (PREM) of Dziewonski and Anderson [1981]. The PREM Q were modeled to agree with the highest quality great circle data. The TRN data give substantially lower Q than the PREM model over their full range of stability, between modes ${}_0S_{20}$ and ${}_0S_{36}$. In this range the TRN data are not contaminated by overtones or by coupled toroidal modes. Like the PTO results of Chapter 1, the raw

TRN Q may be significantly biased due to the effects of lateral heterogeneities. In the next chapter, observations of the actual aspherical component of the Earth's structure are exploited to estimate this bias.

Chapter 4

MODELING THE TRN RECORD FOR THE HETEROGENEOUS EARTH

A physical explanation of the bias in antipodal Q measurements induced by a laterally heterogeneous structure was presented in the Introduction to Chapter 2 of this thesis. In that chapter, the bias in Q from the PTO record was constrained using the consistency of those Q results without any a priori knowledge about the distribution and magnitude of the heterogeneities. This was done because there were no reliable observations of the lateral phase velocity variations in the period range of those measurements (120 to 250 s).

Measurements of Q from the TRN record of the Sumbawa earthquake (Fig. 3.7) yielded abnormally low values which certainly include some bias due to lateral heterogeneities. In this chapter, the bias is studied by realistically modeling the effects of the Earth's aspherical structure on the TRN record. To do this, recent observations of the lateral Rayleigh wave phase velocity variations at periods between 205 and 630 s [Masters et al., 1982] are exploited. These observations employed a large body of data which produced well-resolved, consistent results.

The propagation of surface waves on a slightly heterogeneous sphere has been studied by Dahlen [1979a, 1980] using first order perturbation theory. A routine based on this theory is used to

generate a synthetic of the TRN record which incorporates the heterogeneity effects observed by Masters et al. [1982].

Measured Heterogeneity

Masters and Gilbert [1982] measured the eigenfrequencies of the fundamental modes ${}_0S_8$ to ${}_0S_{46}$ from 557 digital IDA records. An average of 118 reliable measurements were made for each mode. In a subsequent study, Masters et al. [1982] examined the lateral heterogeneity of the Earth by plotting these eigenfrequency measurements as a function of the orientation of the great circle connecting the epicenter and station. The orientation of a great circle is defined by the colatitude Θ and longitude Φ of its positive pole. The eigenfrequency $\omega_\ell(\Theta,\Phi)$ of the mode ${}_0S_\ell$ observed along a specified great circle can be expressed as

$$\omega_\ell(\Theta,\Phi) = \bar{\omega}_\ell + \delta\omega_\ell^{ell}(\Theta) + \sum_{s=2}^{\infty} P_s(0) \sum_{t=-s}^{s} (\delta\omega_\ell^{local})_s^t \, Y_s^t(\Theta,\Phi) \qquad 4.1$$

where $Y_s^t(\Theta,\Phi)$ are the normalized surface spherical harmonics defined by Edmonds [1960], $(\delta\omega_\ell^{local})_s^t$ are the coefficients of the harmonics, P_s are Legendre polynomials, and $\bar{\omega}_\ell$ is the degenerate eigenfrequency of the spherically symmetric component of the Earth's structure. The term $\delta\omega_\ell^{ell}(\Theta)$ represents the perturbation to the eigenfrequency due to the Earth's ellipticity of figure. This is given by [Dahlen, 1975]

$$\delta\omega_\ell^{ell}(\Theta) = \bar{\omega}_\ell \chi_\ell (1-3\cos^2\Theta) \qquad 4.2$$

The ellipticity splitting parameter χ_ℓ appropriate here is obtained by dividing the parameter $\chi_2(T)$, tabulated in Dziewonski and Sailor [1976], by the factor c/U (the ratio of phase to group velocity). In this analysis the perturbation to the degenerate eigenfrequency reflects the influence of lateral variations in elastic parameters. Equation 4.1 is valid in the geometric optics limit, i.e., when the wavelength of the heterogeneity is much greater than that of the mode [Jordan, 1978].

The heterogeneity harmonics with odd angular order (s-odd) do not affect great circle eigenfrequency measurements [Backus, 1964]. This property is included in Equation 4.1 through the factor $P_s(0)$, which vanishes for odd s. Because of this, great circle data cannot be inverted to give the coefficients of the odd-order harmonics of the heterogeneity. Furthermore, the effects of the lower even-order harmonics are preferentially emphasized on such measurements [Kawakatsu, 1983; Nakanishi and Anderson, 1983a]. The factor $P_s(0)$ decreases uniformly with increasing even values of s. The resolution should thus be best for the lower order coefficients.

Masters et al. [1982] performed least-squares inversions of the ellipticity-corrected eigenfrequency data of Masters and Gilbert [1982] to obtain the degenerate eigenfrequencies $\bar{\omega}_\ell$ and the harmonic

coefficients $(\delta\omega_\ell^{local})_s^t$. Three consecutive modes were included in each inversion to stabilize the results. The inversions were done first with $s_{max}=2$ (degree-two inversion) and then again with $s_{max}=6$ (degree-six inversion). The degree-two inversions gave a median variance reduction of 60% for the modes ${}_0S_9$ to ${}_0S_{42}$. The degree-six inversions offered no real improvement on this, so only the degree-two results were presented and discussed in detail. The data and best-fitting degree-two pattern for the mode triplet $\ell=21,22,23$ are shown in Figure 4.1. The data are plotted as deviations from the estimated degenerate eigenfrequencies. The patterns were very consistent over the range of modes studied.

Because the very nature of their experiment excluded the odd-order and emphasized the lower even-order harmonics, the true geographic pattern of the heterogeneity cannot be determined from the results of Masters et al. [1982]. Those authors suggested that a heterogeneity localized at 420 to 670 km depth would explain the data. However, Kawakatsu [1983] and Souriau and Souriau [1983] have since shown that some regionalized Earth models would give similar patterns, and certainly the heterogeneities observed at the Earth's surface (e.g., continents and oceans) have some effect. The regionalized Earth models assume that the heterogeneity at depth correlates perfectly with that at the surface, and this may not be valid. The patterns observed by Masters et al. [1982] do not lend themselves to unambiguous geophysical interpretations.

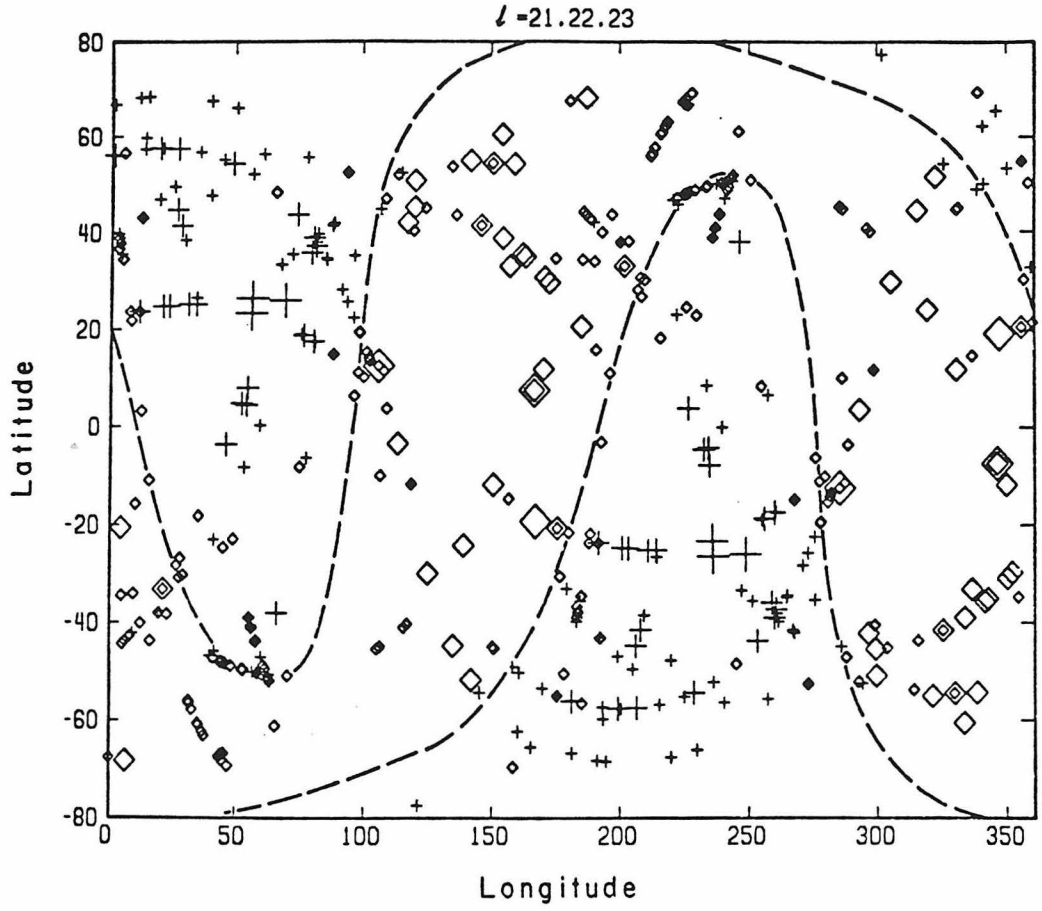

Figure 4.1 Center frequency measurements of the mode ${}_oS_{22}$ plotted at the poles of the great circles between sources and stations. The data are plotted as deviations from their harmonic average value. Positive deviations are denoted by plus signs, negative deviations by diamonds. Symbol size gives the magnitude of the deviation. Dashed curves are the nodes of a spherical harmonic inversion of the data. From Masters et al. [1982].

On the other hand, the results of Masters et al. [1982] are useful here simply as observations of the effects of lateral heterogeneities on great circle phase velocities. The degree-two harmonic coefficients can be used to estimate the deviation of the phase velocity from its average value which would be observed for any particular great circle. The data and the degree-two coefficients give very similar geographic patterns (Fig. 4.1). The variance reduction (>60%) realized by the harmonic expansion is comparable to that of the best regionalized Earth models [Souriau and Souriau, 1983; Nakanishi and Anderson, 1983a] and it demonstrates the accuracy with which a given great circle's behavior can be predicted. An antipodal signal can be thought of as the 'stack' of a continuum of great circle signals, combining the energy radiated at all azimuths from the source. The signal recorded at the antipode is sensitive only to the cumulative effects of propagation around complete orbits of the great circles. To accurately model the effects of the Earth's true lateral heterogeneity on an antipodal seismogram, then, one need only be able to predict the average phase velocity of any great circle through the source. Knowledge of the actual geographic distribution of the heterogeneities is not required. The event's radiation pattern can then be incorporated to generate the weighted stack of the energy arriving at the antipode from all azimuths, i.e., the antipodal seismogram. The degree-two harmonic coefficients of Masters et al. [1982] provide the necessary mechanism for doing this.

Theory

Many authors have studied the effects of aspherical structure on the Earth's normal modes [Usami, 1971; Woodhouse and Dahlen, 1978; Geller and Stein, 1978; Dahlen, 1979a, 1980; Woodhouse and Girnius, 1982]. The theory discussed in this section was developed by Dahlen [1979a, 1980] and is employed in the following section to generate a realistic synthetic of the TRN seismogram.

The vertical component of the normal mode multiplet ${}_0S_\ell$ at the observation point $\underline{r}$ is obtained by summing the constituent singlets

$$S(\underline{r},t) = -\sum_{j=-\ell}^{\ell} A^j(\underline{r})c^j(t) \qquad 4.3$$

Each singlet has a time domain form given by

$$c^j(t) = \exp(-\alpha t)\cos(\omega^j t) \qquad 4.4$$

where α is the attenuation coefficient and ω^j is the eigenfrequency of the j^{th} singlet. The attenuation is assumed to be spherically symmetric: only lateral perturbations in the elastic parameters are considered here. A singlet's amplitude is determined from

$$A^j(\underline{r}) = \underline{M}:\underline{\varepsilon}^j(\underline{r}_s)s^j(\underline{r}) \qquad 4.5$$

[Gilbert, 1970] where $\underline{M}$ is the source moment tensor (a step function source is assumed), $s^j(\underline{r})$ is the vertical component of the singlet eigenfunction and $\underline{\varepsilon}^j(\underline{r}_s)$ is the strain tensor at the source associated with the j^{th} eigenfunction. On a spherically symmetric Earth the eigenfrequencies are degenerate: $\omega^j=\overline{\omega}$. The eigenfrequencies ω^j and the eigenfunctions s^j of a slightly aspherical Earth are determined using perturbation theory. (See Butkov [1968] for a discussion of perturbation theory in the case of degenerate eigenvalues.) The first order eigenfrequencies are expressed as

$$\omega^j = \overline{\omega} + \delta\omega^j \qquad 4.6$$

and the zeroth order eigenfunctions are linear combinations of the orthogonal eigenfunctions chosen for the unperturbed spherical Earth

$$s^j = \sum_{m=-\ell}^{\ell} b_m^j \, s^m \qquad 4.7$$

The index m represents parameters of the spherical Earth, j the perturbed Earth. The quantities $\delta\omega^j$ and $\underline{b}^j=(b_{-\ell},\ldots,b_{\ell})^j$ are the eigenvalues and eigenvectors of the perturbation matrix $\underline{H}$, i.e.,

$$\sum_{m'=-\ell}^{\ell} H_{mm'}b_{m'}^j = \delta\omega^j \, b_m^j \qquad 4.8$$

$\underline{H}$ is a $2\ell+1$ by $2\ell+1$ Hermitian matrix whose elements are linear functions of the perturbation.

To calculate the synthetic seismogram for a heterogeneous Earth model, begin by determining the eigenfrequency $\bar{\omega}$ and eigenfunctions s^m of a mode of the unperturbed spherical model [Alterman et al., 1959]. Specify the desired perturbations to this model, and from these perturbations calculate the matrix elements $H_{mm'}$, using the formulas given by Woodhouse and Dahlen [1978]. Then invert the matrix $\underline{H}$ to find its eigenvalues $\delta\omega^j$ and associated eigenvectors $\underline{b}^j$. Substitute into Equations 4.6 and 4.7 to find the eigenfrequency and eigenfunction of each singlet, and then into 4.4 and 4.5 to determine each singlet's time series. Finally, sum the singlets to produce the entire multiplet (Eqn. 4.3). This process must be repeated for all angular orders ℓ to obtain the complete fundamental mode seismogram.

Unfortunately, there are some drawbacks to using the theory as it stands. To begin with, a routine to implement this procedure would be computationally intensive. The evaluation of each matrix element $H_{mm'}$ would involve a numerical integration of the perturbations to the elastic parameters [Woodhouse and Dahlen, 1978]. Next would follow an inversion of the $2\ell+1$ by $2\ell+1$ matrix $\underline{H}$, with consequent considerations of numerical stability. The evaluation and inversion of $\underline{H}$ would have to be done separately for each multiplet included in the synthetic. The most serious drawback is that the velocity and density

perturbations must be specified as functions of location. In the previous section it was argued that this cannot be unambiguously done using existing observations. At present, the heterogeneity can only be characterized by its effect on great circle averages of the Rayleigh wave phase velocity. Further development of the theory is necessary.

Dahlen [1979a, 1980] has extended the theory through an asymptotic approximation of the singlet sum in Equation 4.3

$$S(\underline{r},t) = -\exp(-\alpha t) \int_0^{2\pi} a(\underline{r},\psi)\cos(\omega_\ell(\psi)t)d\psi \qquad 4.9$$

Here, ψ is the take-off azimuth at the source (measured counterclockwise from south). The time dependence of this expression is identical in form to that of Equation 4.3, except that the singlet eigenfrequency ω^j there is replaced by $\omega_\ell(\psi)$, which is the apparent center frequency of ${}_0S_\ell$ observed along the great circle at azimuth ψ. The great circle at azimuth ψ from the source $\underline{r}_s$ has a pole at $(\Theta(\psi),\Phi(\psi))$, so that

$$\omega_\ell(\psi) = \omega_\ell(\Theta(\psi),\Phi(\psi)) = \omega_\ell(\Theta,\Phi) \qquad 4.10$$

Equation 4.1 and the coefficients tabulated in Masters et al. [1982] can be used to determine $\omega_\ell(\Theta,\Phi)$. The term $a(\underline{r},\psi)$ in Equation 4.9 incorporates the source moment tensor and geometrical spreading.

Explicit formulas for $a(\underline{r},\psi)$ for all three components of motion are given in Equations 75-80 of Dahlen [1980].

Equation 4.9 can be viewed as a diffraction integral over all ray directions from the source. Along any particular direction, a ray travels at the average phase velocity for that great circle. Each ray is weighted by the source radiation pattern and by the asymptotic geometrical spreading factor $\sqrt{\Delta/\sin\Delta}$. There is an additional component to the weighting term $a(\underline{r},\psi)$ which, away from the epicenter and its antipode, is highly oscillatory except near the azimuths of the minor and major great circle arcs to the station. Because of this oscillatory term, the dominant contribution to the motion at some distance from the source and its antipode comes from the great circle connecting the source and station, as expected. Approaching the epicenter or the antipode this oscillatory behavior diminishes. In these regions the observed signals are formed by the interference of the arrivals from all azimuths. The aspherical perturbation to the Earth affects only the time-dependent term of Equation 4.9, by altering $\omega_\ell(\psi)$. The amplitude term $a(\underline{r},\psi)$ is unchanged by the heterogeneity. This is the result of using perturbation theory to first order in the eigenfrequencies and zeroth order in the eigenfunctions.

There are four formal conditions which must be met for the theory presented here to be valid. The theory is appropriate for the surface-wave-equivalent modes ${}_nS_\ell$, for which

$$n << \ell \qquad 4.11a$$

The truncated perturbation theory imposes the restrictions

$$|\delta m/m_o| << 1 \qquad 4.11b$$

and

$$\ell << \frac{s_{min}}{|\delta m/m_o|} \qquad 4.11c$$

The first of these is the standard perturbation theory constraint that the perturbations δm to the original model parameters m_o be small. In the next condition (Eqn. 4.11c) s_{min} is the minimum significant degree in the harmonic expansion of the heterogeneity. This condition results from using zeroth order eigenfunctions: at high frequencies (large ℓ) these become poor approximations of the true eigenfunctions of the perturbed model [Dahlen, 1979c]. The asymptotic approximations of Equations 4.1 and 4.9 require that

$$s_{max} << \ell \qquad 4.11d$$

where s_{max} is the maximum significant degree of the heterogeneity. This is the geometrical optics condition which states that the wavelengths must be much shorter than the smallest heterogeneity length scale. The restrictions here are equivalent to the assumption

that lateral refractions and scattering of the surface waves are negligible. The waves propagate around great circle paths at the average velocity dictated by the heterogeneity distribution.

Measurements from the TRN record represented the fundamental (n=0) spheroidal modes with angular orders $\ell \geq 10$, so condition 4.11a is satisfied. The extent to which the other conditions are satisfied is less clear, because all three require a knowledge of the heterogeneity. The observations of Masters et al. [1982] (Fig. 4.1) show that the patterns of great circle average phase velocities are dominated by the harmonics of low angular order, suggesting that condition 4.11d is met. Individual measurements deviated by less than 0.4% from the mean for any mode, so the perturbations should be sufficiently small (condition 4.11b). Using $s_{min}=2$, condition 4.11c becomes

$$|\delta m/m_o| \ll 2/\ell \qquad 4.12$$

For angular orders ℓ below 40, the right-hand side of this expression is above 5%. This is more than an order of magnitude greater than the deviations in the phase velocity measurements. Observations of the effects of the Earth's lateral variations therefore indicate that the restrictions to the theory above are all reasonably well satisfied.

Modeling

Two synthetic versions of the TRN seismogram were generated in order to evaluate the bias in measurements from that record. The first synthetic was for a spherically symmetric Earth. The modes ${}_0S_4$ to ${}_0S_{60}$ of the elastic model 1066A [Gilbert and Dziewonski, 1975] were summed to produce this synthetic, using the mode Q values given by PREM [Dziewonski and Anderson, 1981]. The Sumbawa event was represented as a point source at 45 km depth with a focal mechanism as determined by Given and Kanamori [1980]. The second synthetic modeled the laterally heterogeneous Earth: it was generated by substituting the best-fit patterns of the lateral eigenfrequency variations of Masters et al. [1982] (Eqn. 4.1) into the asymptotic integral of Equation 4.9. This integral was evaluated numerically for the modes ${}_0S_4$ to ${}_0S_{60}$, although the heterogeneity effect was included only for ${}_0S_9$ to ${}_0S_{42}$. Except for the heterogeneity the second synthetic used the same Earth and source parameters as the first. Both synthetics covered the same 17.5 hour time span as the original record.

Figure 4.2 shows the first 8 hours of the spherical and heterogeneous Earth synthetics as well as the actual TRN data. Comparing the peak-to-peak amplitude of the data with that of the heterogeneous Earth synthetic gave a seismic moment of 3.5×10^{28} dyne-cm for the Sumbawa earthquake. This is in close agreement with the values determined by Given and Kanamori [1980] and Silver and

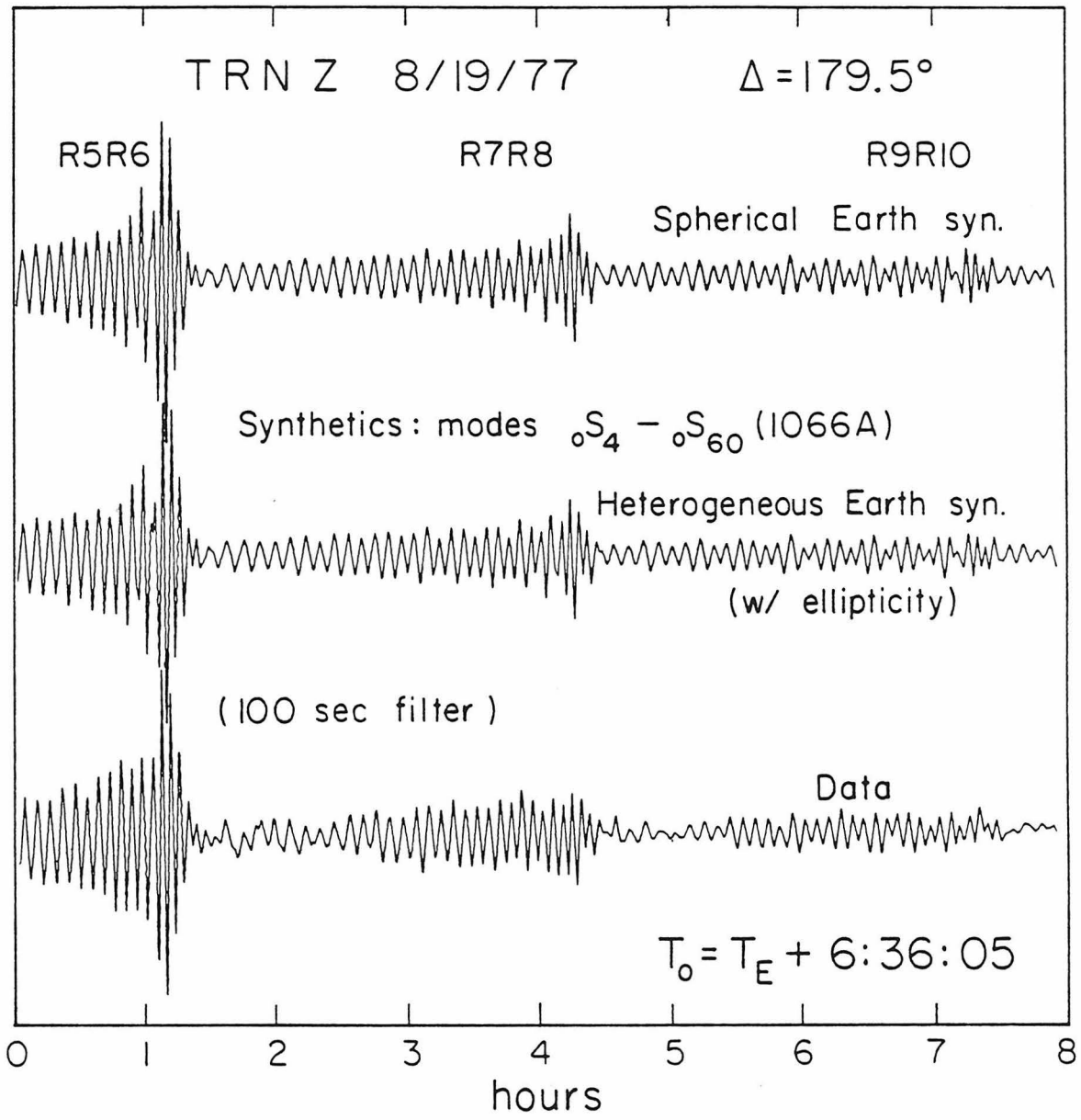

Figure 4.2 Synthetics of the TRN seismogram of the Sumbawa earthquake (Δ=179.5°). The topmost trace is the synthetic for a spherical Earth model. The middle trace includes the effects of the heterogeneity observed by Masters et al. [1982] and the Earth's ellipticity. The actual TRN record is shown at the bottom.

Jordan [1983] (4.0 and 2.4 $\times 10^{28}$ dyne-cm, respectively). Qualitatively both synthetic waveforms give good fits to the data. Amplitude and phase match very well across the entire window. Most striking in Figure 4.2 is the agreement near the Airy phases of the R5R6 and R7R8 arrivals. Surprisingly, the heterogeneous Earth synthetic is virtually indistinguishable from the spherical Earth one. Introducing the heterogeneity provides no visual improvement of the fit between data and synthetic. The heterogeneity does however have an appreciable effect on attenuation and dispersion measurements made from the synthetics.

Analysis of the synthetics for attenuation and dispersion followed the same procedure used on the data (Chapter 3). Phase and group velocities for the spherical Earth synthetic were identical to the 1066A values, as they should have been. This was a reassuring test of the measurement techniques. The apparent Q for the spherical Earth synthetic is plotted in Figure 4.3. This figure shows the results for both boxcar (solid line) and Hanning (dashed line) windowing of the trace. Ideally, one would like to recover the PREM values (open circles). The finite record length causes the measured curves to diverge from PREM at low frequencies, an effect which must be taken into account. The boxcar window is clearly superior to the Hanning for measuring Q, since it introduces less bias from the true values. In the frequency domain, the boxcar has a much narrower main lobe than the Hanning (Oppenheim and Schafer, 1975), so convolving its

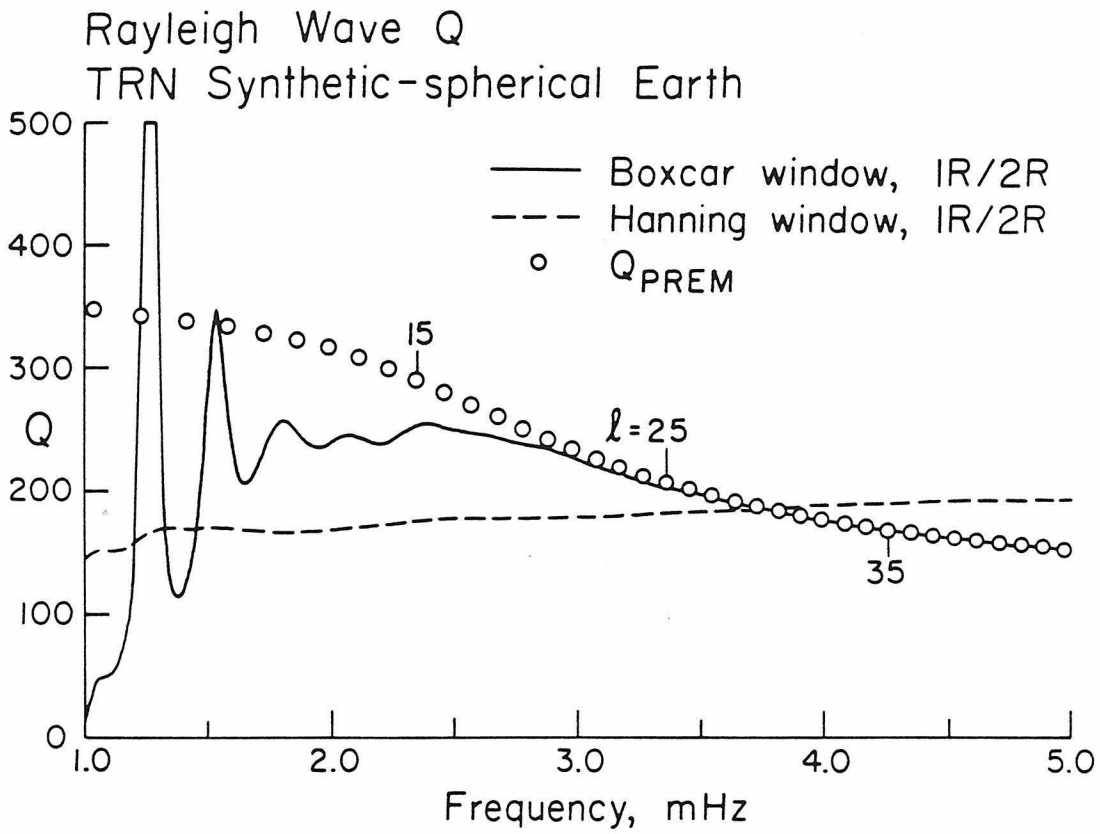

Figure 4.3 Q measured from the spherical Earth synthetic of the TRN record. The dashed curve is the result when the synthetic is Hanning windowed. The solid curve results from boxcar windowing. The open circles give Q of the modes ${}_0S_\ell$ for the PREM model, which was used to generate the synthetic.

spectrum with that of the data has a smaller effect on the widths of the normal mode peaks. This contradicts Masters and Gilbert [1982], who asserted that Q measurements from boxcar windowed traces are unreliable.

Figures 4.4 and 4.5 show respectively the phase and group velocities measured from the heterogeneous Earth synthetic. The deviations of the curves from their 1066A baselines is due to the combined effects of lateral velocity variations and the Earth's ellipsoidal shape. The Q taken from the heterogeneous Earth synthetic are shown in Figure 4.6. The two curves show the 1R/2R and 1R/3R measurements, based on spectral ratios of the autocorrelogram 'arrivals' (see Chapter 3). The difference between these curves is negligible, despite the significant bias of both curves from the PREM values. This implies that the separation of the 1R/2R and 1R/3R curves is not a sufficiently sensitive indicator of the amount of bias due to heterogeneity. Estimating the bias in the TRN Q measurements requires independent knowledge of the magnitude of lateral velocity variations. If the observations of Masters et al. [1982] are reliable, then the shift of the curves in Figure 4.6 from the PREM Q trend should be an accurate measure of the bias in Q from the TRN record.

Figures 4.4, 4.5 and 4.6 demonstrate that the Earth's lateral heterogeneity can bias antipodal estimates of dispersion and attenuation away from the proper global average values. The amount of

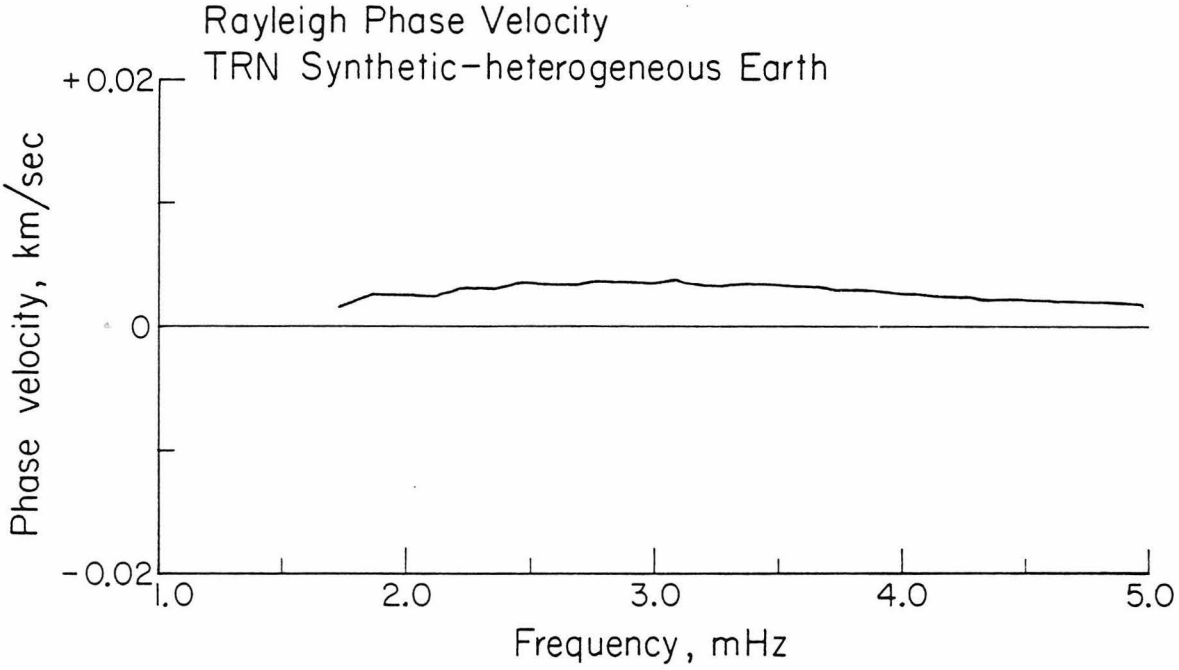

Figure 4.4 Phase velocity measured from the heterogeneous Earth synthetic. The zero line corresponds to 1066A, the spherical Earth base model used in the synthesis.

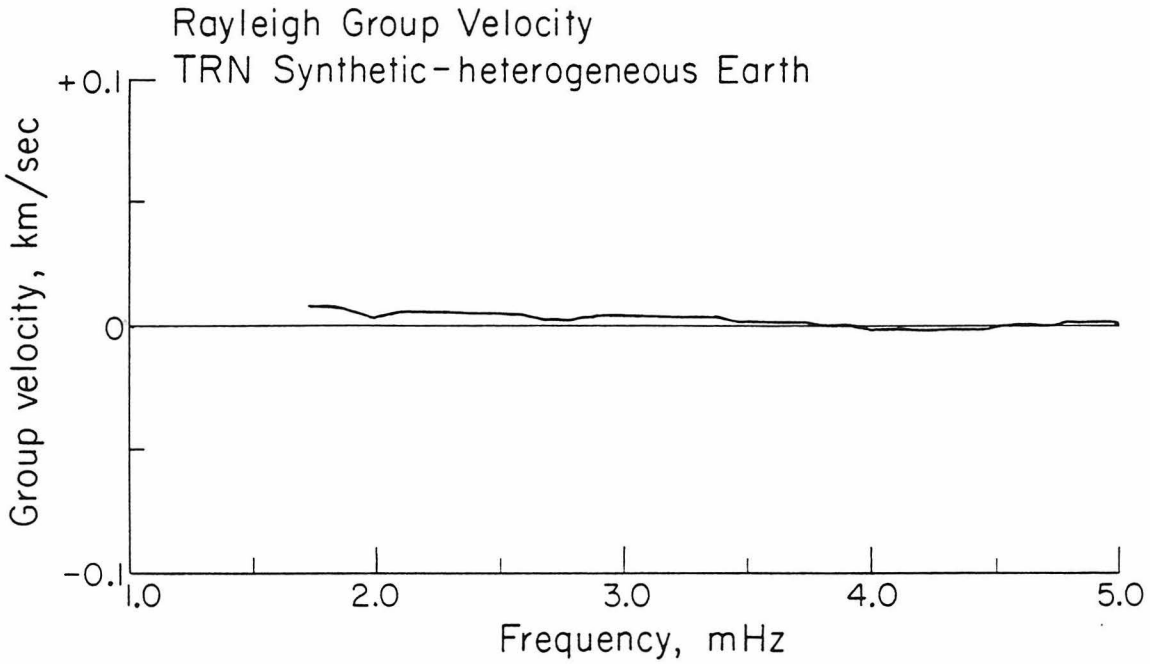

Figure 4.5 Group velocity measured from the heterogeneous Earth synthetic. The zero line corresponds to 1066A, the spherical Earth base model used in the synthesis.

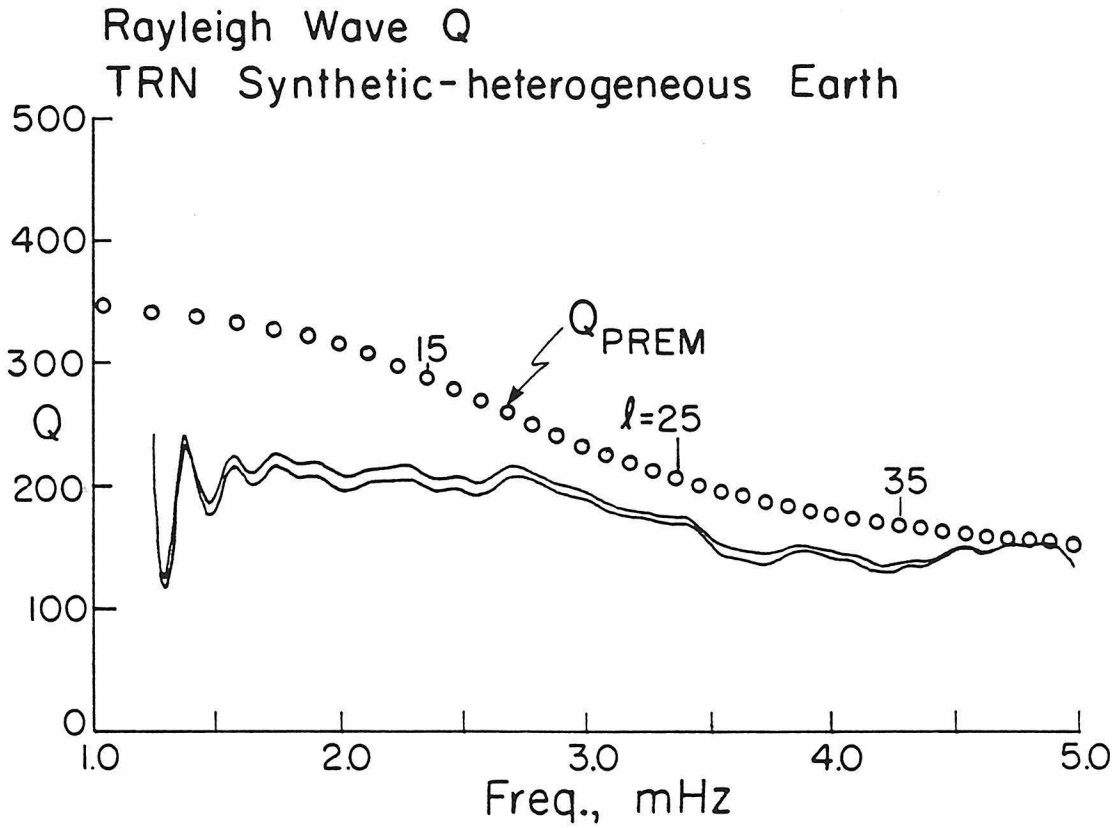

Figure 4.6 Q measured from the heterogeneous Earth synthetic (boxcar windowed). The upper and lower solid curves give the 1R/2R and 1R/3R results. The PREM Q were used to produce the synthetic.

bias in such measurements should depend on the manner in which the Earth's lateral heterogeneity is sampled. The exact nature of the sampling is a function of both the event's location and its radiation pattern. The error bounds on focal mechanism determinations are usually rather large, and observations of surface wave amplitude as a function of azimuth deviate widely from the predicted radiation patterns. Because of this it is important to consider the sensitivity of the dispersion and attenuation biasing to changes in the focal mechanism. P-wave first motions for the Sumbawa event dictate a dominantly normal slip mechanism, but leave large uncertainties in the strike. Heterogeneous Earth synthetics were generated for different values of fault plane strike, with all other model parameters held constant.

The phase velocity biasing was found to be very sensitive to the focal mechanism. A rotation of the strike by only 30^{o} sufficed to change the phase velocity residuals from the significant positive values plotted in Figure 4.4 to slightly negative values. Because of this sensitivity, the antipodal phase velocity measurements are subject to large uncertainties (>0.1%) even if the heterogeneity is well known. Averages from a large number of conventional great circle measurements have standard errors of about 0.05%. One must conclude that individual antipodal records cannot be used to determine improved average Earth phase velocities.

The group velocity deviations induced by the heterogeneity

(Fig. 4.5) are less than 0.01 km/s at all frequencies, near the level of the intrinsic errors in measurements from the TRN data. The magnitude of the group velocity bias was no larger than this for any fault plane orientation. In other words, lateral heterogeneities apparently cause no resolvable biasing of antipodal group velocities. The bias in antipodal Q values is significant (Fig. 4.6), but tests showed the bias to be virtually insensitive to focal mechanism variations. The bias is always toward lower Q: it is a function of the change in phase velocity over the azimuth range sampled, not of the average phase velocity in that range.

Results

Table 4.1 lists the observed eigenperiods of the modes ${}_0S_8$ to ${}_0S_{40}$. The periods were estimated directly from the peaks in the spectrum of the Hanning-windowed TRN trace. They are in general agreement with the phase velocities obtained in a residual dispersion analysis of the record (Fig. 3.5). No corrections have been made for bias in the center frequencies due to sampling of the Earth. Modeling has shown such bias to be very sensitive to the event's radiation pattern.

Analysis of synthetic seismograms demonstrates that the actual TRN record should produce unbiased group velocity estimates. The observed group velocity values (Fig. 3.6) for the modes ${}_0S_{10}$ to ${}_0S_{43}$

Table 4.1 - Mode ${}_0S_\ell$ Eigenperiod

ℓ	Period[a], s	1066A[b]	PREM[c]
8	709.26	707.82	707.47
9	632.59	633.95	633.61
10	578.94	579.55	
11	538.95	537.26	536.94
12	502.58	502.72	502.42
13	472.16	473.55	473.28
14	447.65	448.40	448.15
15	426.67	426.40	426.19
16	406.55	406.98	406.80
17	389.17	389.69	389.55
18	374.06	374.19	374.07
19	360.09	360.21	360.11
20	347.12	347.51	347.42
21	335.74	335.90	335.83
22	325.08	325.25	325.18
23	315.08	315.40	315.34
24	306.24	306.27	306.20
25	297.87	297.75	297.68
26	289.47	289.78	289.70
27	282.48	282.29	282.20
28	274.90	275.23	275.13
29	268.59	268.55	268.44
30	262.14	262.21	262.09
31	256.40	256.19	256.06
32	250.14	250.46	250.32
33	244.90	244.98	244.83
34	239.88	239.74	239.59
35	235.06	234.73	234.57
36	230.11	229.92	229.76
37	225.36	225.30	225.14
38	221.11	220.87	220.70
39	216.72	216.59	216.43
40	212.78	212.48	212.32

[a]From spectrum of Hanning-windowed TRN record.
[b]Gilbert and Dziewonski [1975].
[c]Dziewonski and Anderson [1981].

are compiled in Table 4.2, together with the observed averages of Dziewonski and Steim [1982] and the values for the models 1066A and PREM. The various values agree to within 0.01 km/s across most of the range. For modes ${}_0S_{30}$ to ${}_0S_{36}$, the TRN group velocities are slower than those of Dziewonski and Steim [1982] by about 0.02 km/s. Results in this range from the PTO antipodal record (Chapter 1) show almost no difference from the Dziewonski and Steim [1982] values. The discrepancies between the group velocity estimates are always below 0.6%. Because of the intrinsic errors in measuring group velocities from the TRN record, the results here do not improve the resolution of global average group velocities provided by conventional studies. Such studies obtain small standard errors by averaging measurements from many different paths which differ by only a few percent. Still, it is rather remarkable that results from individual antipodal seismograms agree as closely as they do with the averages of other studies. This is strong evidence that the antipode 'sees' average global properties and that the lateral heterogeneities have a relatively small effect on the focusing.

Modeling the effects of a laterally varying Earth has shown that the Q estimates from the TRN record are biased toward low Q by about 20% for the modes ${}_0S_{20}$ to ${}_0S_{36}$ (Fig. 4.6). In Figure 4.7 the observed Q are compared to the apparent Q of the heterogeneous Earth synthetic (plotted as a heavy line which averages the two curves of Fig. 4.6). From ${}_0S_{20}$ to ${}_0S_{36}$ the observed and synthetic trends agree

Table 4.2 - Mode ${}_0S_\ell$ Group Velocity

ℓ	U^a, km/s	$U_{1066A}{}^b$	$U_{PREM}{}^c$	$U_{DS}{}^d$
10	5.67	5.65	5.648	5.654
11	5.29	5.26	5.254	5.255
12	5.04	5.00	4.997	5.001
13	4.84	4.82	4.813	4.819
14	4.68	4.67	4.665	4.672
15	4.54	4.54	4.533	4.542
16	4.41	4.42	4.411	4.421
17	4.30	4.31	4.298	4.310
18	4.19	4.20	4.193	4.204
19	4.11	4.11	4.097	4.109
20	4.02	4.02	4.011	4.021
21	3.94	3.94	3.934	3.944
22	3.87	3.87	3.866	3.875
23	3.81	3.81	3.808	3.816
24	3.76	3.76	3.758	3.765
25	3.72	3.72	3.716	3.722
26	3.68	3.68	3.681	3.687
27	3.65	3.65	3.652	3.658
28	3.62	3.63	3.629	3.633
29	3.60	3.61	3.611	3.614
30	3.58	3.59	3.597	3.600
31	3.57	3.58	3.586	3.588
32	3.56	3.58	3.578	3.580
33	3.55	3.57	3.573	3.574
34	3.55	3.57	3.569	3.571
35	3.55	3.57	3.568	3.569
36	3.55	3.57	3.568	3.569
37	3.56	3.57	3.569	3.570
38	3.56	3.57	3.571	3.572
39	3.57	3.58	3.573	3.575
40	3.57	3.58	3.577	3.578
41	3.59	3.59	3.580	3.582
42	3.59	3.59	3.584	3.586
43	3.60	3.60	3.588	3.591

[a] From residual dispersion analysis (Fig. 3.6).
[b] Gilbert and Dziewonski [1975].
[c] Dziewonski and Anderson [1981].
[d] Dziewonski and Steim [1982].

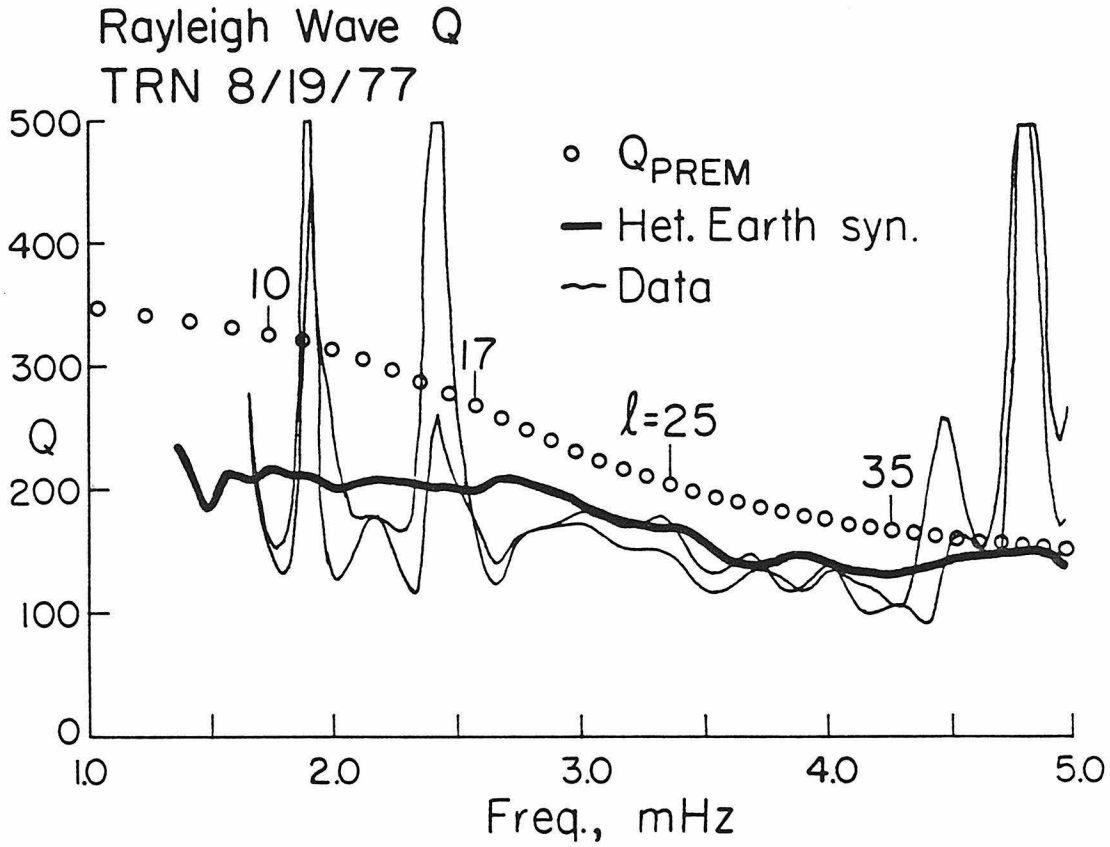

Figure 4.7 Comparison of Q measured from the observed TRN record (light curves) and from the heterogeneous Earth synthetic (heavy curve).

closely. If the Earth's lateral heterogeneities are faithfully reflected in the observations of Masters et al. [1982], then this agreement means that the globally-averaged attenuation is accurately represented by the PREM Q. Dziewonski and Steim [1982], using conventional great circle data, obtained average Q values which also support the PREM model in this range.

By themselves the TRN measurements of apparent Q constrain only the trade-off between intrinsic attenuation and the magnitude of lateral velocity variations. Higher intrinsic Q would require a more heterogeneous Earth (a greater range in great circle phase velocities) in order to explain the antipodal data. Masters and Gilbert [1982] obtained average Q values which are approximately 10% higher than the averages observed by Dziewonski and Steim [1982] for the modes ${}_0S_{20}$ to ${}_0S_{36}$. The TRN results indicate that the average Q given by Masters and Gilbert [1982] are incompatible with the heterogeneity observations of Masters et al. [1982]. The heterogeneity introduced in the modeling biased the Q by about 20%. The additional 10% shift necessary to rationalize the TRN results with the average Q of Masters and Gilbert [1982] would thus require an increase of about 50% in the magnitude of the lateral velocity variations. The errors in individual phase velocity measurements are much smaller than the differences between paths, so it would seem unlikely that Masters et al. [1982] underestimated the range in great circle velocities by so much. It seems most reasonable to interpret the TRN data as

supporting average Earth Q for ${}_0S_{20}$ to ${}_0S_{36}$ comparable to the PREM values.

CONCLUSIONS

This thesis has demonstrated that long period antipodal ($\Delta \sim 180^{o}$) seismograms can be used to study global average properties of the Earth. The attenuation and dispersion of surface waves and normal modes have been measured for periods between 100 and 500 s. The aspherical structure of the Earth corrupts the focusing of surface waves at the antipode and complicates the attenuation and dispersion analyses. A beneficial result of this phenomenon is that antipodal records can constrain the aspherical structure.

The antipodal record of the 1968 Inangahua, New Zealand earthquake from station PTO produced measurements of Rayleigh wave Q for periods from 120 to 280 s. The effects of lateral heterogeneities on this record were constrained using the consistency of the Q measured between repeated Rayleigh arrivals. The range in great circle average phase velocities estimated by this method agrees well with observations and with some regionalized Earth models. Corrected for bias, the PTO data yielded an average Earth Q of 127 at a period of 170 s. This is about 10% below the value predicted by the PREM attenuation model [Dziewonski and Anderson, 1981]. The difference between PREM and the PTO results increased slightly at shorter periods and decreased to nearly zero for periods longer than 230 s.

Rayleigh wave attenuation at 250 to 350 s periods was measured from an antipodal record (station TRN) of the 1977 Sumbawa, Indonesia

earthquake. This seismogram was modeled by including the heterogeneity parameters determined by Masters et al. [1982] in an algorithm based on the asymptotic/perturbation theory presented by Dahlen [1979a, 1980]. The apparent Q from a synthetic seismogram for a heterogeneous Earth were compared with the measurements from the data. This comparison demonstrated that global average Rayleigh wave attenuation in the 250 to 350 s band is accurately represented by the PREM model. Extending these results to longer periods will require an antipodal seismogram somewhat longer than the 17.5 hr TRN record.

Analysis of synthetic seismograms for a heterogeneous Earth indicated that antipodal data give nearly unbiased estimates of global average group velocity. Results from the PTO and TRN records agree closely with the best conventional studies [Dziewonski and Steim, 1982; Nakanishi and Anderson, 1982]. A few antipodal seismograms, preferably of longer duration than those used here, could improve existing average Earth group velocity estimates.

The accuracy of the phase velocity and mode eigenfrequency measurements presented in this thesis is limited by the available record lengths. Heterogeneous structure may also have biased the results by as much as 0.1% from global average values. The exact amount of such biasing is strongly dependent on the radiation pattern of the event and thus it cannot be accurately determined. Because of these sources of uncertainty, several antipodal records of long duration (~50 hrs) would be needed to determine accurate average Earth

phase velocities.

Antipodal records of spheroidal overtones and Love waves have also been analyzed. The data presented in this thesis agree well with synthetic seismograms, proving the potential of the antipode for investigating these modes. In addition, the work here suggests that antipodal records are useful for studying mode coupling and earthquake source properties.

REFERENCES

Aki, K. and P. G. Richards (1980). Quantitative Seismology: Theory and Methods, Volume II, pp. 636-639, W. H. Freeman and Co., San Francisco, CA.

Alterman, Z., H. Jarosch and C. L. Pekeris (1959). Oscillations of the Earth, Proc. Roy. Soc. Lond. A, 252, 80-95.

Anderson, D. L. and J. W. Given (1982). Absorption band Q model for the Earth, J. Geophys. Res., 87, 3893-3904.

Anderson, D. L. and R. S. Hart (1978). Attenuation models of the Earth, Phys. Earth Planet. Inter., 16, 289-306.

Anderson, D. L. and J. B. Minster (1981). The physics of creep and attenuation in the mantle, in Anelasticity in the Earth, F. D. Stacey, M. S. Paterson and A. Nicholas, eds., Am. Geophys. Union / Geol. Soc. Am., 5-11.

Anderson, D. L., A. Ben-Menahem and C. B. Archambeau (1965). Attenuation of seismic energy in the upper mantle, J. Geophys. Res., 70, 1441-1448.

Anderson, D. L., H. Kanamori, R. S. Hart and H. P. Liu (1977). The Earth as a seismic absorption band, Science, 196, 1104-1106.

Backus, G. E. (1964). Geographical interpretation of measurements of average phase velocities of surface waves over great circular and great semi-circular paths, Bull. Seism. Soc. Am., 54, 571-610.

Ben-Menahem, A. (1965). Observed attenuation and Q values of seismic

surface waves in the upper mantle, J. Geophys. Res., 70, 4641-4651.

Brune, J. N. (1962). Attenuation of dispersed wave trains, Bull. Seism. Soc. Am., 52, 109-112.

Brune, J. N. and J. Dorman (1963). Seismic waves and Earth structure in the Canadian shield, Bull. Seism. Soc. Am., 53, 167-210.

Brune, J. N., J. E. Nafe and L. E. Alsop (1961). The polar phase shift of surface waves on a sphere, Bull. Seism. Soc. Am., 51, 247-257.

Buland, R., J. Berger and F. Gilbert (1979). Observations from the IDA network of attenuation and splitting during a recent earthquake, Nature, 277, 358-362.

Butkov, E. (1968). Mathematical Physics, pp. 665-669, Addison-Wesley Publ. Co., Inc., Reading, MA.

Dahlen, F. A. (1968). The normal modes of a rotating elliptical Earth, Geophys. J. R. astr. Soc., 16, 329-367.

Dahlen, F. A. (1969). The normal modes of a rotating elliptical Earth - II. Near-resonance multiplet coupling, Geophys. J. R. astr. Soc., 18, 397-436.

Dahlen, F. A. (1975). The correction of great circular surface wave phase velocity measurements for the rotation and ellipticity of the Earth, J. Geophys. Res., 80, 4895-4903.

Dahlen, F. A. (1979a). The spectra of unresolved split normal mode multiplets, Geophys. J. R. astr. Soc., 58, 1-33.

Dahlen, F. A. (1979b). Exact and asymptotic synthetic multiplet spectra on an ellipsoidal Earth, Geophys. J. R. astr. Soc., 59, 19-42.

Dahlen, F. A. (1979c). Geometrical optics and normal mode perturbation theory: a comparison in one dimension, Bull. Seism. Soc. Am., 69, 1391-1407.

Dahlen, F. A. (1980). A uniformly valid asymptotic representation of normal mode multiplet spectra on a laterally heterogeneous Earth, Geophys. J. R. astr. Soc., 62, 225-247.

Dahlen, F. A. (1982). The effect of data windows on the estimation of free oscillation parameters, Geophys. J. R. astr. Soc., 69, 537-549.

Derr, J. (1969). Free oscillation observations through 1968, Bull. Seism. Soc. Am., 59, 2079-2099.

Dziewonski, A. M. (1970). On regional differences in dispersion of mantle Rayleigh waves, Geophys. J. R. astr. Soc., 22, 289-325.

Dziewonski, A. M. and D. L. Anderson (1981). Preliminary reference Earth model, Phys. Earth Planet. Inter., 25, 297-356.

Dziewonski, A., S. Bloch and M. Landisman (1969). A technique for the analysis of transient seismic signals, Bull. Seism. Soc. Am., 59, 427-444.

Dziewonski, A. M. and F. Gilbert (1972). Observations of normal modes from 84 recordings of the Alaskan earthquake of 28 March

1964, Geophys. J. R. astr. Soc., 27, 393-446.

Dziewonski, A. M. and F. Gilbert (1973). Observations of normal modes from 84 recordings of the Alaskan earthquake of 28 March 1964, part II: spheroidal overtones, Geophys. J. R. astr. Soc., 35, 401-437.

Dziewonski, A. and M. Landisman (1970). Great circle Rayleigh and Love wave dispersion from 100 to 900 seconds, Geophys. J. R. astr. Soc., 19, 37-91.

Dziewonski, A., J. Mills and S. Bloch (1972). Residual dispersion measurement - a new method of surface-wave analysis, Bull. Seism. Soc. Am., 62, 129-139.

Dziewonski, A. M. and R. V. Sailor (1976). Comments on 'The correction of great circular surface wave phase velocity measurements from the rotation and ellipticity of the Earth' by F. A. Dahlen, J. Geophys. Res., 81, 4947-4950.

Dziewonski, A. M. and J. M. Steim (1982). Dispersion and attenuation of mantle waves through wave-form inversion, Geophys. J. R. astr. Soc., 70, 503-527.

Edmonds, A. R. (1960). Angular Momentum in Quantum Mechanics, pp. 19-24, Princeton University Press, Princeton, NJ.

Furumoto, M. and I. Nakanishi (1983). Source times and scaling relations of large earthquakes, J. Geophys. Res., 88, 2191-2198.

Geller, R. J. and S. Stein (1978). Normal modes of a laterally

heterogeneous body: a one-dimensional example, Bull. Seism. Soc. Am., 68, 103-116.

Geller, R. J. and S. Stein (1979). Time-domain attenuation measurements for fundamental spheroidal modes ($_0S_6$ to $_0S_{28}$) for the 1977 Indonesian earthquake, Bull. Seism. Soc. Am., 69, 1671-1691.

Gilbert, F. (1970). Excitation of the normal modes of the Earth by earthquake sources, Geophys. J. R. astr. Soc., 22, 223-226.

Gilbert, F. and A. M. Dziewonski (1975). An application of normal mode theory to the retrieval of structural parameters and source mechanisms from seismic spectra, Phil. Trans. Roy. Soc. Lond. A, 278, 187-269.

Given, J. W. and H. Kanamori (1980). The depth extent of the 1977 Sumbawa, Indonesia earthquake, EOS Trans. Am. Geoph. U., 61, 1044.

Goodman, N. R. (1960). Measuring amplitude and phase, J. Franklin Inst., 260, 437-450.

Hart, R. S., D. L. Anderson and H. Kanamori (1977). The effect of attenuation on gross Earth models, J. Geophys. Res., 82, 1647-1654.

Jackson, D. D. and D. L. Anderson (1970). Physical mechanisms of seismic wave attenuation, Rev. Geophys. Space Phys., 8, 1-63.

Jeffreys, H. (1965). Damping of S waves, Nature, 208, 675.

Jordan, T. H. (1978). A procedure for estimating lateral variations

from low-frequency eigenspectra data, Geophys. J. R. astr. Soc., 52, 441-455.

Jordan, T. H. and S. A. Sipkin (1977). Estimation of the attenuation operator for multiple ScS waves, Geophys. Res. Lett., 4, 167-170.

Kanamori, H. (1970a). Synthesis of long-period surface waves and its application to earthquake source studies - Kurile Islands earthquake of October 13, 1963, J. Geophys. Res., 75, 5011-5027.

Kanamori, H. (1970b). Velocity and Q of mantle waves, Phys. Earth Planet. Inter., 2, 259-275.

Kanamori, H. and K. Abe (1968). Deep structure of island arcs as revealed by surface waves, Bull. Earthquake Res. Inst., 46, 1001-1025.

Kanamori, H. and D. L. Anderson (1975). Theoretical basis of some empirical relations in seismology, Bull. Seism. Soc. Am., 65, 1073-1095.

Kanamori, H. and D. L. Anderson (1977). Importance of physical dispersion in surface wave and free oscillation problems: review, Rev. Geophys. Space Phys., 15, 105-112.

Kawakatsu, H. (1983). Can 'pure-path' models explain free oscillation data?, Geophys. Res. Lett., 10, 186-189.

Liu, H. P., D. L. Anderson and H. Kanamori (1976). Velocity dispersion due to anelasticity; implications for seismology and

mantle composition, Geophys. J. R. astr. Soc., 47, 41-58.

Luh, P. C. (1973). Free oscillations of the laterally inhomogeneous Earth: quasi-degenerate multiplet coupling, Geophys. J. R. astr. Soc., 32, 187-202.

Luh, P. C. (1974). Normal modes of a rotating, self-gravitating inhomogeneous Earth, Geophys. J. R. astr. Soc., 38, 187-224.

Madariaga, R. (1972). Toroidal free oscillations of the laterally heterogeneous Earth, Geophys. J. R. astr. Soc., 27, 81-100.

Madariaga, R., and K. Aki (1972). Spectral splitting of toroidal-free oscillations due to lateral heterogeneity of the Earth's structure, J. Geophys. Res., 77, 4421-4431.

Masters, G. and F. Gilbert (1982). Attenuation in the Earth at low frequencies, Phil. Trans. Roy. Soc. Lond. A, in press.

Masters, G., T. H. Jordan, P. G. Silver and F. Gilbert (1982). Aspherical Earth structure from fundamental spheroidal-mode data, Nature, 298, 609-613.

Masters, G., J. Park and F. Gilbert (1983). Frequency shifts and amplitude variations in aspherically coupled multiplets, in preparation.

Mendiguren, J. A. (1973). Identification of the free oscillations of spectral peaks for 1970 July 31, Columbian deep shock using the excitation criterion, Geophys. J. R. astr. Soc., 33, 281-321.

Mills, J. M. and A. L. Hales (1977). Great-circle Rayleigh wave attenuation and group velocity, I, Phys. Earth Planet. Inter.,

14, 109-119.

Mills, J. M. and A. L. Hales (1978). Great-circle Rayleigh wave attenuation and group velocity, II, Phys. Earth Planet. Inter., 17, 209-231.

Minster, J. B. (1980). Anelasticity and attenuation, in Physics of the Earth's Interior, A. Dziewonski and E. Boschi, eds., Proc. Enrico Fermi Intern. Sch. Phys., Academic Press, 151-212.

Nakanishi, I. (1979). Phase velocity and Q of mantle Rayleigh waves, Geophys. J. R. astr. Soc., 58, 35-59.

Nakanishi, I. and D. L. Anderson (1982). Worldwide distribution of group velocity of mantle Rayleigh waves as determined by spherical harmonic inversion, Bull. Seism. Soc. Am., 72, 1185-1194.

Nakanishi, I. and D. L. Anderson (1983a). Measurements of mantle wave velocities and inversion for lateral heterogeneity and anisotropy, part I: analysis of great circle phase velocities, in preparation.

Nakanishi, I. and D. L. Anderson (1983b). Measurements of mantle wave velocities and inversion for lateral heterogeneity and anisotropy, part II: analysis by single-station method, in preparation.

Okal, E. A. (1977). The effect of intrinsic oceanic upper mantle heterogeneities on regionalization of long-period Rayleigh-wave phase velocities, Geophys. J. R. astr. Soc., 49, 357-370.

Oppenheim, A. V. and R. W. Schafer (1975). Digital Signal Processing, pp. 239-250, Prentice-Hall, Inc., Englewood Cliffs, NJ.

Rial, J. A. (1978a). On the focusing of seismic body waves at the epicentre's antipode, Geophys. J. R. astr. Soc., 55, 737-743.

Rial, J. A. (1978b). Seismic waves at the epicentre's antipode, Ph.D. thesis, Calif. Inst. of Technol., Pasadena, CA.

Robinson, R., W. J. Arabasz, and F. F. Evison (1975). Long term behavior of an aftershock sequence: The Inangahua, New Zealand, earthquake of 1968, Geophys. J. R. astr. Soc., 41, 37-49.

Sailor, R. V. (1978). Attenuation of low frequency seismic energy, Ph.D. thesis, Harvard Univ., Cambridge, MA.

Sailor, R. V. and A. M. Dziewonski (1978). Measurements and interpretation of normal mode attenuation, Geophys. J. R. astr. Soc., 53, 559-581.

Saito, M. and H. Takeuchi (1966). Surface waves across the Pacific, Bull. Seism. Soc. Am., 56, 1067-1091.

Satô, Y. (1958). Attenuation, dispersion, and the wave guide of the G wave, Bull. Seism. Soc. Am., 48, 231-251.

Silver, P. G. and T. H. Jordan (1982). Fundamental spheroidal mode observations of aspherical heterogeneity, Geophys. J. R. astr. Soc., 64, 605-634.

Silver, P. G. and T. H. Jordan (1983). Total-moment spectra of fourteen large earthquakes, J. Geophys. Res., 88, 3273-3293.

Sleep, N. H., R. J. Geller, and S. Stein (1981). A constraint on the Earth's lateral heterogeneity from the scattering of spheroidal mode Q^{-1} measurements, Bull. Seism. Soc. Am., 71, 183-197.

Souriau, A. and M. Souriau (1983). Great circle Rayleigh wave phase velocities, tectonics and ellipticity, Geophys. J. R. astr. Soc., in press.

Stewart, G. S. (1978). Implications for plate-tectonics of the Aug. 19, 1977 Indonesian decoupling normal-fault earthquake, EOS Trans. Am. Geoph. U., 59, 326.

Toksöz, M. N. and D. L. Anderson (1966). Phase velocities of long-period surface waves and structure of the upper mantle. I. Great-circle Love and Rayleigh wave data, J. Geophys. Res., 73, 3801-3806.

Usami, T. (1971). Effect of horizontal heterogeneity on the torsional oscillation of an elastic sphere, J. Phys. Earth, 19, 175-180.

Woodhouse, J. H. (1980). The coupling and attenuation of nearly resonant multiplets in the Earth's free oscillation spectrum, Geophys. J. R. astr. Soc., 61, 261-283.

Woodhouse, J. H. and F. A. Dahlen (1978). The effect of a general aspherical perturbation on the free oscillations of the Earth, Geophys. J. R. astr. Soc., 53, 335-354.

Woodhouse, J. H. and T. P. Girnius (1982). Surface waves and free oscillations in a regionalized Earth model, Geophys. J. R. astr. Soc., 68, 653-673.

APPENDIX

The PTO seismograms were modeled in Chapters 1 and 2 using the method of Dahlen [1979b], who gave equations only for the vertical component of motion. This appendix gives the complete expressions for the amplitude term $A_\ell^m(\underline{r})$ in Equation 2.1 of this thesis for all three components.

Definitions:

$\underline{r}_s = (r_s, \theta_s, \phi_s)$ = source location

$\underline{r} = (r, \theta, \phi)$ = receiver location

$X_\ell^m(\theta)\exp(im\phi) = Y_\ell^m(\theta, \phi)$ = surface spherical harmonics

$U_\ell(r)$, $V_\ell(r)$ = radial eigenfunctions

M_{ij} = moment tensor elements

$\partial_r = \partial/\partial r$, $\partial_\theta = \partial/\partial\theta$

The indices ℓ and m are now suppressed for clarity, e.g., $X_\ell^m(\theta)$ is replaced by $X(\theta)$ and $U_\ell(r)$ by $U(r)$. Let $A(\underline{r})$, $B(\underline{r})$ and $D(\underline{r})$ replace $A_\ell^m(\underline{r})$ in Equation 2.1 for the displacement components u_r, u_θ and u_ϕ, respectively. Then

$$A(\underline{r}) = U(r)X(\theta)\{ [E_s X(\theta_s) + F_s \partial_\theta X(\theta_s)]\cos[m(\phi-\phi_s)] + [G_s X(\theta_s) + H_s \partial_\theta X(\theta_s)]\sin[m(\phi-\phi_s)] \}$$

$$B(\underline{r}) = V(r)\partial_\theta X(\theta)\{ [E_s X(\theta_s) + F_s \partial_\theta X(\theta_s)]\cos[m(\phi-\phi_s)] + [G_s X(\theta_s) + H_s \partial_\theta X(\theta_s)]\sin[m(\phi-\phi_s)] \}$$

$$D(\underline{r}) = m\frac{V(r)}{\sin\theta}X(\theta)\{\ [G_s X(\theta_s) + H_s \partial_\theta X(\theta_s)]\cos[m(\phi-\phi_s)] - [E_s X(\theta_s) + F_s \partial_\theta X(\theta_s)]\sin[m(\phi-\phi_s)]\ \}$$

where

$$E_s = \Gamma(m)\{\ M_{rr}\partial_r U(r_s) + M_{\theta\theta}\big(U(r_s)/r_s - [\ell(\ell+1)-m^2/\sin^2\theta_s]V(r_s)/r_s\big) + M_{\phi\phi}\big(U(r_s)/r_s - [m^2/\sin^2\theta_s]V(r_s)/r_s\big)\ \}$$

$$F_s = \Gamma(m)\{\ M_{r\theta}[U(r_s)/r_s + \partial_r V(r_s) - V(r_s)/r_s] - (M_{\theta\theta}-M_{\phi\phi})\cot\!\text{an}(\theta_s)V(r_s)/r_s\ \}$$

$$G_s = \frac{2m}{\sin\theta_s}\{\ M_{r\phi}[U(r_s)/r_s + \partial_r V(r_s) - V(r_s)/r_s] - 2M_{\theta\phi}\cot\!\text{an}(\theta_s)V(r_s)/r_s\ \}$$

$$H_s = \frac{4m}{\sin\theta_s}M_{\theta\phi}V(r_s)/r_s$$

$$\Gamma(m) = \begin{cases} 1, & m=0 \\ 2, & m\neq 0 \end{cases}$$